Von der Carl-Friedrich-Gauß-Fakultät für Mathematik und

Informatik der Technischen Universität Braunschweig

genehmigte Dissertation

zur Erlangung des Grades eines

Doktor-Ingenieurs (Dr.-Ing.)

Autor : **Antonio Fazzolari, Dott. in Fisica**

Titel: **An Aero-Structure Adjoint Formulation for Efficient Multidisciplinary Wing Optimization**

Datum der Promotion (Tag der mdl. Prüfung): 12.12.2005

1. Referent: Prof. H. G. Matthies, Ph. D.
2. Referent: Prof. Dr. rer. nat. N. R. Gauger

eingereicht am: 12.07.2005

Eidesstattliche Erklärung

Hiermit erkläre ich an Eides statt, daß ich die vorliegende Arbeit selbständig angefertigt habe. Alle benutzten Hilfsmittel sind angegeben. Diese Arbeit ist bisher weder veröffentlicht noch an einer anderen Hochschule zum Zweck der Promotion oder als sonstige Prüfungsarbeit eingereicht worden.

Braunschweig, im Juli 2005

Zusammenfassung

CFD (Computational Fluid Dynamics) ist heutzutage ein zuverlässiges Werkzeug für die Analyse von Strömungen und kommt deshalb in der Luftfahrtindustrie mehr und mehr zum Einsatz. Ein Flugzeugflügel ist jedoch ein Aero-Struktur-System, weshalb die durch die aerodynamischen Kräfte verursachte statische Deformation des Flügels während seines Entwurfes berücksichtigt werden muss. Wenn der Entwurf mittels deterministischen gradientenbasierten Optimierungsverfahren erfolgt, müssen demzufolge die statisch elastischen Effekte bei der Sensitivitätenberechnung mit einfließen und modelliert werden. Um sowohl auf der Struktur als auch auf der Aerodynamikseite hochgenaue und damit rechen- und zeitaufwändige Berechnungsverfahren verwenden zu können, wir ein gekoppeltes Aero-Struktur-Adjungiertenverfahren hergeleitet, implementiert sowie validiert und für den so genannten AMP-Flügel erprobt. Auf der Strömungsseite wird der DLR-Löser FLOWer und auf der Strukturseite der kommerzielle FEM-Löser MSC-NASTRAN verwendet. Schließlich wird eine multidisziplinäre Reichweitenoptimierung, mit der Breguet-Formel für die Reichweite als Zielgröße, für den AMP-Flügel durchgeführt – und zwar unter Berücksichtigung der statischen Deformation und der aerodynamischen Nebenbedingung, dass der Auftrieb konstant bleiben muss. Hierbei ermöglicht das effiziente gekoppelte Aero-Struktur-Adjungiertenverfahren die Parametrisierung des Flügels mit einer großen Anzahl an Entwurfsvariablen.

Abstract

Computational fluid dynamics is today a reliable tool for the analysis of the flow past wings, and is increasingly used in aircraft design. Since the wing is a coupled fluid-structure system, stationary elastic deflection has to be taken into account during the design. If the design is performed by means of gradient-based optimization techniques, it is necessary to include the effect of static elasticity in the gradient computation, since this can significantly alter the values of the sensitivities. On the other hand, the prediction of highly non-linear effects such as shock arise in transonic flow, and shock-shock interaction in supersonic flow is critical to perform a detailed optimization; this demands the use of high fidelity flow models. Since these models are extremely computationally expensive, an efficient computation of the gradient in turn requires the use of an advanced mathematical tool: the adjoint method. Both these critical requirements can be met by a coupled aero-elastic adjoint formulation, where the coupling is carried out firstly in the physical variables of the two systems, and then in the adjoint variables, which are subsequently used to calculate the sensitivity. The multidisciplinary extension of the adjoint method also allows the evaluation of gradients of cost functions or constraints containing terms coming from the structure side, as in the case of the Breguet formula for aircraft range. In the present work, a completely continuous formulation of the aeroelastic coupled adjoint method is presented and applied to test cases relevant to aircraft design, through an implementation within the software FLOWer from DLR and MSC-Nastran. The test cases are based on the AMP wing in the transonic regime, while the shape parametrization is based on the free-form deformation method. A comparative study of optimization histories is presented, showing the necessity of a high number of design variables to maximize the effectiveness of the optimization, as well as the necessity for accurate sensitivities that contain the effect of aeroelasticity. The sensitivities obtained from the coupled adjoint have allowed to perform in relatively short time optimizations with high number of design variables, aimed to reduce drag at constant lift and angle of attack and to increase range by means of the Breguet formula, assuming a stress penalty for the structural weight and again constant lift and angle of attack. A comparison of these two cases shows that the aerodynamically optimal minimal drag design differs from the multidisciplinary optimal design.

Acknowledgements

I would like to thank in the first instance Prof. Nicolas R. Gauger, who supervised this work from the very beginning and appears as co-referee of the thesis. His deep mathemathical insight and his friendly attitude have been invaluable during the various phases of this work. No less helpful has been Joël Brezillon, who shared with me his experience in design and has been a constant help in the implementation the various optimization chains. A big thanks to Richard Dwight for his knowledge of the Linux environment and to Dr. Ralf Heinrich, who developed the interpolation module.
I would also like to show my gratitude to Prof. Norbert Kroll and to Prof. Cord-Christian Rossow, for giving me (having a purely theoretical background) the opportunitiy of challenging myself with the programming of complex, state-of-the-art codes like FLOWer and Nastran, and to gain experience in the fascinating fields of aerodynamic design and multidisciplinary optimization, and to Prof. Hermann G. Matthies, who allowed turning this experience into a Ph. D. thesis.
This work has been supported by a grant from the Graduiertenkolleg “Wechselwirkung von Struktur und Fluid” of the Technical University of Brunswick, Germany.

Contents

1 Nomenclature

The following conventions will be adopted in the text:

$\mathbf{R}$	Residual flux for the fluid problem, 5 dimensional field, partial differential operator acting on the flow field ω.
$\mathbf{f}_{i=1,2,3}$	Convective Flux along the i space direction for the Euler flow equation in Cartesian coordinates, 5 dimensional field.
ω	Vector of the conservative flow variables in Cartesian coordinates, 5 dimensional field.
$\mathbf{F}_{i=1,2,3}$	Convective Flux along the i space direction for the Euler flow equation in body-fitted coordinates, 5 dimensional field.
$\mathbf{W}$	Vector of the conservative flow variables in body-fitted coordinates, 5 dimensional field.
P, E, H, ρ	Fluid pressure, energy density, enthalpy density, mass density.
ψ	Vector of the adjoint to the conservative flow variables, 5 dimensional field.
V or Ω	Flow volume.
S	Solid wall flow boundary (wing surface).
$\hat{n}$	Unitary ingoing normal to the wing surface in Cartesian coordinates (x_1,x_2,x_3).
$\hat{N}$	Unitary ingoing normal to the wing surface in body fitted coordinates (ξ_1,ξ_2,ξ_3).
$\tilde{z}$	Structural generalized displacement, 6 dimensional field, ordered as $\begin{pmatrix}\vec{z}\\ \overline{z}\end{pmatrix}$.
$\vec{z}$	Translational part of the structural generalized displacement field, 3 dimensional.
$\overline{z}$	Rotational part of the structural generalized displacement field, 3 dimensional.
$\tilde{S}(\tilde{z})$	Residual of the structural PDE, 6 dimensional field, ordered in the same way of $\tilde{z}$, partial differential operator acting on the displacement field $\tilde{z}$.
$\tilde{\phi}$	Field adjoint to the structural generalized displacement field, 6 dimensional, ordered as $\begin{pmatrix}\vec{\phi}\\ \overline{\phi}\end{pmatrix}$.
$\vec{\phi}$	Translational part of the field adjoint to the structural generalized displacement field, 3 dimensional.
$\overline{\phi}$	Rotational part of the field adjoint to the structural generalized displacement field, 3 dimensional.
$\vec{T}$	Traction applied to the structural surface.
Ω'	Structure volume.
N	Number of structural nodes.

$K \in \mathbb{R}^{6N} \otimes \mathbb{R}^{6N}$	Structural stiffness matrix.
a	design variable.
$\boldsymbol{A}=(a_1,...,a_n)$	Vector of design variables.
$\mathbf{B}^T\,\mathbf{C}$	Scalar product of the vectors **B** and **C**.
$b_i c_i$	Scalar product of the vectors **B** and **C** according to Einstein´s sum convention ($b_i c_i = \sum_{i=1}^{3} b_i c_i$).
$\Delta_a \omega$	Finite variation of ω caused by Δa.
δa	Variation of a.
$\delta_a \omega$	Variation of ω caused by δa.
$\frac{dF}{da}$	Total derivative of the function F with respect to a.
$\frac{\partial F}{\partial a}$	Partial derivative of the function F with respect to a.
$D_\omega \mathbf{R}$	Fréchet derivative of the operator **R** with respect to ω.
$\frac{\delta J}{\delta \omega}$	Variational derivative of the functional J with respect to ω.

2 Introduction

2.1 A new discipline

Multidisciplinary Design Optimization (MDO) has evolved as new discipline that provides a body of methods aimed at seeking an optimal engineering design when the interaction between several disciplines must be considered, and when the designer is free to significantly modify the system performance in more than one discipline. The coupling between different disciplines, which reflects the physical behaviour of the system, is usually paid for with an increased size, complexity and solution time of the problem and often by methodological and practical problems in the coupling of different solvers. Furthermore, not only the computational cost of multidisciplinary analysis is often much higher than the sum of the computational costs of the single disciplines solutions, but also the coupling itself can give rise to non-linear behaviour, even if the individual codes show linear behaviour. For example, the coupling of aerodynamics and elasticity can be obtained at a low accuracy level using a linear aerodynamics code, which gives the pressure distribution, and a linear elastic code, which gives the displacement as function of the pressure distribution. Since the dependence of the pressure on the displacement can be non-linear, this problem shows a higher level of non-linearity than the individual disciplines. In some cases the coupling of single discipline codes can give an ill-conditioned system that requires special treatment in order to obtain convergence.

On the other hand, the struggle to carry out an MDO is often worth it, since multidisciplinary optimal designs have been shown in numerous cases to be better than designs obtained with singledisciplinary optimization methods, especially when the optimal design implies a trade-off between the different disciplines. For example the goal of minimizing the cost of a vehicle while maintaining some acceleration capability can be reached either reducing the structural weight or adding engine power, but the cost of these two operations can be different. This is thus a multidisciplinary optimization problem that involves propulsion and structural design. In similar way, electronic packaging optimization involves coupling between electronic and thermal analysis. But the most important example of a multidisciplinary optimization problem, and historically the one that has sparked research in this field, comes from aerospace design and deals with aero-structural optimization. In this case, slender shapes are associated with lower drag values but are heavier than stubby, more draggy shapes. The trade-off between the exigency of light structure and the exigency of low drag is reached in a multidisciplinary optimal design point, which is different from the design obtained with singledisciplinary (e. g. pure aerodynamic) methodology. Furthermore, this bidisciplinary design problem is part of the wider multidisciplinary problem of aircraft design, which can include, beyond aerodynamics and static elasticity, fluttering, propulsion, mission design, and flyover noise. In a similar way, ship design involves the disciplines of hydrodynamics, structures, propulsion, and cost estimation and automotive design implies the analysis of noise and vibration, crash performance and weight.

All these problems, which are very varied in disciplines and solution techniques, share thus a common formal structure and have been the motivation for the development of a great number of multidisciplinary optimization strategies. A survey of such strategies and their applications can be found in the work of Kodiyalamand and Sobiesky [**1**] or in the reports [**2**] and [**3**], while in Sobiesky and Haftka [**4**] the focus is in particular on methods and test cases that are relevant for aircraft design.

2.2 Computational fluid dynamic analysis and optimization in aircraft design

Before entering into the matter of multidisciplinary optimization, which is one of the latest developments for aircraft design, it is worth seeing how the computational science has entered into the aircraft design process. The fruitful interaction of computational science and engineering has generated computational fluid dynamics based analysis and optimization tools that are today widely used for the design of engineered products like airplanes and vehicles. An established CFD based optimization methodology is the prerequisite to its extension to multidisciplinary optimization and the two methods often make use of the same optimization strategies.

2.2.1 Computation fluid dynamics from analysis to optimization

The first aircraft that has been designed using also a CFD technology was probably the Anglo-French supersonic transport aircraft Concorde. Designed in the late 1960s, of which the last exemplar was retired, after 30 years of duty, during the development time of this work. The great sensitivity of the supersonic wave drag to the details of the design made necessary to support the empirical cut-and-try method with computational methods, while the supersonic flow over a slender body was susceptible to being described by the linearized supersonic models embedded in the first CFD codes. These codes ran on an IBM7094 machine, which was equipped with 32 Kilobytes memory and cost about 3.5 million dollars.

By the mid 1970s, several panel-method codes were implemented and researchers started to use them in conjunction with optimization strategies, based on finite-difference gradient evaluation [**5**]. One of the successful applications of this technology was the design of the B747 Space Shuttle Carrier Aircraft [**6**]. This technology also provided a better understanding of the interference phenomenon between wing and turbine nacelle that led to the design of longer engine bodies. However it required about ten years to overcome all difficulties associated with boundary conditions, numerical problems and geometry definition. Panel codes with automatic panelling tools are in use still today in preliminary design and MDO [**7**]. However, the inability of the potential (Laplace) equation to predict non-linear phenomena like shocks in transonic flow and shock interaction in supersonic flow seriously limits their applicability [**6**]. A first step to overcome this problem was taken with the formulation of a fully conservative finite volume scheme to solve the full potential equation, performed by Jameson and Caughey in 1977 [**8**]. The full potential equation is a non-linear partial differential equation for the potential flow derived assuming compressible, irrotational, isentropic flow, and mass and energy conservation at potential jumps, but not momentum conservation. Since the last assumption is unphysical, it is no wonder that this equation is unable to correctly predict shock strength and position even in case of moderate shocks. It has been recently shown [**9**] that replacing the isentropic assumption with a non-isentropic one and enforcing momentum conservation leads to solutions much closer to that of the Euler equations, which, by making use of the Rankine-Hugoniot conditions, correctly describe the behaviour across flow discontinuities. Despite this limitation, tools based on the full potential equation coupled with a boundary-layer model were intensively used in 1980s to study transonic flow for complex wing-body-nacelle geometries. The non-linear behaviour of this equation posed for the first time the problems of convergence speed and of the volume mesh generation, features which are also today critical for the solution of high-fidelity flow equations. In the middle of 1980s, the parallel developments in computational power and in numerical methods, allowed the solution of the Euler equations with a finite volume formulation on structured grids [**10**]. In the

early 1990s, thanks to the development of turbulence models, Navier Stokes solvers based on finite volume schemes on structured grids were available for use in design. However the extremely high computational cost of the solution of the Euler and Navier-Stokes equations limited the applicability of these achievements to optimization problems until the major breakthrough of shape sensitivity analysis through the continuous adjoint formulation (sometimes called also control theory), in 1996. This method allowed the simultaneous use of a high-fidelity model and a high number of design variables in conjunction with a gradient-based optimization strategy [**11**]. In the following years, this method has been widely applied to transonic and supersonic design. The continuous adjoint method was later extended to the Reynolds Averaged Navier-Stokes equations with the Baldwin-Lomax turbulence model [**12**], [**13**]. In the meantime, the technology for the calculation of these high fidelity flow models and their sensitivities has been enriched by two alternative methodologies, namely the unstructured grid finite volume formulation and the discrete adjoint method for the sensitivity evaluation. The unstructured grid methodology is based on grid cells that are not necessarily orthogonal with respect to a body-fitted coordinate system. Its main advantage is the much shorter time required to generate an unstructured grid as compared to a structured one. In the continuous adjoint formulations one formulates the optimization problem prior to the discretization, while the discrete adjoint method is obtained by discretizing the flow equations and then deriving the sensitivities, in order to perform the optimization. Both of these new methodologies have been used in design, so that we can find discrete adjoint methods based on structured solver [**14**] and continuous adjoint methods based on unstructured solvers [**15**], [**16**], as well as discrete adjoint methods based on unstructured solvers. A study on the relative merits of the two approaches for can be found in [**17**].

Once a reliable and efficient methodology to evaluate sensitivities from high-fidelity flow models via the adjoint approach has been achieved, the next step has been to include the effect of static elasticity in these sensitivities, in order to transfer all the advantages of the adjoint formulation into an MDO framework. This method, which requires some analytical effort to formulate a system of coupled adjoint equations for the flow and for the structure, has been recently successfully applied to gradient based optimization of a supersonic business jet using a continuous adjoint formulation for inviscid flow, a discrete formulation for the coupling, and taking an approximation of the Breguet range formula as cost function [**18**]. The same coupled sensitivities approach, but based on the three field-formulation for aeroelasticity and using a totally discrete adjoint formulation, was applied to the aero-structural optimization of a transonic wing, assuming inviscid flow [**19**]. All the optimizations reported above were based on the evaluation of the sensitivity of cost functions and constraints with respect to a set of design variables, they were thus gradient-based optimizations. However, this is not the only strategy that leads to a wing shape optimization or even a multidisciplinary optimization. Evolutionary strategies and Nelder-Mead Simplex methods have also been successfully applied to many optimization problems, based on single and multidisciplinary analysis, as reported in the following paragraphs.

2.2.2 Optimization strategies

To give an overview on the rich and constantly evolving field of optimization techniques is beyond the scope of this work. What the reader can find here is a very concise exposition of the most common techniques and their applicability to problems in aircraft design. The exposition does not pretend to be exhaustive, but just to offer to the reader a perspective for the use of a gradient-based adjoint approach, which is the subject of the present work. Optimization

strategies can be divided in the two big classes: deterministic and non-deterministic, according whether or not they use information from preceding sets of design variables to evaluate the new set or they apply a random perturbation [**20**].

2.2.2.1 Evolutionary strategies

These methods, belonging to non-deterministic methods, replicate the biological processes of mutation-crossover-selection in a population of individuals belonging to the same species but with different genetic characters. The genetic character is embodied by a design vector, which is randomly altered during mutation, randomly crossed with other design vectors belonging to the actual "population" during the crossover phase, and subsequently selected according to some cost function criterion. In this way the population evolves toward fitter designs. If constraints are present, they are taken into account by introducing penalty terms in the cost function. Since the whole procedure contains a considerable number of random operations, it tends to become inefficient with large numbers of design variables (and thus with big design vectors). On the other hand, the optimal designs obtained in this way are likely to be global optima, which is not necessarily true for deterministic strategies. A wide number of different kinds of genetic algorithms have been developed and applied to aircraft design optimization. Some of them use gradient information to drive the mutation process, increasing the effectiveness of the method [**21**]. Another possibility is to use an evolutionary strategy to "explore" a wide number of configurations in the design space and then to use a gradient-based strategy to perform the final, detailed optimization. Such multi-strategic approach has been applied recently to the multidisciplinary optimization of a supersonic transport aircraft [**22**].

2.2.2.2 Nelder-Mead Simplex method

The Nelder-Mead Simplex is a widely used deterministic approach, due to its simplicity and robustness [**23**]. The optimizer builds a regular simplex with n+1 points in the n-dimensional design space, and evaluates the cost function on these points. The point with the worst value of the cost function is replaced with its mirror image with respect to the geometric mean of the other points, and the procedure restarts. In this way the optimizer performs a search in the design space, following a path that leads to the nearest minimum of the cost function. Since the number of evaluations required increases linearly with the number of dimensions, the method becomes extremely inefficient in high dimensional design spaces. An interesting way to overcome this problem is given by Multilevel Shape Parametrization [**24**]. By using a set of shape functions that support easily degree-elevation, the optimization is started with the coarser set of design variables, and reaches the finest level - the most accurate and expensive - only in the final stage. In this way many evaluations are saved and the convergence is greatly improved.

2.2.2.3 Gradient based methods

Gradient-based methods are determistic methods which require the evaluation not only of the value of cost functions and constraints at a given design point, but also the evaluation of their sensitivities to small perturbations in the neighbourhood of the design point. The gradients are used to build a linear approximation of the cost function and of the constraints. For this reasons, these methods are termed 1^{st} order determistic methods, while the Nelder-Mead Simplex algorithm use only 0^{th} order information. Once values and gradients are evaluated, the gradient-based optimizer faces the problem of finding a search direction that will bring the maximum decrease of the cost function. If the problem is unconstrained, this is achieved simply by

moving in the direction opposite to the gradient, according the *steepest-descent* method. The optimizer performs thus a line-search until the cost function starts to increase. At this point, the search direction is updated with new gradient evaluation followed by a new line search, until convergence to a local minimum. Often it is more efficient to retain some information from the past gradients in establishing a new search direction, as in the *conjugate-gradient* method. These methods apply to unconstrained optimization. If constraints are present, the direction-finding problem must reject all directions that decrease the cost function causing a violation of the constraints, and thus an *infeasible* design. This is realized by the *method of feasible direction*. Also the line search must take into account the presence of constraints before a new gradient evaluation is requested. This is accomplished by adding some *push-off* factors in the direction-finding problem that prevent the optimizer from violating the constraint [**25**].

Gradient-based methods are the methods that most efficiently move in the design space towards the nearest minimum. However, the cost of a gradient evaluation conducted by direct evaluation of the perturbed states (finite-differences) can seriously limit its applicability to a low number of design parameters. Therefore gradient-based methods are often paired with efficient gradient evaluation methodologies like automatic differentiation, direct differentiation or adjoint methods.

2.2.2.4 Higher order methods

The convergence criterion for unconstrained optimization problems requires that the gradient of the cost function F with respect to a set of design variables $\mathbf{A} = (a_1, ..., a_N)$ vanishes at the optimal design point. In the neighbourhood $\mathbf{A}_0 + d\,\mathbf{A}$ of a design point $\mathbf{A}_0$, the gradient of F can be found to the first order in $d\boldsymbol{A}$ as function of the gradient of F in $\mathbf{A}_0$ and of the Hessian of F in $\mathbf{A}_0$, $H(F)(\mathbf{A}_0) = \left.\frac{\partial^2 F}{\partial a_i \partial a_j}\right|_{\mathbf{A}=\mathbf{A}_0}$. Such gradient takes the form:

$$\nabla F(\mathbf{A}_0 + d\,\mathbf{A}) = \nabla F(\mathbf{A}_0) + H(F)(\mathbf{A}_0) d\,\mathbf{A} + O(d\,\mathbf{A}^2). \tag{1}$$

Imposing this expression for the gradient to be zero, a condition that is fulfilled only in the local optimal design point, leads to a value for $d\,\mathbf{A}$ that points towards the sought minimum for F, provided that the Hessian of F is positive definite. The procedure is thus iterated, giving a Newton's method. Since the Hessian matrix is in practice very expensive to evaluate, it is often replaced by an approximation iteratively updated on the basis of the previous values of F and ∇F, and the procedure takes the name of the Quasi-Newton method. In case of constrained optimization, the equality constraints, expressed by $C(\mathbf{A}) = 0$, can be taken into account using a Lagrangian formulation, namely by seeking the unconstrained stationary points (points of vanishing gradient) of the functional

$$L(\mathbf{A}, \lambda) = F(\mathbf{A}) - \lambda C(\mathbf{A}) \tag{2}$$

in the space $(\mathbf{A}, \lambda)$. This implies the first order optimality condition (Kuhn-Tucker condition)

$$\nabla L(\mathbf{A}, \lambda) = 0\,, \tag{3}$$

Where the gradient is evaluated with respect to $(\mathbf{A}, \lambda)$. The Lagrangian multiplier λ has the same dimension of the number of constraints. Since a constrained minimum for *F* is not an unconstrained minimum for *L*, but only a stationary point, the search for the optimal design point must be lead under additional assumptions on the Hessian of *L:*

$$d^T \left(H(L) \right) d > 0\,, \tag{4}$$

where *d* is such that $\nabla C^T d = 0$. If one applies Newton's method to the Lagrangian *L*, the result is a quadratic minimization problem, and the method takes the name of Sequential Quadratic Programming. Alternatively, the Lagrangian can be augmented by a penalty factor that assures that the condition (4) is fulfilled

$$L(\mathbf{A}, \lambda) = F(\mathbf{A}) - \lambda C(\mathbf{A}) + \frac{\rho}{2} C^2(\mathbf{A})\,. \tag{5}$$

It can be shown that a value ρ_0 exists, such that for $\rho > \rho_0$ the constrained minimum of *F* is also an unconstrained minimum of the augmented Lagrangian *L*. In this way, the same methods used for unconstrained optimization problems can be applied to constrained ones. This method, however, can be extremely sensitive to the choice of the value of ρ_0. An exhaustive treatment of various optimization methods can be found in [**26**].

2.2.2.5 Optimization strategy adopted

In the work of the following sections, a modification of the method of the feasible direction was used [**27**]. The modification consists of adding a constraint recovery routine, which is activated if the line search, despite the *push-off* factors, brings the design point into a violated constraint zone. In that case, the successive line search is aimed principally at recovering the constraint and only in the second instance to decrease the cost function. The method of feasible direction is maybe not as efficient as higher-order methods, but the absence of the Hessian matrix and associated approximations is likely to make the method more robust in high dimensional (~10^2 parameters) design spaces.

2.2.3 Shape parametrization for optimization in aircraft design

Once a strategy to move in the design space has been chosen, it is necessary to choose a parametrization of the wing geometry that defines the design space for a particular test case. Here, many different approaches have been successfully applied. The most simple geometry parametrization can be obtained by simply taking every mesh point coordinate as design variable. This approach has the principal drawback that the sensitivity of a cost function with respect to point coordinates is of a lower smoothness class than the wing shape. This implies that successive deformations of the shape according to this sensitivity degrade the smoothness of the surface, possibly giving unusable "corrugated" surfaces. A solution to this problem has been found in so-called gradient smoothing [**28**]. Another drawback is that a wing surface is discretized usually by order 10^3 points, which gives $3\text{x}10^3$ design variables, a number that

cannot be considerably reduced without risk of decreasing the efficiency of the optimization. For this reason, this method can be used only in conjunction with an adjoint sensitivity evaluation that allows the evaluation of gradients independently of the number of design variables. Alternatively, one can choose a set of smooth functions that create a basis for the bumping applied to the surface. The bumping method is more likely to preserve the smoothness of the surface but, on the other hand, if the set of bumping functions is not wide enough, the optimal design point obtained will be only an approximation of the real optimal design. If the set of bump functions supports the degree-elevation, the already cited Multivelel Shape Parametrization [**24**] is a possible solution of this problem. Within this approach, a huge number of algorithms have been written to parametrize the deformation of the wing, based on functions sets like nonuniform rational b-splines (NURBS) [**29**], Hicks-Henne bump functions [**30**] and Bezier Polynomials. The bumping can be applied to the wing surface or to the thickness, camber-line, and twist distributions, depending on the constraints that are prescribed for the geometry, which can be sometimes quite complex. In this case, it is essential to choose a geometry parametrization compatible with the geometrical constraints, in order to perform a successful optimization, as for example in Ref. [**31**].Lately, a method firstly developed for visual editing [**32**], called free-form deformation, has been also successfully applied to aircraft design [**33**]. The method is based on a 3D generalization of a Bezier curve defined by *n* control points, giving thus a 3D mesh of control points that enclose the object to be deformed [**34**].

A separate citation is due to the optimization of high-lift devices of commercial planes. Here, design variables are principally the positions of extended slat and flap, target are again lift and drag, and constraints come from various aspect of the mission design, like climb and glide path angles, or flyover noise [**20**].

2.2.4 Gradient evaluation methods

Several methods are available to evaluate the sensitivities of cost functions and constraints that are used in gradient-based optimization of airfoils. In the pioneering works on this topic [**35**], [**36**] the method used was finite-differencing of the solution of the full-potential flow equation on an airfoil. A method derived from finite-difference is the complex step method, which supposes all calculations in the CFD code to be extended in the complex field $\mathbb{C}$ [**37**]. The geometry alteration is thus obtained by applying an increment in the imaginary direction. The error in the so obtained sensitivity shows a better behaviour as the step size goes to zero with respect to the real finite differencing. The use of finite-difference with high-fidelity flow models limits drastically the number of design variables, thus this method has been abandoned in favour of the more powerful approaches described in the following paragraphs, and it is used as reference for the validation of sensitivities.

2.2.4.1 Analytic differentiation

Let's consider an optimization problem defined by a function $F(\omega, a)$ that is to be minimized, $\omega \in W \subset \mathbb{R}^n$ being a vector of state variables and $a \in \mathbb{R}$ a design variable. Given a function $\mathbf{R}(\omega, a): W \times \mathbb{R} \to \mathbb{R}^n$ that is continuously differentiable, called state equation, let a point (ω_0, a_0) in $W \times A$ exist, such that $\mathbf{R}(\omega_0, a_0) = 0$. By the implicit function theorem, if $\det\left(\frac{\partial \mathbf{R}(\omega, A)}{\partial \omega}\right) \neq 0$, then $\mathbf{R}(\omega, a)$ implicitly defines a mapping $h: H \subset \mathbb{R} \to V \subset W$ such

that $\mathbf{R}(h(a),a)=0$ for every $a \in H$. The mapping h describes the dependence of ω from a and has the property

$$\frac{\partial h}{\partial a} = -\left(\frac{\partial \mathbf{R}}{\partial \omega}\right)^{-1} \frac{\partial \mathbf{R}}{\partial a}. \tag{6}$$

We can write the *total derivative* of the function $F(h(a),a)$ with respect to a as

$$\frac{dF}{da} = \frac{\partial F}{\partial \omega}\frac{\partial h}{\partial a} + \frac{\partial F}{\partial a}, \tag{7}$$

In optimization context, such quantity is usually referred as *sensitivity* of F with respect to a. Using Eq. (6) the expression for the total derivative becomes

$$\frac{dF}{da} = -\frac{\partial F}{\partial \omega}\left(\frac{\partial \mathbf{R}}{\partial \omega}\right)^{-1} \frac{\partial \mathbf{R}}{\partial a} + \frac{\partial F}{\partial a}. \tag{8}$$

Since F does not appear in Eq. (6), the same solution of Eq. (6) can be used to evaluate sensitivities of different cost functions. However, Eq. (6) must be solved for every component a of the design variables set $\mathbf{A} \in \mathbb{R}^m$. In the case of large iterative problems, like in CFD, the cost of solving Eq. (6) is likely to be the same as for solving the state equation $\mathbf{R}(\omega,a)=0$. This approach is thus not competitive in terms of CPU time with respect to the finite differences method. In the case that the terms in Eq. (6) are derived analytically, however, the outcome is not dependent from the choice of a stepsize for the design parameters, as in the case of finite differences.

2.2.4.2 Adjoint methods

These approaches are derived from an analytic differentiation, when Eq. (6) is multiplied by a Lagrangian multiplier ψ and then added to the expression for the sensitivity Eq. (7) obtaining

$$\frac{dF}{da} = \frac{\partial F}{\partial \omega}\frac{\partial h}{\partial a} + \frac{\partial F}{\partial a} + \psi^T\left(\frac{\partial \mathbf{R}}{\partial \omega}\frac{\partial h}{\partial a} + \frac{\partial \mathbf{R}}{\partial a}\right) \tag{9}$$

If one imposes the Lagrangian multiplier to be a solution of the adjoint equations

$$\frac{\partial F}{\partial \omega} + \psi^T \frac{\partial \mathbf{R}}{\partial \omega} = 0, \tag{10}$$

then the sensitivity can be calculated as

$$\frac{dF}{da} = \frac{\partial F}{\partial a} + \psi^T \frac{\partial \mathbf{R}}{\partial a}. \tag{11}$$

Since this expression does not contain $\frac{\partial h}{\partial a}$, but only the adjoint field ψ, the solution of the adjoint Eq. (10), the sensitivity of F can be obtained from Eq. (11) without solving the state equation n times for n design parameters as in the case of Finite Differencing. In the case that the state equation is a high fidelity flow equation like the Euler or Navier-Stokes equations, this method allows a great increase in the computational efficiency.

2.2.4.2.1 Continuous adjoint and discrete adjoint

In the case of high-fidelity CFD models, like the ones given by the Euler and Navier-Stokes equations, the state equation in the Cartesian coordinates x_i takes the form

$$\mathbf{R}(\omega) = \frac{\partial \omega}{\partial t} + \frac{\partial \mathbf{f}_i(\omega)}{\partial x_i} = 0, \tag{12}$$

where $\omega(t,x_i)$ is the vector of conservative variables and $\mathbf{f}_i(\omega)$ are the residual flux vectors which contains the convective and viscous flux terms. In the numerical solution of Eq. (10), one can choose to first discretize Eq. (12) and then calculate the derivatives with respect to the discrete flow field ω_h, which are necessary to assembly the adjoint equation:

$$\frac{\partial F_h}{\partial \omega_h} + \psi_h^T \frac{\partial \mathbf{R}_h(\omega_h)}{\partial \omega_h} = 0. \tag{13}$$

In particular for a finite volume scheme the divergence term in Eq. (12) is replaced by a sum of fluxes of $\mathbf{f}_i(\omega)$ at the cell boundaries, evaluated on the basis of a stencil of values of the discrete flow vector ω_h in the nearby cells. To evaluate the discrete adjoint Eq. (13) this sum of fluxes and the discretized cost function F_h have then to be differentiated with respect to the discrete flow field ω_h. Alternatively, one can evaluate the derivative with respect to ω in Eq. (10) analytically and discretize the obtained expression according the same discretization scheme used for the solution of the primal problem. In this case, the method takes the name of continuous adjoint.

2.2.4.3 Automatic differentiation

In the automatic differentiation (AD) method, a program automatically differentiates every relevant quantity in the main code using the chain-rule, as done e.g. in Eq. (7), in order to obtain an expression to be solved for the sensitivity. The so obtained code is usually much bigger than the original one and requires much more memory. The cost of a sensitivity evaluation is the same as a finite difference evaluation in “forward mode”, while it is independent of the number of design variables if the “reverse mode” is used. The reverse mode is equivalent to a discrete adjoint formulation, where the derivatives of the quantities appearing in the adjoint

equation with respect to the discrete flow field ω_h are obtained by automatic differentiation. The applicability of this method is nowadays limited by the complexity of the code to be differentiated. A survey on various AD programs on Fortran CFD codes can be found in [**38**], while theoretical foundations can be found in [**39**].

2.3 Multidisciplinary optimization in aircraft design

The definition of multidisciplinarity is in some way blurred. In some cases, it refers to the mere exchange of information between discipline analysis codes, or as *a methodology for design and analysis of complex engineering systems and subsystems which coherently exploits the synergism of mutually interacting phenomena* [**40**]. Aside from abstract definitions, the multidisciplinary optimization implemented for aircraft design can practically be divided in two big classes. To the first class, and historically the oldest, belong problems for which quantities belonging to different disciplines are to appear in the optimization cost function or constraints. The second class is embodied by problems which take also the name of *multi-field* or *multi-physics* problem, like aeroelasticity, thermoelasticity, aeroacustics, etc., where the physical system of interest is made of two interacting sub-systems, and a complete analysis of this interaction is carried out. These two definitions are not mutually exclusive, nevertheless often a multidisciplinary optimizations of the first class has been performed without, or on the base of approximated, analysis of the second class. Only recently have the two methodologies been applied together in fully consistent multidisciplinary frameworks like the ones described in [**18**] and [**19**].

2.3.1 Optimizations with a multidisciplinary cost function

Multidisciplinary issues have been constantly present in aircraft design. The elliptic lift distribution law, which 1915 was derived analytically by L. Prandlt using a potential flow model, has been later modified with a correction factor to allow for constraining the root bending moment, which is a measure of the stress the structure must undergo [**41**]. A meaningful application of this correction is represented by the optimization of the airplane range. The range can be calculated from the Breguet range formula as

$$R \propto \frac{L}{D} \ln\left(\frac{W + M_F}{W}\right), \tag{14}$$

where L is the Lift, D the drag, W the weight of the aircraft and M_F is the fuel weight. In the search for an optimum for such cost function, a trade-off must be made between the requirement for an elliptical distribution (aerodynamics) and the requirement for a low bending moment (structure). The result is that the lift distribution appears more “triangular” with respect to the elliptic loading, while the total lift, represented by the area under the distribution, remains unchanged. The outcomes of the analytic calculations discussed above are associated to simplifications in the flow (lifting line theory) and in the structure (absence of structure model, since only the bending moment is taken into account) modelling, so that a computational analysis is necessary to increase the accuracy of the result. Some CFD panel codes [**42**], [**43**], [**44**] have been extended to the treatment of the root bending constraint, based on different structural beam models. Since an analytic solution of the multidisciplinary optimization

problem is not possible, these codes use an iterative approach to evaluate a lift load distribution associated with a bending moment that does not exceed a maximum value. The weight of the wing is assumed to be linear function of the local bending moment. These procedures have been then tested on a realistic design of long-range commercial airplane. The result is again a more triangular distribution (see Figure 1).

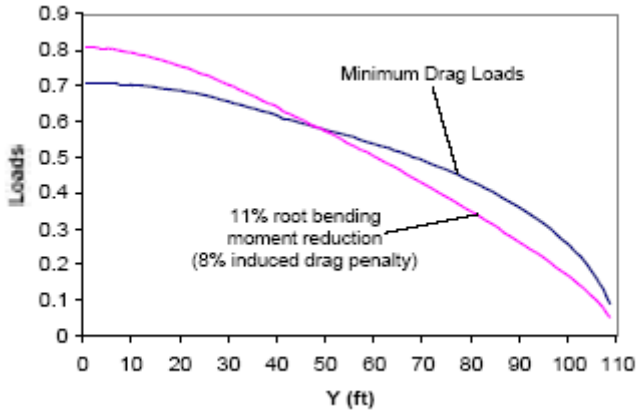

Figure 1. Span load distribution for minimum induced drag and for an 11% root bending moment reduction for a B-777 type configuration, picture from ref. [42]

If we consider the aircraft range fixed, and solve (14) with respect to the fuel weight, we obtain

$$M_F \propto W\left(e^{\frac{D}{L}R}-1\right). \tag{15}$$

We see that it is possible to reduce the fuel consumption, assuming an increase in the drag, if we get an appropriate decrease in the weight. According to the calculations of [**42**]**,** this trade-off between weight and aerodynamics reflects a 0.5% fuel saving for a Boeing-777 class aircraft. This ratio is better for smaller, shorter-range aircraft, because of the smaller R factor that multiply the drag penalty in (15), or if the aircraft is optimized for reduced range missions. According to a recent paper [**45**], commercial airplane wings designed in the ´70 and ´80 are poorly optimized, and a RANS multipoint optimization based on sensitivities evaluated with adjoint approach and analytical weight model lead to a range improvement of more than 10%.

2.3.2 Optimizations with multidisciplinary (multi physics) coupling

An aircraft in flight is subject to complex interactions between aerodynamics, structures, control and propulsion systems. Traditionally, these disciplines were uncoupled and solved separately. In the early 1990s started the first organic programs aimed, like the NASA series on High Speed Civil Transport, to a multidisciplinary optimization that covers all these disciplines. Due to the great number of task to be integrated, these early studies relied on some approximations of the coupling between the disciplines. For example, the aeroelastic coupling was taken into account only during a single aeroelastic analysis before the optimization, and

then supposed constant [**46**]. A systematic analysis performed on coupled CFD and CSM codes showed that coupled sensitivities for shape design can show big deviations with respect to singlediscipline sensitivities, showing sometimes also changes in sign [**47**]. The first study was based on the transonic small disturbance equation and for an analytic flat plate model for the structure, while a few years later a similar task was performed using unstructured Euler flow solver and finite element structural modelling [**48**]. As a consequence, NASA´s and similar multidisciplinary frameworks [**49**], [**29**] now make use of a complete sensitivity analysis by finite-difference, according the so-called *all-in-one* or *multidisciplinary feasible* approach. The extremely high computational costs of a gradient evaluation by finite-differences, however, forces these frameworks to be run on supercomputers even for a low number of design variables, or, alternatively, to make use of response surface approximations of the high-fidelity flow models [**50**].

2.3.3 Collaborative optimization and other distributed approaches

Although probably the most popular, the inclusion of the elasticity effect into the sensitivity is not the only way to carry out a multidisciplinary optimization in presence of aeroelastic coupling. Several methods have been developed, in order to decompose a multidisciplinary optimization into many linked single discipline optimizations, controlled by a global operator, that operates at the higher level (system-level), and defines the single discipline optimization targets. These approaches present the advantage that each single discipline optimization can be carried out with its own strategy and code, eliminating thus the necessity of building a global sensitivity. This can be done if the coupling variables, which carry the coupling between disciplines, are considered as design variables of which the “optimal” value is the one that minimizes a given interdisciplinary inconsistency. By introducing interdisciplinary consistency functions the single disciplines are thus decoupled. In collaborative optimization, the disciplines are given the autonomous task of minimizing system-level inconsistency while maintaining disciplinary design feasibility. In optimization by hierarchical decomposition, reversely, the disciplines are given the task of minimizing disciplinary infeasibility while maintaining system-level consistency [**51**]. In general these methods require many system-level iterations to reach an optimal design, and the computational cost is significantly higher than using a tightly coupled method like the multidisciplinary feasible approach. A typical way of alleviating the computational cost is to use this method with simpler discipline models like response surfaces [**52**], or to use a modal analysis to reduce the exchange of information (the so-called bandwidth) between the codes [**53**]. The idea of using the coupling variables as design variables characterizes also the simultaneous aerodynamics and structural design optimization (SASDO) approach, in which the convergence is brought simultaneously in the analysis and in the optimization, as in the singlediscipline *one-shot* approaches. This approach allows reducing the cost of a multidisciplinary aeroelastic optimization, as shown in [**54**], but the gain is limited to a 26% saving in the CPU-time. A survey on the application of such methods to MDO in aircraft design can be found in [**40**].

2.3.4 Recent developments in sensitivity-based MDO

Once the necessity of including in the sensitivity the effect of elasticity is recognized, the most challenging task is finding a way to compute it efficiently. The problem is similar to the singlediscipline one, but with a rise in complexity due to the fact that aeroelastic coupling problem is usually solved by two different codes, each with it’s own discretization method and mesh. The use of automatic differentiation tools for the whole problem is thus evidently

impossible. An analytic differentiation that gives the sensitivity for a coupled system has been carried out by Sobiesky [**55**], and applied to a 3D wing in transonic regime by Newman et al. [**56**] and to the HSCT test case by Giunta and Sobiesky [**57**]. In general, this method presupposes to obtain the sensitivity matrices (1^{st} term of Eq. (6)) from the two codes, which can be done analytically or using some automatic differentiation tool. These matrices are then used to assemble a system of global sensitivity equations, of which the solution is the coupled sensitivity. Unfortunately, this system can be solved by explicit factorisation methods only for small sized problems, due to the excessive memory requirements. For larger problems, the Gauss-Seidel iteration must be used, and the computational cost is not dissimilar to a finite-difference evaluation of the primal problem.

2.3.4.1 Sensitivity evaluation by coupled adjoint method

An alternative to the solution of the global sensitivity equations and to finite-differences can be found in the coupled adjoint formulation. The derivation is similar to that of the singlediscIplinary adjoint, but the presence of two state equations requires the use of two Lagrangian multipliers, which are solutions of a system of two coupled adjoint equations. If a three-field formulation for the aero-elastic coupling is used, the three state equations (fluid equation, structure equation and mesh movement pseudo-structural equation) give rise to a system of three coupled adjoint equations. The choice between a discrete and a continuous adjoint formulation must be made, or a mixture of both. Maute et al. [**19**] built the adjoint of the system of discrete equations associated with the three field formulation of aeroelasticity, and applied it to the optimization of a wing in the transonic regime aimed at increasing the lift/drag ratio, assuming constraints on the lift and on the stress. Martins et al. [**58**], [**59**], [**60**], [**18**], used a continuous adjoint formulation for the Euler flow problem and a discrete formulation for the adjoint structural problem and for the coupling terms. The test case was the optimization of the range of a supersonic business jet at constant lift and assuming constraints on the element stresses, expressed through a functional (lumping functional) of the stress distribution, instead that constraining the stress element by element. Design variables were in both cases shape parameters and thickness parameters for the structure. The necessity of using a functional to lump the element stress constraints can be explained by the fact that an adjoint formulation is much more efficient than the global sensitivity approach in the case that the number of constraints (for each of which an adjoint problem must be solved) is smaller than the number of design variables. Adjoint based optimizations are thus efficient in the case of few constraints and several hundreds of design variables, while the global sensitivity approach make it possible to handle hundreds of constraints but only few (e. g. several tens) of design variables.

2.4 Aim of the work

This work is aimed at the development and implementation of a completely continuous coupled adjoint formulation for the evaluation of sensitivities in presence of static aeroelastic interaction and to its testing on cases relevant to aircraft design, like drag reduction at constant lift and angle of attack, and range increase by means of the Breguet formula, assuming a stress penalty for the structural weight, and again constant lift and angle of attack. To offer a justification for the development of such an approach a comparative study of optimization schemes and strategies has been performed, showing the necessity of a high number of design variables to maximize the effectiveness of the optimization, as well as the necessity of accurate sensitivities that contain the effects of aeroelasticity. The implementation is based on the block structured flow solver for the Euler and Navier-Stokes equations FLOWer, which has

been developed within the MEGAFLOW project [**61**], and on the finite element structural solver MSC-NASTRAN [**62**]. During the development of this work preliminary results have been presented as proceedings in the papers [**63**],[**64**],[**65**] and [**66**].

2.4.1 CFD model

All optimization schemes and strategies have been tested using the AMP wing model [**67**], with a value of 2.83° for the angle of attack and at Mach 0.78. With these parameters, the flow presents a strong normal shock on the upper surface of the wing. To make use of the FLOWer single-disciplinary adjoint feature, the flow has been assumed inviscid, governed by the Euler equation; although, given a Navier-Stokes adjoint option in FLOWer, an extension of the method to the viscous case should not present any difficulties. The CFD domain has been discretized through a two block structured mesh with a total number of 280000 nodes, generated with the DLR software MEGACADS [**68**].

2.4.2 CSM model

The wing structure, assumed linearly elastic, has been modelled using 126 nodes, all lying on the wing surface, connected by 422 tria/quad shell and 198 beam elements, as shown in Figure 2. Such model, unlike its fluid counterpart, does not represent the state of the art, but is sufficient to demonstrate the features of the method. Moreover, since realistic CSM wing models can have thousands of nodes, it is common procedure to extract a simplified model with the same properties of bending and torsional stiffness, the so-called stick models [**69**], which can be more easily used in aero-elastic analysis. In order to make clear the effect of aero elasticity, the thickness of the bar elements of the wing has been tuned in order to reach a deflection at wing tip of about 10% of the wing span. Such deflection is large enough to model a realistic cruise flight condition, but also small enough to allow using a pseudo-elastic mesh movement algorithm to deform the mesh, which cannot be done in case of large deformations.

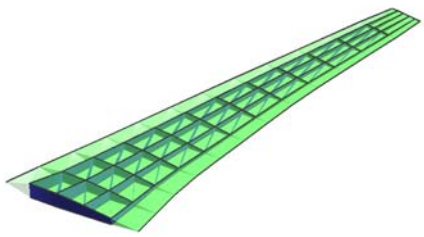

Figure 2. AMP wing structural model.

2.4.3 Comparison of optimization schemes

With *optimizations schemes* different ways of combining coupling information during the optimization are indicated. The inclusion of the aeroelastic coupling effect into the state and sensitivities evaluation gives rise to the *multidisciplinary feasible* (MDF) approach, where no approximations are made. In all other cases, we talk of low fidelity optimization, not referring to the flow model, but to the use of approximations in the coupling. All test cases are based on the previously described CFD and CSM models. In the preliminary study, a comparison is

made between the performance of low fidelity optimizations and MDF optimization, with the same shape parametrization and strategy. The strategy used is the method of feasible direction, while the parameterisations are typically obtained by bumping functions or with the free-form deformation method. In the second part of this work, a study is performed to select the most effective shape parametrization, and the use of the method of feasible direction is compared with the simpler projection strategy.

Finally, the MDF sensitivities are applied to optimizations with a purely aerodynamical cost function (drag) and with multidisciplinary cost function (a range-like expression), both with constant lift.

2.4.3.1 Low fidelity optimization schemes

The adjoint approach allows obtaining the sensitivities of cost function and constraints efficiently in the case of large number of design variables. In the case of a single discipline (aerodynamics), the optimization follows the scheme:

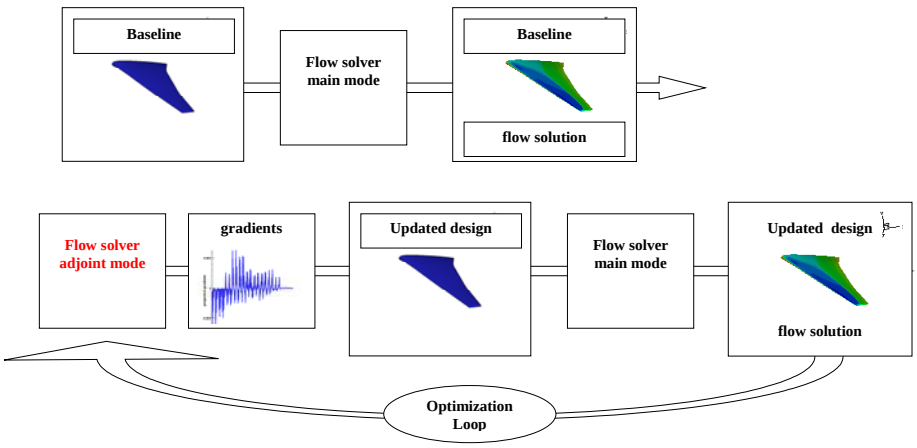

After the solution of the flow equations (Flow solver main mode), a solution of the adjoint flow equations is calculated (Flow solver adjoint mode) from which the sensitivities can be derived (gradients). These are used by the optimizer to update the design (Updated design). On the updated configuration a new flow calculation is performed and, if requested by the optimizer, a new adjoint flow and sensitivity evaluation. The sequence of gradients evaluations, design updates and state evaluations gives the optimization history.

Since in a modern commercial airplane the aeroelastic deflection can alter the shape of the wing, affecting the value of quantities like drag and lift up to 20% with respect to the undeflected shape, this effect must be taken into account in some way during the design of the wing. The simplest method consists in performing an initial multidisciplinary analysis to evaluate the effect of the elastic deflection, and then to assume that loads, and thus deflections, are constant for design changes made during the optimization. This assumption has been tested in the present work by implementing the following optimization scheme:

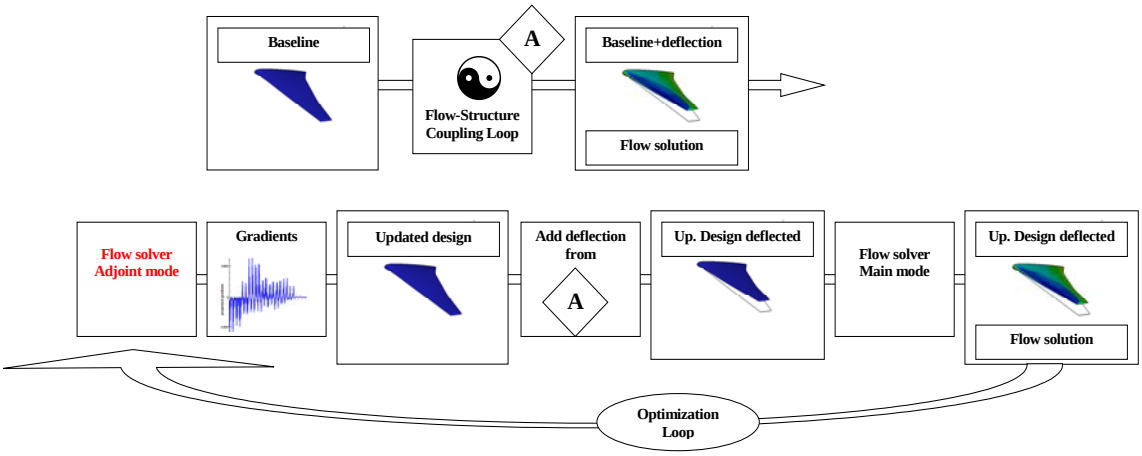

First, we observe that the presence of the aeroelastic coupling loop forces us to distinguish between the shape of the wing before and after the aeroelastic deflection. Design updates are performed on the first one, while aerodynamic values like drag and lift are read on the second one. As shown in the scheme, we first perform a coupling loop (stage A) that gives a deflected geometry and a flow solution, and we store the value of the deflection for future use. From the deflected geometry and flow solution a singlediscipli-nary adjoint solution is evaluated, which gives singlediscipliinary sensitivities. These are used to update the design. Now the effect of coupling must be taken into account. This is done by assuming a constant deflec-tion (evaluated in the initial analysis at stage A). On the thus obtained geometry, a new flow solution, and eventually adjoint solution, are evaluated. The value of deflection calculated at stage A is used in all the state and sensitivities evaluations occurring during the optimization.

An optimization aimed at reducing drag at constant lift and angle of attack has been per-formed following this scheme. To test the consistency of the scheme, after the optimization the optimized wing was brought to an aeroelastic stationary state, by applying a flow-structure coupling loop. This caused a variation in the lift value of about 7%, bringing the wing into an off-design condition from which it can be difficult to recover.

A more sophisticated approach consists in performing a multidisciplinary analysis each time the design is altered, but keeping the sensitivities singlediscipliinary. This method is referred to as 0-th order coupling [**47**]. Since the sensitivities are assumed to be singlediscipliinary, they can still be computed with the singlediscipliinary adjoint method, according to the scheme:

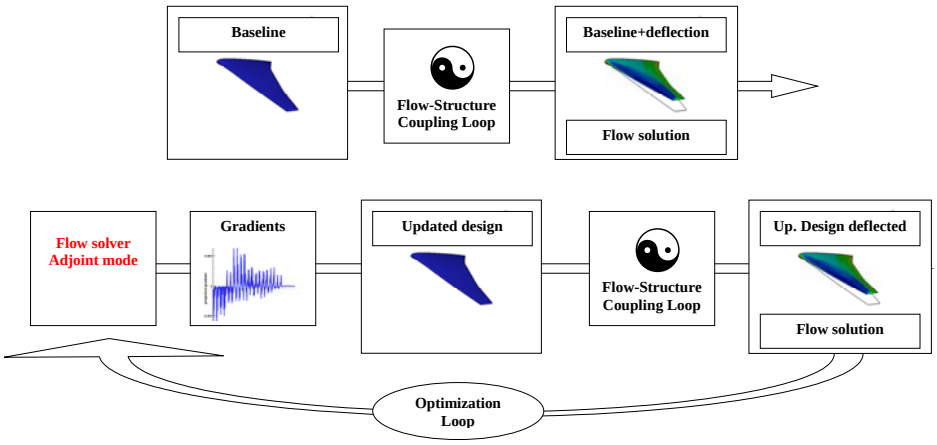

In this scheme, we introduce a consistent aeroelastic analysis. This means that for each design updating, a new coupling loop is performed and a new stationary state (characterized by a new deflection value) is calculated.

Nevertheless, the lack of information about the aeroelastic effect in the sensitivities translates into a low gradient accuracy, which caused for this test case a 60% decrease in effectiveness of the optimization, defined as the amount or drag decrease obtained. This is due to the fact that the optimizer tries to keep the constraint (in this case the lift) constant on the base of inaccurate gradient information, and this causes a reduction of the step in the feasible direction.

2.4.3.2 High fidelity optimization scheme using coupled adjoint approach

To coherently extend the adjoint approach to the coupled case requires the solution of a direct coupling loop to get the aeroelastic stationary state followed by the solution of an adjoint coupling loop to obtain two adjoint fields, which are used to evaluate the sensitivities. The overall optimization scheme takes the form

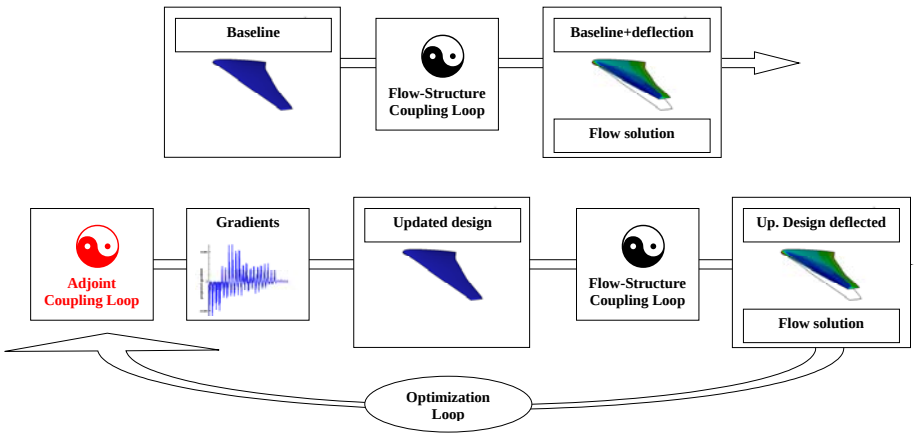

According to the scheme, a design updating is applied to the undeflected shape. The execution of the aeroelastic coupling (flow-structure coupling loop) gives then the associated deflection and flow solution, which constitute the stationary state. On the basis of these, an adjoint coupling loop is performed and sensitivities evaluated. In the adjoint loop, the flow adjoint equation is coupled to the structural adjoint equation through the boundary conditions. As result, after convergence of the system, the adjoint flow field contains information about the effect of elasticity, and the sensitivities are accurate.

On a typical optimization involving about 100 state evaluations and 15 sensitivities evaluations, this scheme allows an increase in CPU time-efficiency of about 1800 % with respect to the same optimization performed with finite difference sensitivity evaluation. The relatively high CPU time-efficiency of the adjoint method thus allowed testing different strategies and shape parameterisations, as described in the following section.

2.4.4 Comparison of different optimization strategies and shape parameterisations

Various gradient-based optimization strategies in conjunction with two different shape parameterisations have been applied to the problem of drag reduction at constant lift. Firstly, a pure sequence of line searches in the feasible direction has been performed, to get an idea of the behaviour of the cost function (drag) and of the constraint (lift). The wavy behaviour of the lift indicates the necessity of using an optimizer to assure the constancy of the constraint. A commercial implementation of the method of modified feasible direction has thus been chosen. Secondly, the effect on the optimization of two different shape parameterisations, a bumping based on Bernstein polynomials constrained to be zero on the leading and trailing edges, and a unconstrained free-form-deformation method has been evaluated. The comparison indicated, given a fixed number of 120 design variables, a net superiority of the unconstrained free-form-deformation with respect to the bumping. Thirdly, the number of design parameters, in this case the control points of the free-form-deformation algorithm, has been increased from 120 to 240, causing a superlinear increase in the effectiveness of the optimization (drag decrease). This shows the necessity of using a high number of design variables. Applying all these improvements, an optimization has been performed leading to a 26 % drag

decrease with constant lift, both evaluated at an aeroelastic stationary state. The value of drag decrease, associated with a smearing of the shock, is consistent with similar results obtained using singledisciplinary adjoint-based optimization for rigid wings in a transonic regime [**11**], [**70**].

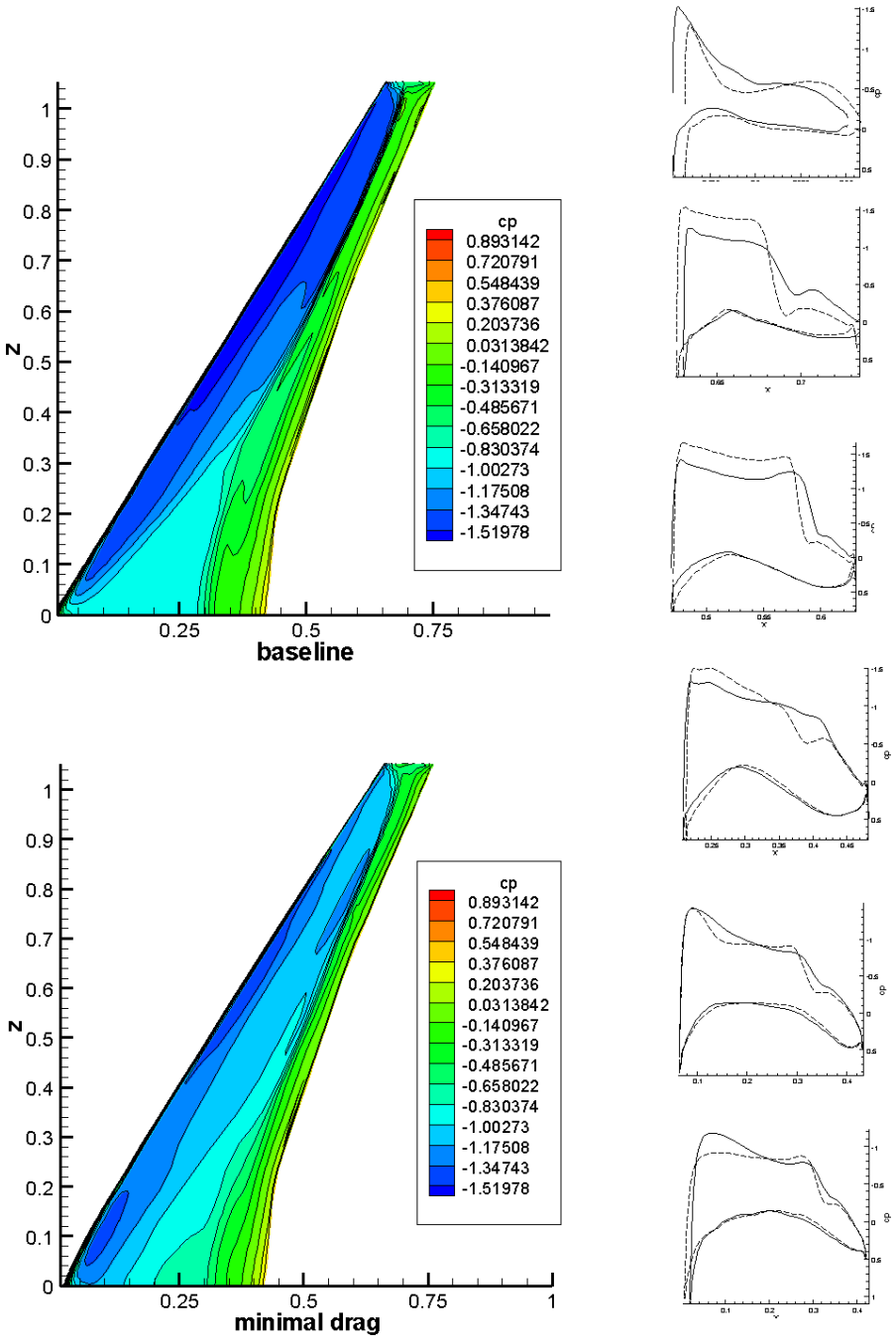

Figure 3. Pressure distribution for the baseline (dashed line) and for the minimal drag optimized design (cont. line). The pressure profiles are from six spanwise equally spaced stations (root station at bottom).

2.4.5 Application to multidisciplinary cost function

The outcome of the previous study leads to the definition of a methodology for shape optimization that allows a successful drag reduction at constant lift and angle of attack for the chosen test case. The successive and final step has been to apply the same combination of strategy, shape parametrization and number of design parameters to the optimization of an aircraft range-like cost function, expressed by the Breguet formula, with a weight penalty factor linked to the bending stress of the structural elements. As discussed before, in this case the multidisciplinarity is not only "hidden" in the sensitivities but also "explicit" since the cost function contains a term that is directly dependent on structural displacements. The trade-off between low drag and low stress instances causes the optimal design point to be different from the pure minimal drag optimal design. The difference can be appreciated in the spanwise lift distribution (Figure 4), showing a more triangular shape (associated with 7% stress reduction for the most stressed structural element), and in the pressure distribution (Figure 5) that shows a slight increase in the shock in the inboard station of the wing (associated with 4% drag increase). The so-obtained design showed an increase of 7% in range with respect to the minimal drag design. The magnitude of the stress decrease (and consequently of the drag increase) can be changed by altering the parameters of the stress penalty in the expression for the weight that enters the Breguet range formula.

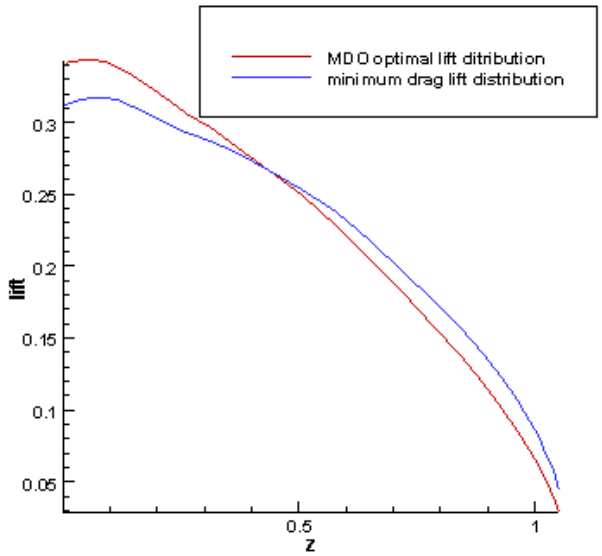

Figure 4. Spanwise lift distribution for the minimal drag and optimal range configurations. The optimal range design presents 7% stress reduction on the most stressed element and 4% drag penalty with respect to the minimal drag design.

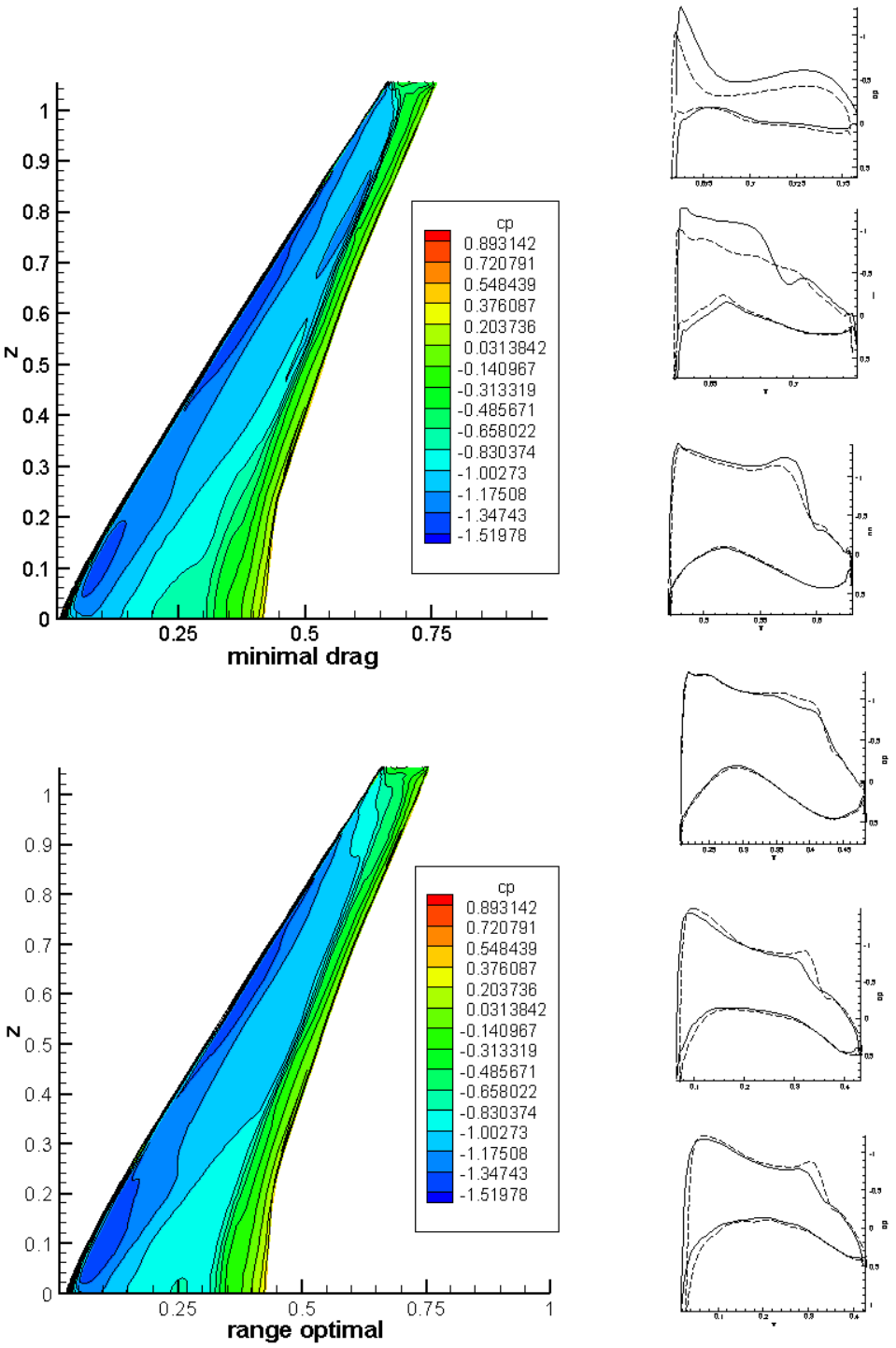

Figure 5. Optimal pressure distribution for the purely aerodynamical (minimal drag – cont. line) and for the multidisciplinary (range optimal – dashed line) optimizations. The pressure profiles are from six spanwise equally spaced stations (wing root station at bottom).

2.5 Structure of the work

The exposition is structured in the following way:

In Chapter 3 the established formalism and implementation of a continuous singlediscipliniary adjoint method for the case of inviscid flow is described, as basis for the extension to the coupled case. The sensitivities are validated by comparison with finite-differences.

In Chapter 4 the aeroelastic coupling is introduced and the solution procedure for the stationary state defined. The so obtained aeroelastic coupling loop is used in conjunction with singlediscipliniary optimization procedures, but without introducing the effect of elasticity in the sensitivity evaluation. A comparison with the outcome of an optimization based on exact sensitivities shows the necessity of embodying the effect of elasticity in the sensitivity evaluation. This instance, together with the need for a high number of design variables, motivates the formulation and implementation of a coupled adjoint method.

In Chapter 5 the continuous adjoint formalism for a general coupled system is defined, and particularized in the case of coupling between inviscid flow and linearly elastic structure. The implementation of the adjoint coupling loop is described and the so obtained sensitivities are validated against finite-differences.

Chapter 6 describes the application of the adjoint coupled sensitivities to drag minimization at constant lift. A preliminary study shows the necessity of using an optimizer based on the method of feasible direction to assure constant lift. Subsequently, combinations of different shape parameterisations and number of design variables are compared to maximize the effectiveness of the optimization. The best combination is then applied to the optimization of the range, as expressed by the Breguet formula with a stress penalty for the weight, at constant lift. A comparison between the range-optimal and the drag-optimal configurations is performed.

3 Singlediciplinary adjoint-based optimization

In this section, the adjoint equations for a single discipline are established and formulated for the case of an inviscid compressible flow. The accuracy of the adjoint sensitivities, obtained with two different formulas, is then evaluated for the 3D transonic test case by comparison with finite differencing. The matter of this section is mainly a recasting of the established formalism as exposed in [**74**], which is reported here as requirement for the further extension to the coupled adjoint case.

3.1 Formulation of the adjoint equations for the inviscid flow

Let $a \in \mathbb{R}$ be a design variable that describes the wing's shape *S(a)* and determines the associated fluid flow $\omega(a)$, ω is the vector field of state variables belonging to some normed space O, and assumed to be the solution of the governing equations of fluid flow

$$\mathbf{R}\left(a, \omega(a)\right) = 0 . \tag{16}$$

$\mathbf{R}\left(a, \omega(a)\right)$ is thus a map from $\mathbb{R} \times O \to \mathbb{R}$. If the shape geometry is now perturbed from $S(a)$ to $S(a + \Delta a)$, it holds that

$$\mathbf{R}\left(a + \Delta a, \omega(a + \Delta a)\right) = 0 . \tag{17}$$

This equation links the variation of ω to the variation of *a*, thus we can define

$$\Delta_a \omega = \omega(a + \Delta a) - \omega(a) . \tag{18}$$

If we assume the map $\mathbf{R}\left(a, \omega(a)\right)$ to be Fréchet differentiable [**71**] with respect to ω, it is possible to expand Eq. (17) in a Taylor series at the point $(a, \omega(a))$ and subtracting $\mathbf{R}\left(a, \omega(a)\right)$ on both sides, one ends up with

$$\Delta_a \mathbf{R} = \mathbf{R}(a + \Delta a, \omega(a) + \Delta_a \omega) - \mathbf{R}(a, \omega(a)) = \frac{\partial \mathbf{R}}{\partial a} \Delta a + \left(D_\omega \mathbf{R}\right) \Delta_a \omega + O\left(\left\|\Delta a\right\|^2\right) = 0 , \tag{19}$$

where $D_\omega \mathbf{R}(\omega)$ is the Fréchet derivative of $\mathbf{R}$ with respect to ω. Taking the limit of Eq. (19) as the finite increment Δa goes to zero defines the total derivative of $\mathbf{R}$ with respect to *a*.

$$\frac{d\mathbf{R}}{da} \equiv \lim_{\Delta a \to 0} \frac{\Delta_a \mathbf{R}}{\Delta a} = \frac{\partial \mathbf{R}}{\partial a} + \left(D_\omega \mathbf{R}\right) \frac{\partial \omega}{\partial a} . \tag{20}$$

Let now $F(a, \omega)$ denote the cost function of the optimization problem. Such function is typically a functional of the form

$$F(a,\omega) = \int_{\Omega} f(a,\omega) d\Omega . \tag{21}$$

For a gradient-based optimization procedure, we have to determine the total derivative (also referred as sensitivity) of F with respect to a as

$$\frac{dF}{da} = \frac{\partial F}{\partial a} + \int_{\Omega} \frac{\delta F}{\delta \omega} \frac{\partial \omega(a)}{\partial a} d\Omega . \tag{22}$$

$\frac{\delta F}{\delta \omega}$ is the variational derivative of the functional F, which in standard variational calculus takes the form [**72**]

$$\frac{\delta F}{\delta \omega} = \frac{\partial f}{\partial \omega} - \frac{\partial}{\partial t}\left(\frac{\partial f}{\partial \omega'} \right). \tag{23}$$

In the case that f has no dependence from the time t and from the time derivative of ω, indicated as ω', Eq. (23) yields

$$\frac{\delta F}{\delta \omega} = \frac{\partial f}{\partial \omega}, \tag{24}$$

and finally Eq. (22) reduces to

$$\frac{dF}{da} = \frac{\partial F}{\partial a} + \int_{\Omega} \frac{\partial f}{\partial \omega} \frac{\partial \omega(a)}{\partial a} d\Omega . \tag{25}$$

The first term of this expression contains the direct effect of the geometry perturbation (due to the variation of the normal vectors to the surface) on the cost function F, while the second embodies the indirect effect, mediated by the alteration of the flow field ω. In order to determine the sensitivity of the cost function with the method of finite-differences, using

$$\frac{dF}{da} = \lim_{\Delta a \to 0} \frac{F\left(a + \Delta a, \omega + \Delta_a \omega\right) - F\left(a, \omega\right)}{\Delta a}, \tag{26}$$

one has to solve Eq. (16) once and Eq. (17) n times for n design parameters. The computational cost is thus proportional to the number of design variables. Alternatively, if we add now Eq. (20), multiplied by an arbitrary Lagrangian multiplier function μ, to Eq. (25), we get:

$$\frac{dF}{da} = \frac{\partial F}{\partial a} + \int_{\Omega} \frac{\partial f}{\partial \omega} \frac{\partial \omega}{\partial a} d\Omega + \int_{\Omega} \mu^T \left(\frac{\partial \mathbf{R}}{\partial a} + \left(D_{\omega} \mathbf{R} \right) \frac{\partial \omega}{\partial a} \right) d\Omega , \tag{27}$$

which can be reordered as

$$\frac{dF}{da}=\left(\frac{\partial F}{\partial a}+\int_{\Omega}\mu^{T}\frac{\partial \mathbf{R}}{\partial a}d\Omega\right)+\int_{\Omega}\left(\frac{\partial f}{\partial \omega}+\mu^{T}\left(D_{\omega}\mathbf{R}\right)\right)\frac{\partial \omega}{\partial a}d\Omega\,. \tag{28}$$

Of the expression above, we are interested in cancelling the terms that multiply the field $\frac{\partial \omega}{\partial a}$, since its evaluation requires a new flow solution. This can be achieved if μ is assumed to be identical with ψ, the solution of the adjoint equations

$$\frac{\partial f}{\partial \omega}+\psi^{T}\left(D_{\omega}\mathbf{R}\right)=0\,. \tag{29}$$

The vector ψ is called the *adjoint* to ω and finally we have

$$\frac{dF}{da}=\frac{\partial F}{\partial a}+\int_{\Omega}\psi^{T}\frac{\partial \mathbf{R}}{\partial a}d\Omega\,. \tag{30}$$

In order to evaluate the adjoint sensitivity, we have to solve Eq. (16) once, and the adjoint Eq. (29) once, operations that are independent of the number of design variables, and finally we have to evaluate Eq. (30) for every design parameter *a*, which requires calculations much less expensive than a flow solution. As a result, we get the sensitivity at a computational cost that is almost independent of the number of design variables.

3.2 Discretization and solution of the primal problem

By neglecting viscous effects, the transonic flow over a wing is described by the Euler equation that can be written as

$$\frac{\partial \omega}{\partial t}+\frac{\partial \mathbf{f}_{i}}{\partial x_{i}}=0\,, \tag{31}$$

where the velocity must fulfil $n_i u_i = 0$ on the wing surface $S = S(a)$, and

$$\omega=\begin{pmatrix}\rho\\ \rho u_1\\ \rho u_2\\ \rho u_3\\ \rho E\end{pmatrix},\mathbf{f}_{i}=\begin{pmatrix}\rho u_i\\ \rho u_i u_1+P\delta_{i1}\\ \rho u_i u_2+P\delta_{i2}\\ \rho u_i u_3+P\delta_{i3}\\ \rho u_i H\end{pmatrix}. \tag{32}$$

Where ρ, u_i, E, H, P are the density, the velocity components in a Cartesian reference frame, the energy, the enthalpy and the pressure of the flow respectively, and δ_{ij} is the Kronecker´s delta. In the far field, free stream conditions are assumed. For a perfect gas the pressure is equal to

$$P = (\gamma - 1)\rho(E - \frac{1}{2}\sum_i (u_i^2)), \tag{33}$$

where γ is the ratio of specific heats. The enthalpy H is defined as $H = E + P/\rho$. The aerodynamic quantities of interest for the flow past a wing are the drag, lift and pitching moment coefficients, defined as:

$$C_D = \frac{1}{S}\int_S C_P(n_1 \cos\alpha + n_2 \sin\alpha)dS, \tag{34}$$

$$C_L = \frac{1}{S}\int_S C_P(-n_1 \sin\alpha + n_2 \cos\alpha)dS, \tag{35}$$

$$C_M = \frac{1}{S^2}\int_S C_P(n_2(x_1 - x_{1m}) - n_1(x_2 - x_{2m}))dS. \tag{36}$$

where x_{1m} and x_{2m} are the coordinates of the moment reference axis, S is the wing surface area and C_P is defined by

$$C_P = \frac{2(P - P_\infty)}{\gamma M_\infty^2 P_\infty}, \tag{37}$$

where M_∞ and P_∞ the Mach number and the pressure at the far field. To solve Eq. (31), the flow solver FLOWer has been developed at the DLR and is intensively used by the DLR itself, the German aircraft industry and universities. FLOWer is a block structured parallel solver for the Euler and Navier-Stokes equations. It makes use of a cell-centered finite volume scheme with a blend of artificial dissipation of 1st and 3rd order following the scheme of Jameson, Schmidt and Turkel [**73**] to damp high frequency oscillations and obtain convergence. The finite volume scheme is the most suited to capture shocks in the flow. According to this scheme, Eq. (31) is integrated within a control volume Ω_{ijk}, belonging to some partitioning of Ω following a structured grid along the body fitted directions *ijk*, such that $\Omega = \bigcup_{ijk} \Omega_{ijk}$,

$$\frac{\partial}{\partial t}\int_{\Omega_{ijk}} \omega d\Omega = -\int_{\Omega_{ijk}} (\frac{\partial \mathbf{f}_i}{\partial x_i})d\Omega. \tag{38}$$

By applying the Gauss divergence theorem, the volume integral on the r.h.s. of Eq. (38) is turned into a sum of fluxes across the cell boundaries

$$\frac{\partial}{\partial t}\int_{\Omega_{ijk}} \omega d\Omega = -\sum_e \int_{S_e} \mathbf{f}_i \, dS_i \,, \tag{39}$$

where the index e spans the six faces of the ijk cell and $d\vec{S} = \hat{n}dS$ is the oriented surface differential. We define the volume average of the flow ω in the cell ijk as

$$\omega_{ijk} = \frac{1}{h_{ijk}} \int_{\Omega_{ijk}} \omega d\Omega_{ijk} \,, \tag{40}$$

where h_{ijk} is the volume of the cell. In the evaluation of the r. h. s. of Eq. (39), the flux $\mathbf{f}_i(\omega)$ at the boundary face S_e of the ijk-cell, the value of ω is approximated using the average of the values of ω_{ijk} at the centers of the cell facing the surface S_e. The r. h. s. of Eq. (39), once evaluated the sum over the Cartesian index i and over the cell face index e, give rise to a 5 dimensional quantity associated with each cell, named the residual flux $\mathbf{R}_{ijk}$, that is dependent on the values of ω_{ijk} in the near cells. It holds:

$$h_{ijk}\frac{\partial \omega_{ijk}}{\partial t} = -\mathbf{R}_{ijk} \,. \tag{41}$$

Since a central averaging of ω_{ijk} is used, the finite volume discretization is on a uniform Cartesian grid equivalent to a second order central difference scheme stabilized by artificial dissipation terms. If the grid is nonuniform, the accuracy depends on the smoothness of the grid. For sufficiently smooth grids, the accuracy is almost second-order. Convergence to steady state is improved using the multi-grid convergence acceleration technique, as well as implicit residual smoothing and local time stepping. For steady flows the unsteady Eq. (31) are integrated using a time-marching 5-stage Runge-Kutta scheme until a steady solution is reached. The calculation can be stopped according to lift convergence or averaged residual magnitude criteria.

3.3 Discretization and solution of the adjoint problem

We can assume the cost functional to be an integral of the flow field ω of the form

$$F(a,\omega) = \int_{\Omega} f(a,\omega) d\Omega \,. \tag{42}$$

If we define a system (ξ_1,ξ_2,ξ_3) of locally orthogonal body-fitted coordinates such that in such coordinates the wing surface is described by $\xi_2=0$, we can write the drag under the form (42), with

$$f(a,\omega) = \frac{1}{S}\frac{2(P-P_\infty)}{\gamma M_\infty^2 P_\infty}(n_1\cos\alpha + n_2\sin\alpha)\delta(\xi_2) \,, \tag{43}$$

Where $\vec{n}$ is the wing surface normal in Cartesian coordinates and δ is the Dirac delta function. We suppose that the fluid obeys the Euler equation already defined in Eq. (31), which in the body fitted coordinates (ξ_1,ξ_2,ξ_3) takes the form

$$\frac{\partial \mathbf{W}}{\partial t}+\frac{\partial \mathbf{F}_i}{\partial \xi_i}=0\,, \tag{44}$$

where the transformed $\mathbf{F},\mathbf{W}$ are appropriate combinations of $\mathbf{f},\omega$

$$\mathbf{W}=J\begin{pmatrix}\rho\\ \rho u_1\\ \rho u_2\\ \rho u_3\\ \rho E\end{pmatrix},\mathbf{F}_i=Q_{ij}\mathbf{f}_j=\begin{pmatrix}\rho U_i\\ \rho U_i u_1+Q_{i1}P\\ \rho U_i u_2+Q_{i2}P\\ \rho U_i u_3+Q_{i3}P\\ \rho U_i H\end{pmatrix}, \tag{45}$$

where $J=\det(B)$, $B_{ij}=\left(\frac{\partial x_i}{\partial \xi_j}\right)$, $Q=JB^{-1}$ and $U_i=Q_{ij}u_j$ are the fluid velocities in body fitted coordinates. Since the surface normal vector in body-fitted coordinates is by definition $\hat{N}=(0,1,0)$, the slip boundary condition $U_iN_i=0$ in this coordinates is simply $U_2=0$. As we have already seen in Eq. (29), the adjoint equation takes the form:

$$\frac{\partial f}{\partial \omega}+\psi^T\left(D_\omega \mathbf{R}\right)=0\,. \tag{46}$$

This equation is equivalent to the differential equation

$$\left(\frac{\partial \psi}{\partial \xi_i}\right)^T\frac{\partial \mathbf{F}_i}{\partial \omega}=0 \tag{47}$$

with the boundary conditions on the wing surface (in the case of the drag)

$$\psi_2 n_1+\psi_3 n_2+\psi_4 n_3+\frac{1}{S_{ref}\gamma M_\infty^2 P_\infty}\left(n_1\cos(\alpha)+n_2\sin(\alpha)\right)=0\,. \tag{48}$$

To show this, it is convenient to bring the differential equation for ψ, Eq. (46) back in integral form, by integrating in the flow domain Ω

$$\int_\Omega \frac{\partial f}{\partial \omega}+\psi^T\left(D_\omega \mathbf{R}\right)d\Omega=0\,. \tag{49}$$

Let's write explicitly the second term of Eq. (49) as

$$\int_{\Omega} \psi^T D_{\omega} \left(\frac{\partial \mathbf{F}_1}{\partial \xi_1} + \frac{\partial \mathbf{F}_2}{\partial \xi_2} + \frac{\partial \mathbf{F}_3}{\partial \xi_3} \right) d\Omega . \tag{50}$$

Integrating by parts with respect to (ξ_i) and dropping the far field surface term, since it is multiplied by ψ which is stated to be zero at the far field, Eq. (50) is equivalent to

$$\int_{S} \psi^T D_{\omega} \left(\mathbf{F}_1 N_1 + \mathbf{F}_2 N_2 + \mathbf{F}_3 N_3 \right) dS - \int_{\Omega} \left(\frac{\partial \psi^T}{\partial \xi_i} D_{\omega} \mathbf{F}_i \right) d\Omega . \tag{51}$$

Since the fluxes $\mathbf{F}_i$ are algebraic point wise functions of ω, the Fréchet derivative D_{ω} reduces to a partial derivative, and Eq. (51) is equivalent to

$$\int_{S} \psi^T \frac{\partial \left(\mathbf{F}_1 N_1 + \mathbf{F}_2 N_2 + \mathbf{F}_3 N_3 \right)}{\partial \omega} dS - \int_{\Omega} \left(\frac{\partial \psi^T}{\partial \xi_i} \frac{\partial \mathbf{F}_i}{\partial \omega} \right) d\Omega \tag{52}$$

Imposing the second term of Eq. (52) to be zero is equivalent to Eq. (47). Now all the surface terms in Eq. (49) have to be collected, in order to obtain the equation in integral form

$$\int_{S} \left(\psi_2 n_1 + \psi_3 n_2 + \psi_4 n_3 + \frac{1}{S_{ref} \gamma M_{\infty}^2 P_{\infty}} \left(n_1 \cos(\alpha) + n_2 \sin(\alpha) \right) \right) \frac{\partial P}{\partial \omega} dS = 0 \tag{53}$$

which is equivalent to Eq. (48). Since $U_2=0$ on the wing surface S, $\mathbf{F}_2$ is just function of P, and we can make use of the chain rule, writing

$$\frac{\partial \mathbf{F}_2}{\partial \omega} = \frac{\partial \mathbf{F}_2}{\partial P} \frac{\partial P}{\partial \omega}, \tag{54}$$

where P is the pressure. Using this property and $N_i = (0,1,0)$ the first term of Eq. (52) becomes

$$\int_{S} \psi^T \frac{\partial \left(\mathbf{F}_2 \right)}{\partial P} \frac{\partial P}{\partial \omega} dS . \tag{55}$$

Since

$$\mathbf{F}_2 = \begin{pmatrix} \rho U_2 \\ \rho U_2 u_1 + Q_{21} P \\ \rho U_2 u_2 + Q_{22} P \\ \rho U_2 u_3 + Q_{23} P \\ \rho U_2 H \end{pmatrix} = \begin{pmatrix} 0 \\ Q_{21} P \\ Q_{22} P \\ Q_{23} P \\ 0 \end{pmatrix}, \tag{56}$$

and

$$\frac{\partial \mathbf{F}_2}{\partial P} = J \begin{pmatrix} 0 \\ \frac{\partial \xi_2}{\partial x_1} \\ \frac{\partial \xi_2}{\partial x_2} \\ \frac{\partial \xi_2}{\partial x_3} \\ 0 \end{pmatrix} = \begin{pmatrix} 0 \\ n_1 \\ n_2 \\ n_3 \\ 0 \end{pmatrix}, \tag{57}$$

it follows that Eq. (55) takes the form

$$\int_S \psi^T \begin{pmatrix} 0 \\ n_1 \\ n_2 \\ n_3 \\ 0 \end{pmatrix} \frac{\partial P}{\partial \omega} dS = \int_S \left(\psi_2 n_1 + \psi_3 n_2 + \psi_4 n_3 \right) \frac{\partial P}{\partial \omega} dS \,. \tag{58}$$

By substituting Eq. (43) in the first term of Eq. (49) we get again a surface integral, which summed to the term coming from Eq. (58) gives Eq. (53), in the case of the drag. Boundary conditions for lift and pitching moment coefficients can be derived easily in the same way. The adjoint method has been implement in the DLR code FLOWer for a cell centred scheme, using the same artificial dissipation scheme as for the primal problem. Also multi grid capability has been implemented in the latest version. For more details on the derivation, the theoretical background of the adjoint Euler equations, and the implementation see [**74**]. The adjoint mode has been used to carry out a number of singlediscipliнary optimizations [**31**].

3.4 Sensitivity for a stress functional in a one-way coupling

As for purely aerodynamic functions, an adjoint formulation as described by Eq. (29) and Eq. (30) is possible for every functional of the form $F(\omega, a)$, also not analytically known, for which it is possible to evaluate separately the terms which appear in the sensitivity Eq. (22):

$$\frac{\partial F}{\partial a}, \frac{\partial F}{\partial \omega}. \tag{59}$$

As first step prior to a multi discipline feasible sensitivity formulation, one can be interested in calculating how the bending stress of an aerodynamically loaded structure varies according

to variations in shape or structural design. This approach, in conjunction with an analytical model for the structure has been used in the redesign of the Boeing 747 wing in Ref. [**45**], and is in line with the "one-way" coupling philosophy of taking into account the influence of aerodynamics on the structure, but neglecting the effect of the structure (elastic deflections) on aerodynamics. This can be considered a first approximation to the fully coupled (two-way) adjoint approach first proposed in [**18**]. In this work, a modification of the method will be proposed, based on a CSM structural model instead that on an analytical structural model. Let's suppose the cost function or constraints to be a functional of the stress distribution associated with a given geometry and flow named *G*. Since the stress distribution is a function of the flow field ω along the wing´s surface *S*, *G* can be written as

$$G(a,\omega) = \int_S g(a,\omega) dS \,. \tag{60}$$

We are interested in the sensitivity of $G(\omega, a)$, which according Eq. (30) is

$$\frac{dG}{da} = \frac{\partial G}{\partial a} + \int_\Omega \psi^T \frac{\partial \mathbf{R}}{\partial a} d\Omega, \tag{61}$$

where we have to solve the adjoint equation

$$\int_S \frac{\partial g}{\partial \omega} dS + \int_\Omega \psi^T \left(D_\omega \mathbf{R} \right) d\Omega = 0 \,. \tag{62}$$

Since we already know how to treat the second term of Eq. (62), we need only to derive the form of the boundary condition associated with the first term in Eq. (62). Now, *G* is a function of the traction (force per unit surface) applied to the structure, which depends on the pressure on the surrounding surface according to

$$\vec{T} = P\vec{n} \,, \tag{63}$$

where $\vec{n}$ is the normal to the wing surface. So *G* can be taken as functional of *P(ω)*. As in Eq. (24) it holds that $\frac{\delta G}{\delta P} = \frac{\partial g}{\partial P}$. It follows, together with the chain rule, that

$$\int_S \frac{\partial g}{\partial \omega} dS = \int_S \frac{\partial g}{\partial P} \frac{\partial P}{\partial \omega} dS = \int_S \frac{\delta G}{\delta P} \frac{\partial P}{\partial \omega} dS \,. \tag{64}$$

This equation together with Eq. (58), implies that the boundary condition for the adjoint problem of the *G* function is given by

$$n_1\psi_2 + n_2\psi_3 + n_3\psi_4 = -\frac{\delta G}{\delta P} \,. \tag{65}$$

The variational derivative on the r. h. s. of Eq. (65) can be easily evaluated with a finite difference procedure by varying the value of the discrete pressure distribution in the *ij* cell of the wing surface mesh. Such surface scalar field can be thus read in by the adjoint flow solver to enforce the boundary condition Eq. (65).

3.5 Reconstruction and validation of the sensitivities

From the adjoint formulation it follows that the sensitivity of some cost function *F* with respect to some design parameter *a* is

$$\frac{dF}{da} = \frac{\partial F}{\partial a} + \int_{\Omega} \left(\psi^T \frac{\partial \mathbf{R}}{\partial a} \right) d\Omega , \tag{66}$$

where **R** is the stationary Euler equation already defined in Eq. (31) and ψ the adjoint field. The first term is the effect of the mesh perturbation on the cost function associated with a shape variation, while keeping the flow field constant. The second term represents the volume integral of the scalar product of the adjoint field ψ and the partial derivative of the flow operator $\mathbf{R}(a,\omega(a))$ with respect to a mesh perturbation induced by a change in *a*, keeping the flow field constant. Since early implementations of adjoint methods in flow solvers, there have been some attempts to replace the volume integration that occurs in the expression Eq. (66) in the case of purely aerodynamical cost functions, with some expression containing a surface integral, such as

$$\frac{dF}{da} = \int_{S} div(\vec{\varphi} + (\omega_H{}^T \psi)\vec{u}) \cdot (n_1 \frac{\partial x_1}{\partial a} + n_2 \frac{\partial x_2}{\partial a} + n_3 \frac{\partial x_3}{\partial a}) dS \tag{67}$$

where $\omega_H = \left(\rho \quad \rho u_1 \quad \rho u_2 \quad \rho u_3 \quad \rho H \right)^T$, $\vec{\varphi}$ is defined by $F = \int_S \vec{\varphi} \cdot \hat{n} dS$ and $\frac{\partial x_i}{\partial a}$ are the surface mesh sensitivities with respect to the shape parameter *a*. The motivation for such expression is that the volume integration over the whole volume mesh in Eq. (66) is a relatively expensive operation, while the surface integration is computationally much cheaper. Such formulas have been derived by Weinerfelt [**75**] and by Jameson [**76**], or by Gauger [**74**]. Although the volume and surface formulas are analytically equivalent, the agreement with the finite-difference sensitivities at the computational level is better for the volume formula, and the discrepancy with the surface formula decreases as the mesh is refined. The differences are mainly localized in regions with high pressure gradients and high mesh curvature, such as occurs at the leading edge, or with rapid variations of the adjoint field, as occur at the stagnation point near the trailing edge.

The matter is relevant also for the implementation of a fluid-structure coupled adjoint method that is discussed later in this work. A term of the form of Eq. (66) occurs not only in the coupled adjoint sensitivity evaluation, but also in the coupled adjoint loop, and it's the most expensive operation after the flow and adjoint flow calculations, requiring *3N* mesh-deformation operations each coupling step, where *N* is the number of structural nodes. The use of faster formulations for evaluating the volume integral would highly benefit also the coupled adjoint calculation. Unfortunately, the surface integral discussed above is not accurate enough for this

purpose, and by experience it causes divergence in the fluid-structure adjoint coupling loop. Thus, the volume formulation has been adopted in this work. Recent developments show that it is possible to eliminate mesh sensitivities from the formula Eq. (66) using an appropriate auxiliary adjoint field [**77**]. The use of this method in the coupled adjoint would lead to a three-field coupled adjoint formulation probably even more computationally efficient than the two-field formulation, but at price of additional complexity in the implementation.

3.5.1 Volume formulation for the sensitivity evaluation

Once an adjoint solution has been obtained we numerically evaluate the sensitivity of F to any arbitrary parameter alteration Δa according to formula Eq. (66) via

$$dF \approx \left(\Delta_a F + \int_{\Omega} \left(\psi^T \Delta_a \mathbf{R} \right) d\Omega \right)_{\omega=\omega_0}, \tag{68}$$

where the subscript $\omega=\omega_0$ on the r. h. s. means that the finite variations $\Delta_a F$ and $\Delta_a \mathbf{R}$ are evaluated keeping the flow field fixed. We can break the volume integral into a sum of integrals over cells volumes

$$\sum_{ijk} \int_{\Omega ijk} \left(\psi_{ijk}{}^T \Delta_a \mathbf{R} \right) d\Omega . \tag{69}$$

After the discretization we can rearrange the integration as

$$\sum_{ijk} \psi_{ijk} \Delta_a \int_{\Omega ijk} \left(\mathbf{R} \right) d\Omega . \tag{70}$$

The integral in Eq. (70) is the residual flux and it's evaluated by FLOWer on every iteration step according the finite volume scheme Eq. (41). Evaluating its variation with respect to a mesh alteration is thus possible using the same routines of FLOWer and a fictitious time step on the deformed mesh, provided that the original residual field has been previously saved and can be read in. A loop over all cells indexes involving the sum of the scalar products of ψ and $\Delta\mathbf{R}$ gives the scalar value represented by Eq. (70). The effect of the geometry variation on the cost function, represented by the first term in Eq. (68), can be evaluated in similar way. The division by the step Δa gives the sensitivity.

3.5.2 Validation of the volume formulation sensitivity

The sensitivity has been evaluated based on primal and adjoint Euler solutions both converged to seven orders of magnitude in the residual, by making use of the finite volume formulation and residual fluxes implemented in the solver FLOWer and according to the surface formulation Eq. (67). As design variables the coefficients of a set of bump functions were used, that were added to the camber line of the wing. The bump functions were Bernstein polynomials in the indices *(i,j)*, spanning the surface mesh. Both results, together with a forward step finite-difference, are shown in Figure 6. As seen in similar results reported in [**76**], the volume integration is more exact with respect to the surface integration (67), showing a mean absolute deviation of 2.3 % against the 4.2 % of the surface method, with respect to the finite difference result, which, after some tuning is assumed to be the reference value for the

sensitivities. The biggest discrepancies occur at the trailing edge (points 1-5 in Figure 6) and at the leading edge (points 11-15 in Figure 6). However, the volume integration is also much more computationally expensive. The mean absolute deviation with respect to finite difference method is shown in Figure 7. Compared applications to optimizations test cases also shows that the volume integration is more robust for handling particularly the design of the trailing edge of a 3D wing, which is often linked with big values in the sensitivities.

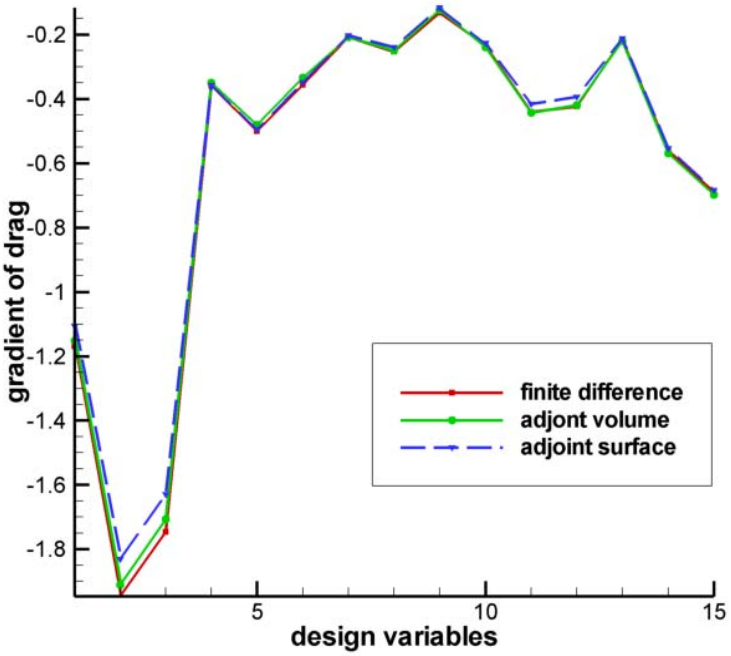

Figure 6. Sensitivity of the drag (3x5 Bernstein bump functions).

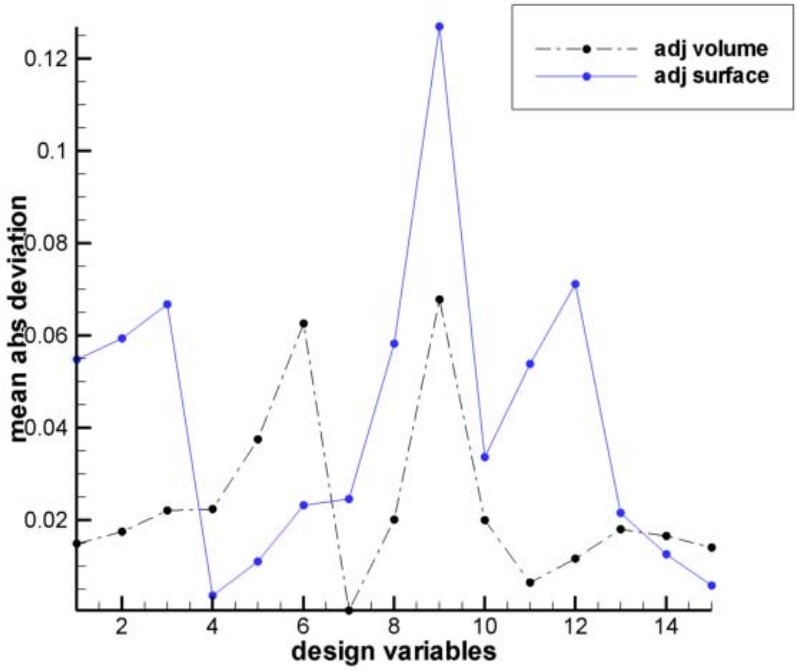

Figure 7. Mean absolute deviations of adjoint sensitivities with respect to finite differences.

3.5.3 Validation of the one-way sensitivity of the Kreisselmeier-Steinhauser functional

The validation proceeds in this case in a very similar way as before, but the cost function is evaluated from the stress distribution associated with the applied forces coming from the pressure distribution. The deflection that the structure undergoes under aerodynamic load causes a stress to arise in every element of the wing structure. Without loss of generality, we can limit our analysis only to one type of element, for example the beams, of which we consider the bending stress at one end. The beam element is a two-nodes finite element related to the classical (Euler-Bernoulli) beam theory [**78**]. It describes a linear structure that shows a bending after an applied transverse load. The bending is described by a displacement field *z(x)*, normal to the longitudinal direction *x*, $x \in [0,L]$. The application of several kinematics, constitutive and equilibrium equations lead to the equation

$$EI \frac{d^4 z(x)}{dx^4} = p$$

where p is the transverse applied force per unit length, E is Young´s modulus and I is the moment of inertia of a beam section around the neutral axis. In particular, only the stress σ_{xx} relative to the longitudinal direction x, which is related with the bending $z(x)$ is considered, and the other stress components, as well as the displacements in the other directions, are neglected. To uniquely define the function $z(x)$ over the element four boundary conditions are necessary of the form $\left(z(0), \frac{dz}{dx}(0), z(L), \frac{dz}{dx}(L) \right)$. The quantity $\frac{dz}{dx}$ is equivalent by the *normality* assumption to the rotation angle θ of the beam cross section around the neutral axis z. In a one-dimensional element, each node i is thus associated with two degree of freedom

(z_i, θ_i) describing displacement and rotation of that node. In a 3-dimensional element, we have a total of six degrees of freedom for each node. A structure wing model of N beam-connected nodes thus possesses a $6N$-dimensional Stiffness matrix. The application of the aerodynamic load to such structure causes a bending stress in each beam. The resulting stress distribution, obtained from the bending stress at one end of each element, is depicted in Figure 8.

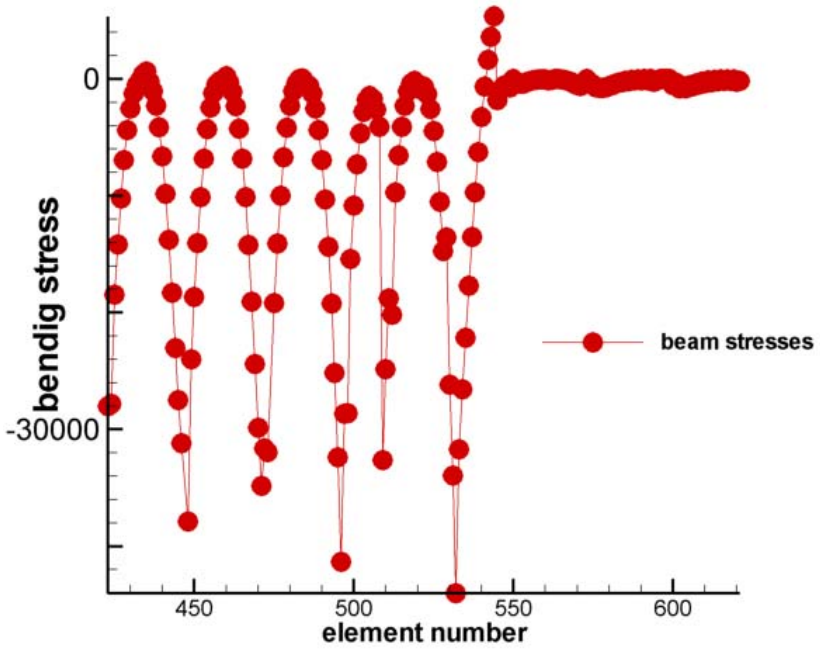

Figure 8. Bending stress distribution for beam elements.

The same distribution (apart from a sign) is shown in Figure 9.

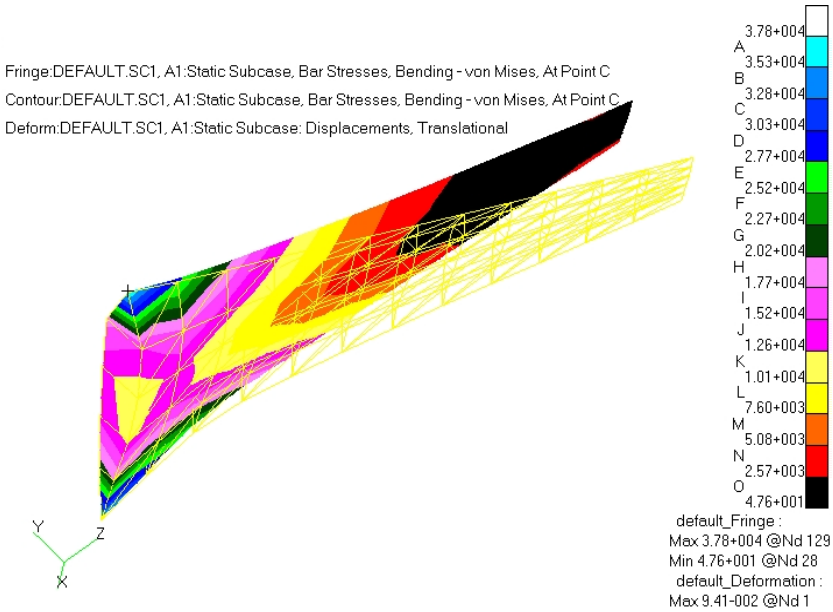

Figure 9. Bending stress and displacement distributions after Nastran calculation.

As may be seen from Figure 9, the stress varies continuously along the wing span, reaching the maximum at the wing root leading and trailing edges and it is very small (in black in the picture) after the middle station of the wing. This implies that the structural model is evidently sub-optimal, since assembled with beams of identical thickness. An internal optimizer exists in Nastran, which can size the elements according the stress, with the aim of reducing the weight of the structure. What Nastran cannot do, is to modify the pressure distribution, and thus the wing shape, in order to constrain the stress to not exceed some maximal value. This could be the task of a multidisciplinary optimization, making use of a cost functional associated to the stress distribution. Since we wish to evaluate the first variation of it, it is also advisable for this functional to be differentiable with respect to the stress of the elements. To examine the beam maximum stress, which is a combination of the absolute values of bending and axial stresses, is in this sense not a good choice and can cause wrong results in the adjoint reconstruction of the sensitivity. We thus build a functional of the distribution of the bending stress according to the formula

$$G(\sigma_n) = \frac{1}{\rho} \ln \sum_n \exp(\rho \frac{\sigma_n - \sigma_0}{\sigma_0}), \tag{71}$$

σ_0 being the maximum allowed stress and ρ a parameter. The functional is smaller than $\ln(n)/\rho$ if no element has stress bigger than σ_0, and bigger in the opposite case (all elements have stresses bigger than σ_0). Furthermore it behaves like a “magnifying glass”, showing a high sensitivity, adjustable by ρ, to variations of the stress in an interval around σ_0, and being in fact transparent if the variation of the stress involves values far below σ_0 . This functional is usually used to lump the stress constraints in structural optimization problems [**79**]. The sensitivity of it can be thus evaluated according the adjoint formulation of the problem described in Chapter 3.4. A comparison with the same sensitivity evaluated with finite forward differencing is shown in Figure 10.

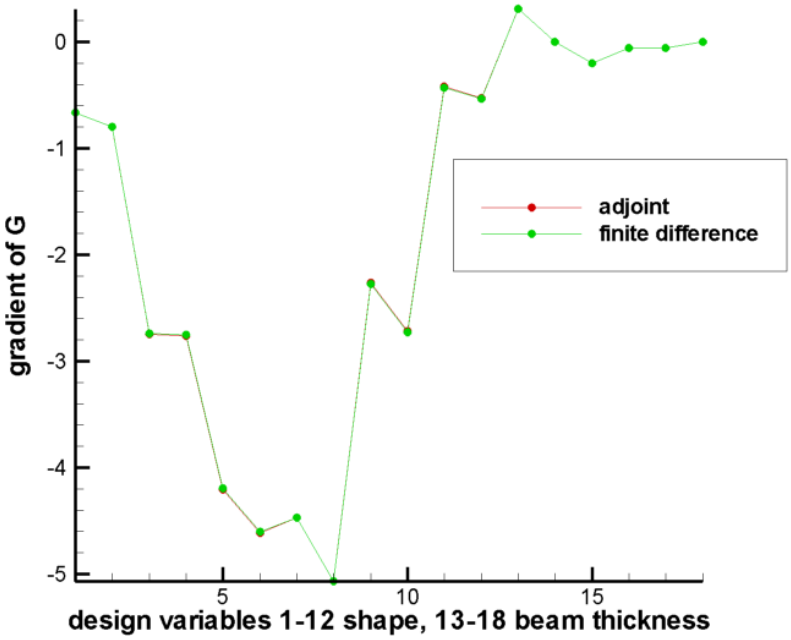

Figure 10. Sensitivity of the Kreisselmeier-Steinhauser stress function for shape alterations based on FFD and for beam thickness alterations, according finite differencing and adjoint formulation.

There is an extremely good agreement between finite-differences and adjoint, with a mean absolute deviation of about 0.4 % for the shape design variables. For the thickness design variable the deviation is identically 0 %, which is obviously due to the fact that thickness alterations does not involve, in the one-way approach, an alteration of the flow field, and thus the effect on the cost function is purely geometric. Although consistent within the “one way” approach, this sensitivity has not been used to carry out any optimization. A two-way coupling will be instead introduced in the following section.

4 Introducing aeroelasticity

The aero-elastic coupled system of interest is part of the class of problems relating to fluid-structure interaction. In these problems, the coupling between the two fields (fluid flow and structural displacement) is not in general limited to the exchange of boundary conditions. However, solution schemes based on single discipline solvers, the so-called *partioned* approaches, are preferred to the *monolithic* approaches, which require the development of dedicated discretization and solution processes. In establishing the coupling between two different solvers, care must be taken in the definition of the singlediscipline problems and boundary conditions, which are discretized and solved according to different methodologies and even different coordinate frames. In particular for fluid-structure interaction problems, the structural problem is formulated and solved in a *Lagrangian* coordinate frame, while for a fluid flow a *Eulerian* coordinate frame is used. Since the latter is usually a body-fixed coordinate system, thus possessing a motion associated with the structural displacement, the Eulerian formulation must be changed in an *Arbitrary Lagrangian Eulerian* or ALE formulation that takes into account the movement of the body. Since this movement is described by an arbitrary field, coupled by some equation with the structural displacement, this is also called the *three-field formulation* for fluid-structure interaction. If one is interested in calculating the static aero-elastic deflection of an elastic body in a fluid flow, the formulation is simplified and a weak coupling procedure can be used to calculate the stationary state. The coupling procedure gives rise to an aeroelastic coupling loop that that after a certain number of iterations between the flow and structural solver converges to the stationary, deflected wing shape. This configuration is generally characterized by values of drag and lift that are substantially different from those of the initial, undeflected geometry. The coupling loop can be thus identified with a multidisciplinary analysis procedure. The incorporation of this procedure into an optimization process can be done in a variety of different ways, the simplest of which consists in performing just one multidisciplinary analysis prior to the optimization. On the other hand, the most accurate approach presupposes the inclusion of the aeroelastic effect in the sensitivity evaluation, according to the so-called *multidisciplinary feasible* approach. In the following chapters, after describing how the aeroelastic coupling is defined and implemented, a comparison of various optimization chains that make use of multidisciplinary analysis is presented.

4.1 Definition of fluid-structure coupled system

In an arbitrary Lagrangian-Eulerian coordinate frame, the Euler equation describing a compressible inviscid flow maintains the form of Eq. (31), but in order to take into account the mesh movement, the flux vectors are corrected according to take into account the convection velocity with respect the mesh (see for example [**80**])

$$\mathbf{f}_i = \begin{pmatrix} \rho(u_i - \dot{X}_i) \\ \rho(u_i - \dot{X}_i)u_1 + P\delta_{i1} \\ \rho(u_i - \dot{X}_i)u_2 + P\delta_{i2} \\ \rho(u_i - \dot{X}_i)u_3 + P\delta_{i3} \\ \rho(u_i - \dot{X}_i)H \end{pmatrix}, \tag{72}$$

where $(\dot{X}_i)$ is the velocity of the ALE coordinate system (CFD mesh). The structure obeys some linear PDE describing linear elasticity, which can be generically written as

$$\tilde{S}(\tilde{z}, \partial_t \tilde{z}, \partial_i \tilde{z}, \partial_i \partial_j \tilde{z}, ...) = 0, \quad \text{with} \quad i, j = 1, ..., 6. \tag{73}$$

The displacement of the mesh is described by $\vec{\chi} = (X_1, X_2, X_3)$ and is coupled to the structural displacement by some pseudo-elastic PDE:

$$A(\vec{\chi}, \partial_i \vec{\chi}, \partial_i \partial_j \vec{\chi}, ..., \tilde{z}) = 0, \quad \text{with} \quad i, j = 1, ..., 6. \tag{74}$$

The system is completed by the boundary conditions

$$\vec{u}(\vec{\chi}(t)) \cdot \hat{n} = \partial_t \vec{z}(\vec{x}_0, t) \cdot \hat{n}, \text{ with } \vec{\chi}(t) = \vec{x}_0 + \vec{z}(\vec{x}_0, t), \tag{75}$$

where $\vec{u}$ is the flow velocity and $\hat{n}$ the unit normal vector to the surface. This equation describes the slip condition between the flow media and a moving solid surface. The traction balance between the two media is represented by

$$Pn_i = \Theta_{ij} n_j, \quad \text{with} \quad i, j = 1, ..., 3. \tag{76}$$

where Θ_{ij} is the stress tensor for the displacement field $\tilde{z}$, and P the pressure of the fluid. In general, solving the system given by Eq. (72), Eq. (73) and Eq. (74) plus b.c., or similar fluid structure interaction systems, by partitioned procedures, and assuring time-accuracy and convergence is a challenging task of computational science, see for example [**81**]. Since we are interested in the stationary solution of the coupled system, some simplifications are possible in the solution algorithm. Firstly, the terms in $(\dot{X}, \dot{Y}, \dot{Z})$ disappear from Eq. (72), giving back the usual Euler flow equations. The time derivative disappears also from Eq. (73) and Eq. (75) , giving in the latter the usual slip-condition. The fields ω, $\vec{\chi}$ and $\tilde{z}$ are supposed dependent on a pseudo-time stepping, and the system can be solved by a serial staggered fixed-point iterative scheme.

4.2 Discretization and solution of an aero-elastic coupled system

In order to solve the coupled equations of the fluid-structure system for the stationary state, a serial staggered partitioning as described in [**82**] and [**58**] has been implemented, where forces are transferred from the flow mesh to the structure mesh to give the nodal loads, and deflections are transferred back from the structure mesh to the flow mesh, which is consequently deformed. The equation that links the mesh movement $\vec{\chi}$ to the structural displacement field $\tilde{z}$, Eq. (74), is obtained from the stationary solution of a spring model, assuming fixed far field boundaries. The fluid flow around the body described by the Euler equation is solved by the DLR solver FLOWer, while the structural problem is solved by MSC-Nastran. The transfer of information between CFD and CSM meshes is traditionally managed using finite element interpolation techniques, as described in [**83**] or [**84**]. Here, we adopted a new method following [**85**], based on the B-spline volume interpolation assuming a linear radial basis

function. This algorithm is *conservative* and *consistent*, and has been adequately validated by comparison with tunnel testing data using the AMP wing model. Typically, 12 exchanges of information between the two codes are enough to reach a converged aero elastic solution, as shown in Figure 11. The remaining small oscillations in the residual are probably due to numerical round-off error in the calculation of forces and displacements, and can be damped using the under-relaxation technique, that is using a weighted mean of the last two displacement to evaluate the new CFD mesh, as done for example in [**86**]. However this is for our test case not strictly necessary, since the oscillation is so small that it has no effect on the value of lift and drag. In order to obtain convergence, a damping factor has been instead applied to the aerodynamic force in the first three coupling steps.

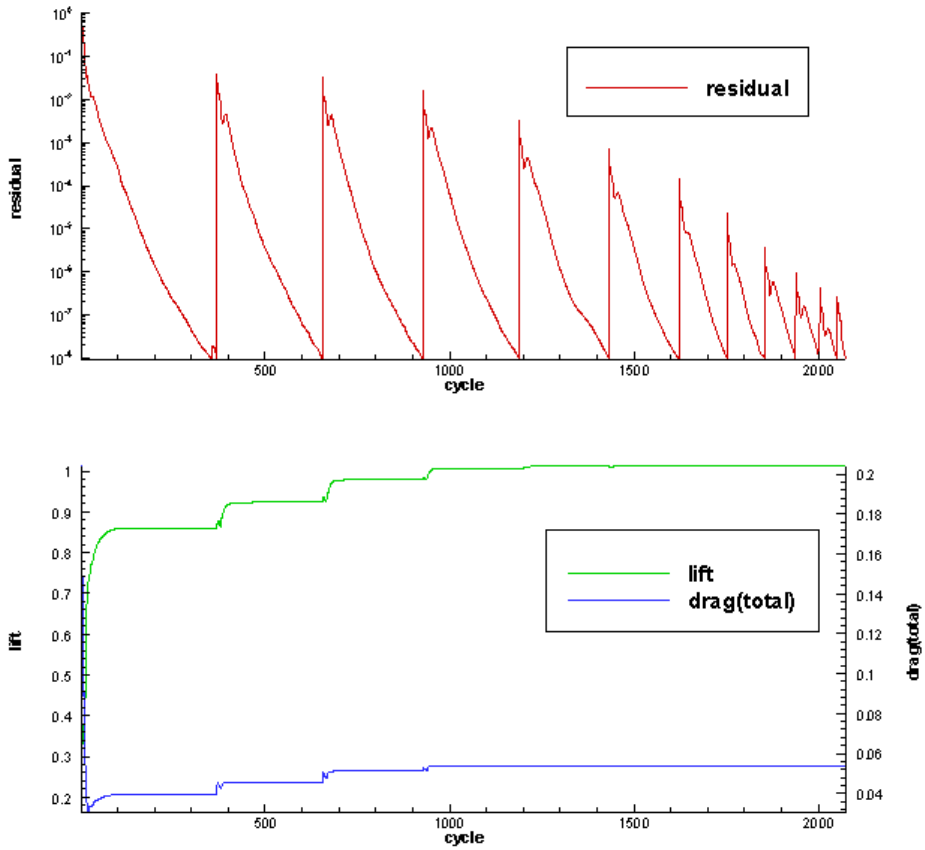

Figure 11. Plot of residual (log scale) of flow equation, lift and drag, during coupled computation. Jumps in the residual indicate exchange of information between CFD and CSM codes.

The coupling flow chart is sketched in the following scheme:

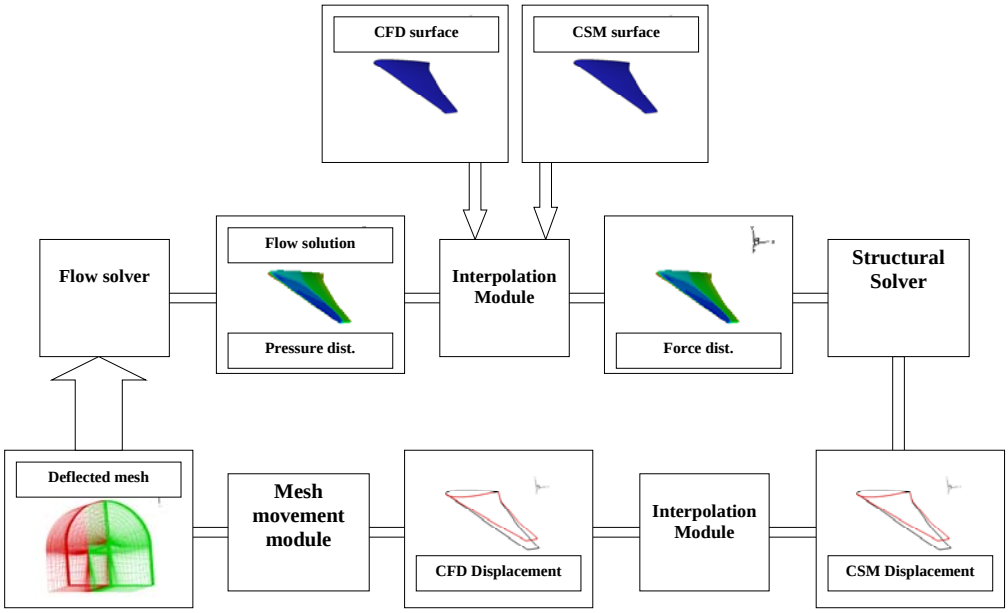

Preliminary to the loop is the generation of the two exchanging meshes for the interpolation of forces and displacements. The CFD exchanging mesh is structured and is derived from the cell center wing surface mesh read from the output of the flow solver on the initial mesh. The CSM exchanging mesh is unstructured and consists of the nodes from the structure model. After a flow solution on the initial grid, the pressure distribution is read in by the interpolation module, which creates a force distribution on the CSM nodes. The structural solver gives the associated displacement field on the CSM nodes, which is interpolated to the CFD side. The mesh movement module reads the displacement field on the CFD surface and extrapolates it to the whole CFD mesh. On the so obtained deformed mesh a new flow calculation is started.

4.3 Need for accurate sensitivity

The fluid-structure coupling loop defined in the preceding Chapter can be inserted into an optimization chain in different ways. If the aeroelastic effect is taken into account in the sensitivity evaluation, we have complete consistency and the method is called *multidisciplinary feasible*. An evaluation of such a sensitivity by means of finite-differences follows the scheme, for the case of the drag:

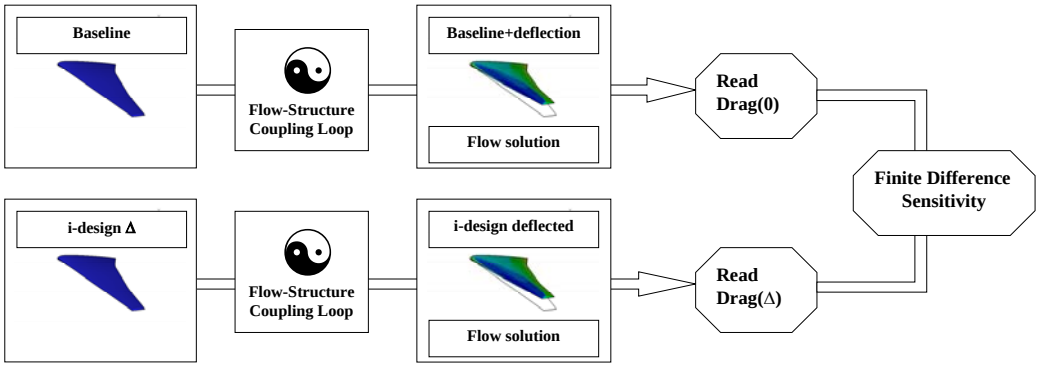

A coupling loop started from the baseline geometry evaluates the stationary deflected state that gives the reference value for the drag. The geometry is then altered by increasing the i-th design variable by a finite (small) amount Δ. The fluid structure coupling loop evaluates the new stationary state and the new value of the drag is obtained. The difference, divided by the finite step Δ, gives the value of the sensitivity of the drag with respect the i-th design parameter. The procedure is thus repeated for each design parameter.

This procedure is extremely expensive, since a fluid structure coupling loop is about 6-times more expensive than a flow solution, and it must be repeated for every design parameter. A less accurate approach can be investigated to avoid this expensive procedure. The simplest method consists of performing one multidisciplinary analysis prior to the optimization, and then assuming that the so calculated deflection is constant during the optimization, according the scheme:

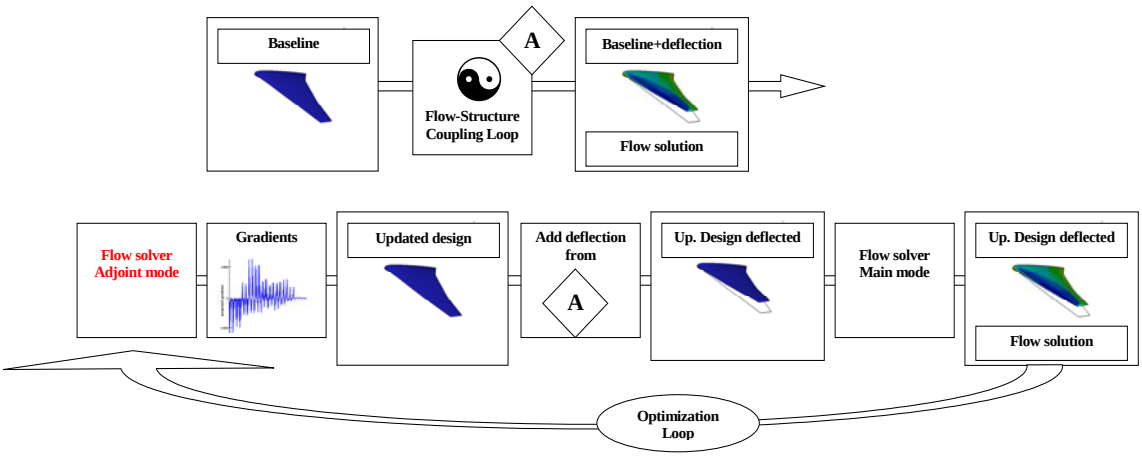

To preserve high computational efficiency, this scheme makes use of the adjoint method to evaluate the sensitivities (gradients) of drag and lift with respect to the shape parameters. The design obtained with this kind of process is optimal from a single disciplinary viewpoint, thus only for the deflection calculated in the previous analysis. Since the design has been altered during the optimization, it is not assured that such a deflection is still physically motivated. In fact, a new application of the flow structure coupling loop to the optimal design gives a different value of the deflection, which in turn causes different values of drag and lift. The out-

come of the optimization and of the subsequent recoupling is summarized in Figure 12. The optimization was aimed at drag reduction at constant lift and angle of attack, by means of the method of feasible direction (the choice of this strategy will be better motivated later on).

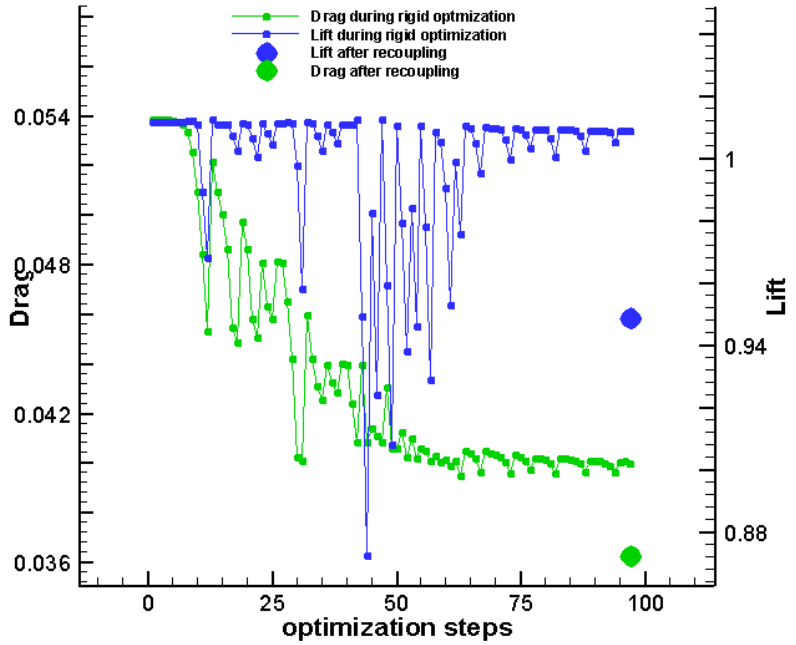

Figure 12. Values of drag and lift during the optimization history (line and spots) and after the recoupling (big spots).

The values of both drag and lift after the recoupling are substantially different from that coming from the optimization. The lift in particular, shows a decrease of about 6%, bringing the wing into an off-design condition. We conclude that to obtain a consistent set of design and deflection that characterize a stationary state, the fluid-structure coupling must be taken into account during the optimization, at every design update and not just once before the optimization. This can be realized by the following scheme:

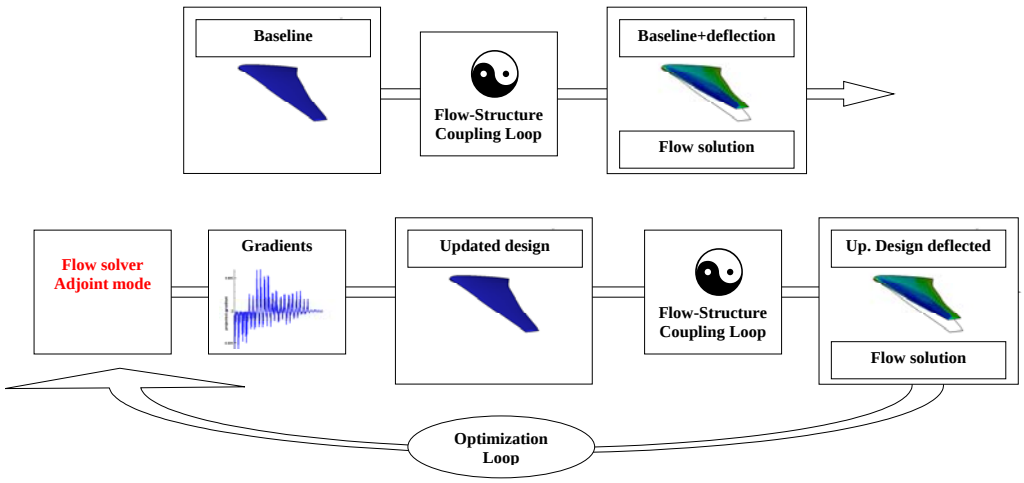

Here a complete multidisciplinary analysis is performed at every design update. The sensitivity, however, is evaluated using a singledisciplinary adjoint method. This introduces an incon-

sistency, since the sensitivity does not contain information about the effect of elastic coupling. For this reason, this method is called 0-th order coupling. The resulting optimization history is compared in Figure 13 with an optimization that uses the same strategy, but complete gradient information, according the 1st order coupling (multi discipline feasible) scheme.

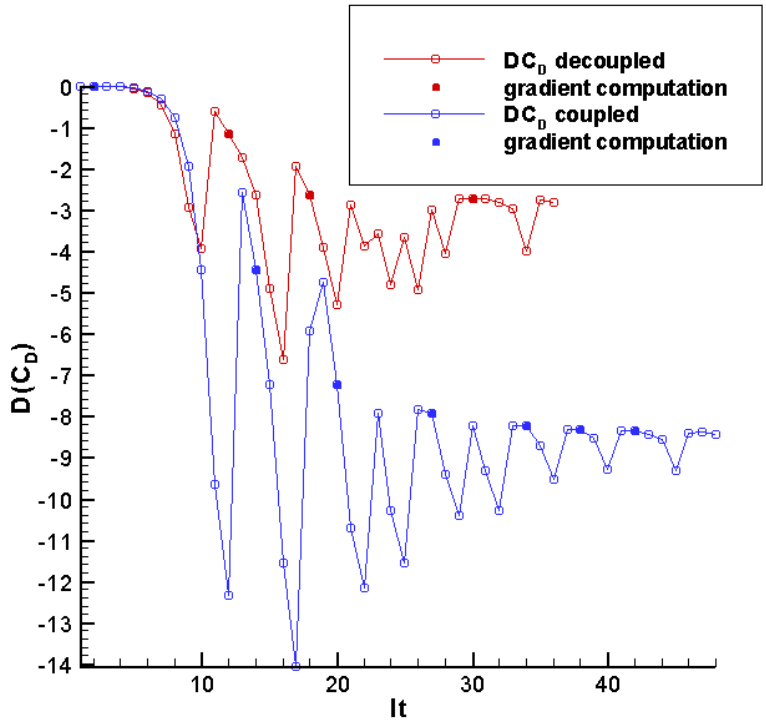

Figure 13. Drag percentage variation during optimizations performed using 0th order coupling (red) and 1st order coupling (blue). The optimization was aimed to drag reduction by constant lift and angle of attack.

Although neither of the two optimizations has been brought to complete convergence, it's evident that the lack of information in the sensitivity about the effect of elasticity reduces the effectiveness of the optimization, diminishing of about 60% the drag decrease. We conclude that to maximize the effectiveness of the optimization, a multidisciplinary feasible formulation must be used. This is in principle possible using the previous discussed finite difference scheme, or other approaches discussed in the introduction like the global sensitivity method. If a high number of design parameters are used, however, the only way to maintain the computational cost acceptable is to use an adjoint formulation. In order to obtain accurate sensitivities, which take into account the fluid structure coupling, the singlediscipline adjoint method previously discussed must be extended to a coupled aero-structure adjoint method, following the scheme:

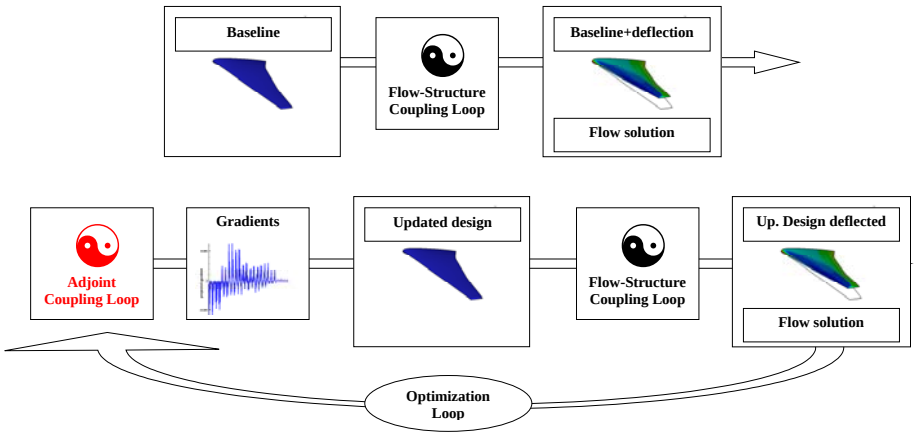

According to this method, after a fluid-structure coupling loop (direct coupling), an adjoint coupling loop is performed and two adjoint fields (one for the flow, one for the elastic displacement field) are calculated. These adjoint fields allow the evaluation of accurate sensitivities. As in the singledisciplinary case, the adjoint coupling loop has to be performed for every cost function and constraint. In the following section, a continuous adjoint formulation for the aero-elastic coupling is presented and explicitly formulated for the case of the Euler equation and linear elasticity.

5 Adjoint formulation for the aeroelastic coupled system

5.1 Formulation of the continuous adjoint equations for a coupled system

The derivation of the adjoint equations in the case of a multidisciplinary problem is similar to that which has been carried out for the purely aerodynamic case, with the difference that we will end up with a dual adjoint variable for each set of state variables of the problem. An adjoint formulation is possible for any problem involving the calculation of the sensitivity of a function of one or more sets of variables obeying one or more state equations. We will restrict ourselves to the case of two sets: one represents the flow variables, the other the structure nodal displacement. $F(a,\omega,\tilde{z})$ denotes the cost function of the optimization problem, dependent now also on the 6-dimensional displacement field $\tilde{z}$, the solution of the structural problem. Following the notation of Eq. (25), the sensitivity takes the form

$$\frac{dF}{da} = \frac{\partial F}{\partial a} + \int_{\Omega} \left(\frac{\partial f}{\partial \omega}\frac{\partial \omega}{\partial a} + \frac{\partial f}{\partial \tilde{z}}\frac{\partial \tilde{z}}{\partial a} \right) d\Omega , \tag{77}$$

or , in terms of first variations,

$$dF = \frac{\partial F}{\partial a}\delta a + \int_{\Omega} \left(\frac{\partial f}{\partial \omega}\delta_a \omega + \frac{\partial f}{\partial \tilde{z}}\delta_a \tilde{z} \right) d\Omega . \tag{78}$$

The fields $\omega, \tilde{z}$ are the solution of the system of partial differential equations and b. c.

$$\mathbf{R}(a,\omega,\tilde{z}) = 0 \text{ in } \Omega, \tag{79}$$

$$\tilde{\mathbf{S}}(a,\tilde{z}) = 0 \text{ in } \Omega', \tag{80}$$

$$\Theta(\tilde{z})\hat{n}(a) = P(\omega)\hat{n}(a) \text{ in } S, \tag{81}$$

$$\vec{v}(\omega)^T \hat{n}(a) = 0 \text{ in } S. \tag{82}$$

Here Ω indicate the flow field volume, and Ω' the wing internal volume. The two open volumes have a common boundary *S*, which represents the wing surface. Eq. (79) are the flow, and Eq. (80) the structural equations, while Eq. (81) represents the boundary condition for the structural equation, assigned by equating the structural stress normal to *S* with the aerodynamic force, being $\Theta(\tilde{z})$ the structural stress tensor and *P(ω)* the aerodynamic pressure. Eq. (82) represents the usual slip boundary condition for an inviscid flow. Just as in Eq. (19), we take the first variation of the PDEs and of the boundary condition Eq. (81) consequent to the variation δa of the design variable *a*:

$$d\mathbf{R} = \frac{\partial \mathbf{R}}{\partial a}\delta a + \left(D_{\omega}\,\mathbf{R}\right)\delta_a \omega + \left(D_{\tilde{z}}\,\mathbf{R}\right)\delta_a \tilde{z} = 0 , \tag{83}$$

$$d\tilde{\mathbf{S}} = \frac{\partial \tilde{\mathbf{S}}}{\partial a}\delta a + \left(D_{\tilde{z}}\tilde{\mathbf{S}}\right)\delta_a \tilde{z} = 0 , \tag{84}$$

$$\left(D_{\tilde{z}}\Theta(a,\tilde{z})\right)\hat{n}(a)\delta_a \tilde{z} - \frac{\partial P(\omega)}{\partial \omega}\hat{n}(a)\delta_a \omega = 0 . \tag{85}$$

We multiply Eq. (83) with the Lagrangian multiplier ψ and we perform a volume integration in Ω. Similarly we multiply Eq. (84) for the Lagrangian multiplier $\tilde{\phi}$ restricted to the open Ω´ and integrate over Ω´. To take into account the boundary condition Eq. (85), which is a 3-dimensional equation defined on the boundary of Ω´, S, we multiply it for the Lagrangian multiplier $\tilde{\phi}$ restricted to its traslational part $\vec{\phi}$ and integrate over S. We add these three terms to the expression Eq. (78) , obtaining after a reordering of terms:

$$\begin{aligned} dF = & \left(\frac{\partial F}{\partial a} + \int_{\Omega} \left(\psi^T \frac{\partial \mathbf{R}}{\partial a} \right) d\Omega + \int_{\Omega'} \left(\tilde{\phi}^T \frac{\partial \tilde{\mathbf{S}}}{\partial a} \right) d\Omega' \right) \delta a \\ & + \left(\int_{\Omega} \left(\frac{\partial f}{\partial \omega} + \psi^T \left(D_{\omega} \mathbf{R} \right) \right) d\Omega - \int_{S} \vec{\phi}^T \frac{\partial P(\omega)}{\partial \omega} \hat{n}(a) dS \right) \delta_a \omega \\ & + \left(\int_{\Omega} \left(\psi^T \left(D_{\omega} \mathbf{R} \right) + D_{\tilde{z}} f \right) d\Omega + \int_{\Omega'} \left(\tilde{\phi}^T \left(D_{\tilde{z}} \tilde{\mathbf{S}} \right) \right) d\Omega' + \int_{S} \vec{\phi}^T \left(D_{\tilde{z}} \Theta(\tilde{z}) \right) \hat{n}(a) dS \right) \delta_a \tilde{z}. \end{aligned} \tag{86}$$

Since we want to avoid recalculation of the $(\omega, \tilde{z})$ fields, we cancel the terms multiplying $\delta_a \omega$ and $\delta_a \tilde{z}$ in $\delta_a F$ by imposing the fields $\tilde{\phi}, \psi$ to be solution of the equations

$$\int_{\Omega} \left(\frac{\partial f}{\partial \omega} + \psi^T \left(D_{\omega} \mathbf{R} \right) \right) d\Omega - \int_{S} \vec{\phi}^T \frac{\partial P(\omega)}{\partial \omega} \hat{n}(a) dS = 0 , \tag{87}$$

$$\int_{\Omega} \left(\psi^T \left(D_{\omega} \mathbf{R} \right) + \left(D_{\tilde{z}} f \right) \right) d\Omega + \int_{\Omega'} \left(\tilde{\phi}^T \left(D_{\tilde{z}} \tilde{\mathbf{S}} \right) \right) d\Omega' + \int_{S} \vec{\phi}^T \left(D_{\tilde{z}} \Theta(\tilde{z}) \right) \hat{n}(a) dS = 0 . \tag{88}$$

These are the adjoint equations in integral form for the problem of coupled aero elasticity. After solving these equations, the sensitivity can be recovered from the expression

$$dF = \frac{\partial F}{\partial a} \delta a + \int_{\Omega} \left(\psi^T \frac{\partial \mathbf{R}}{\partial a} \delta a \right) d\Omega + \int_{\Omega'} \left(\tilde{\phi}^T \frac{\partial \tilde{\mathbf{S}}}{\partial a} \delta a \right) d\Omega' , \tag{89}$$

as

$$\frac{dF}{da} = \frac{\partial F}{\partial a} + \int_{\Omega} \left(\psi^T \frac{\partial \mathbf{R}}{\partial a} \right) d\Omega + \int_{\Omega'} \left(\tilde{\phi}^T \frac{\partial \tilde{\mathbf{S}}}{\partial a} \right) d\Omega' . \tag{90}$$

5.2 Form of the equations for the fluid-structure coupling

At this point, no hypothesis has been yet made concerning the form of the flow or structure state equations, or their discretization. In the following paragraphs, this will be done in two distinct steps. First, the continuous adjoint formulation will be carried out for the coupling of an Euler flow and a linear elastic structure. Then, the so obtained equations will be discretized and solved.

5.2.1 Continuous coupled adjoint formulation

In the previous Section the continuous adjoint equations for a general coupled system have been derived:

$$\int_{\Omega}\left(\frac{\partial f}{\partial \omega}+\psi^{T}\left(D_{\omega}\,\mathbf{R}\right)\right)d\Omega-\int_{S}\vec{\phi}^{T}\,\frac{\partial P(\omega)}{\partial \omega}\hat{n}(a)dS=0\,, \tag{91}$$

$$\int_{\Omega}\left(\psi^{T}\left(D_{\omega}\,\mathbf{R}\right)+\left(D_{\tilde{z}}\,f\right)\right)d\Omega+\int_{\Omega'}\left(\tilde{\phi}^{T}\left(D_{\tilde{z}}\tilde{\mathbf{S}}\right)\right)d\Omega'+\int_{S}\vec{\phi}^{T}\left(D_{\tilde{z}}\Theta(\tilde{z})\right)\hat{n}(a)dS=0\,, \tag{92}$$

and it has been shown that the sensitivity takes the form

$$\frac{dF(\omega,\tilde{z},a)}{da}=\frac{\partial F}{\partial a}+\int_{\Omega}\left(\psi^{T}\,\frac{\partial\,\mathbf{R}}{\partial a}\right)d\Omega+\int_{\Omega'}\left(\tilde{\phi}^{T}\,\frac{\partial\,\tilde{\mathbf{S}}}{\partial a}\right)d\Omega'\,. \tag{93}$$

In this paragraph, the specialization to the case of Euler flow and a linear elastic structure is derived. The formulation is continuous with respect to both state equations, which means that no discretization is assumed at this stage. Let's examine first Eq. (91), which expresses the adjoint flow equation and its boundary conditions. It has been already shown in Section 3.3 that the second term in the volume integral on the l. h. s. of Eq. (91) after integration by parts gives a volume term

$$\int_{\Omega}\left(\left(\frac{\partial\psi}{\partial\xi_{i}}\right)^{T}\frac{\partial\,\mathbf{F}_{i}}{\partial\omega}\right)d\Omega=0\,, \tag{94}$$

and a surface term expressed by

$$\int_{S}\left(\psi_{2}n_{1}+\psi_{3}n_{2}+\psi_{4}n_{3}\right)\frac{\partial P}{\partial\omega}dS\,. \tag{95}$$

Thus, the adjoint flow equation remains identical with respect to the uncoupled case given by Eq. (47) and Eq. (48). This implies that although Euler flow has been assumed, no substantial differences arise in the adjoint coupling procedure when viscous adjoint equations are assumed. The coupling with the structural adjoint equation follows thus from the boundary conditions. These are expressed by the first and third term of Eq. (91) and by the term of Eq. (95). The first term of Eq. (91) has been already shown to be equivalent to, e. g. in the case of the drag sensitivity

$$\int_{\Omega}\frac{\partial f}{\partial\omega}d\Omega=\int_{S}\frac{\partial f}{\partial\omega}dS=\int_{S}\frac{\partial P}{\partial\omega}\frac{1}{S}\frac{2}{\gamma M_{\infty}^{2}P_{\infty}}(n_{1}\cos\alpha+n_{2}\sin\alpha)dS\,. \tag{96}$$

Collecting all the surface integrals in Eq. (91), namely Eq. (95), Eq. (96) and the third term of Eq. (91), we get (in the case of drag sensitivity)

$$\psi_2 n_1 + \psi_3 n_2 + \psi_4 n_3 + \frac{2}{S\gamma M_\infty^2 P_\infty}\left(n_1 \cos(\alpha) + n_2 \sin(\alpha)\right) - \vec{\phi}^T \hat{n} = 0. \tag{97}$$

These are the boundary conditions for the adjoint flow coupled with the adjoint structure equation. Compared to the single discipline case, the boundary conditions are enriched by a term which contains the coupling, and which depends of the translational part of the structural adjoint displacement field $\tilde{\phi}$, indicated by $\vec{\phi}$. If the cost function does not contain explicit dependency on ω, the term of Eq. (96) is zero, and the boundary condition becomes

$$\psi_2 n_1 + \psi_3 n_2 + \psi_4 n_3 - \vec{\phi}^T \hat{n} = 0\,. \tag{98}$$

This is the case, for example, for a structural cost function like the function G defined in (71). The use of the above described boundary condition differentiates the method from the already implemented coupled adjoint methods. In particular, the evaluation of the coupling term in the adjoint flow equation in the continuous form $\vec{\phi}^T \hat{n}$ is likely to be more efficient than its evaluation in discrete form implemented in [**58**]

$$\frac{\partial \tilde{\mathbf{S}}}{\partial \omega} = \left(\frac{\partial P}{\partial \omega}\right)_h \left(\frac{\partial \tilde{\mathbf{S}}}{\partial P}\right)_h, \tag{99}$$

which involves the calculation of wide matrices and the differentiation of the interpolation algorithm. Let's now consider Eq. (92), which represents the structural adjoint equation and its boundary conditions. The derivative $D_{\tilde{z}}\,\tilde{\mathbf{S}}$ in Eq. (92) represents the Fréchet derivative of the operator $\tilde{\mathbf{S}}$, which is in turn a linear operator. Its transpose is applied to the adjoint structural field $\tilde{\phi}$, giving the equation

$$\int_{\Omega'} \left(D_{\tilde{z}}\,\tilde{\mathbf{S}}\right)^T \tilde{\phi} d\Omega = -\int_{\Omega} \left(\left(D_{\tilde{z}} f\right) + \psi^T \left(D_{\tilde{z}}\,\mathbf{R}\right)\right) d\Omega\,. \tag{100}$$

By equating the remaining term in (92) to zero, we obtain

$$\int_S \left(D_{\tilde{z}} \Theta(\tilde{z})\right)^T \vec{\phi}\,\hat{n}(a) dS = 0\,. \tag{101}$$

This completes the continuous adjoint formulation for the coupled fluid-structure interaction. However, the discretization to be adopted still remains to be discussed.

5.2.2 Discretization and solution of the coupled adjoint system

As for the primal problem, the coupling between the two state equations occurs by means of the boundary conditions. This makes it possible to solve the system by a serial staggered iterative scheme, and to preserve existing discretization and solution techniques for the singlediscipliplinary problems. In particular, the treatment of the coupled adjoint flow equations does not present any difference to the singlediscipliplinary case, except for the presence of a coupling term that must be evaluated at every step of the coupling procedure. The FLOWer code in adjoint mode has thus been modified to be able to read a scalar field defined on the surface of

the wing, and to add it to the boundary conditions according Eq. (97). The coupled adjoint structure Eq. (100) deserves more explanation. If we discretize the structural part of the equation within the same method used for the primal problem, we get the equation

$$H^T \tilde{\phi}_h = -\int_{\Omega} \frac{\partial f}{\partial \tilde{z}_h} d\Omega - \int_{\Omega'} \left(\psi^T \frac{\partial \mathbf{R}}{\partial \tilde{z}_h} \right) d\Omega , \tag{102}$$

where $\tilde{\phi}_h$ is the discrete structural adjoint field and *H* the stiffness matrix associated with the operator $D_{\tilde{z}} \tilde{\mathbf{S}}$. To lighten the notation, the aerodynamical part is not discretized, understood that it follows the same discretization already discussed. Since $\tilde{z}$ is now a discrete quantity, the Fréchet derivatives with respect to $\tilde{z}$ have been replaced by partial derivatives to be evaluated numerically. On the other hand, since $\tilde{\mathbf{S}}(\tilde{z})$ is a linear operator with respect to $\tilde{z}$, its Fréchet derivative with respect to $\tilde{z}$ coincides with the operator itself, and thus *H* coincides with the stiffness matrix of the primal problem *K*. Since this is a symmetric matrix, the product $K^T \tilde{\phi}_h$ can be replaced by $K \tilde{\phi}_h$. We obtain

$$K \tilde{\phi}_h = -\int_{\Omega} \frac{\partial f}{\partial \tilde{z}_h} d\Omega - \int_{\Omega'} \left(\psi^T \frac{\partial \mathbf{R}}{\partial \tilde{z}_h} \right) d\Omega . \tag{103}$$

Thus, the same solver can be used for the structural direct and adjoint equation. Eq. (101) can be seen as the following boundary condition in integral form:

$$\left(D_{\tilde{z}} \Theta(\tilde{z}) \right)^T \vec{\phi} \hat{n}(a) = 0 \text{ on } S. \tag{104}$$

Since the stress tensor Θ is a linear differential operator, this is equivalent to

$$\left(\Theta(\vec{\phi}) \right) \hat{n}(a) = 0 \text{ on } S, \tag{105}$$

which simply prescribes that no stress must be transmitted to the adjoint structural field through the surface *S*. The force applied to the adjoint problem is instead represented by the right hand side terms in equation (103). The first of these terms is equivalent to

$$-\frac{\partial F}{\partial \vec{z}_h} , \tag{106}$$

that is minus the partial derivative of the cost function with respect to a structural degree of freedom of translational type. The second term, namely

$$-\int_{\Omega} \left(\psi^T \frac{\partial \mathbf{R}}{\partial \tilde{z}_h} \right) d\Omega , \tag{107}$$

represents the integral of the scalar product of the adjoint field ψ and the partial derivative of the flow operator $\mathbf{R}(a,\omega,\tilde{z})$ with respect to a structural degree of freedom, thus keeping constant the flow field and the design variables. Since the fluid mesh, and thus $\mathbf{R}(a,\omega,\tilde{z})$, does not change after a pure rotation of some structural node, this term can also be restricted to its translational part

$$\int_{\Omega}\left(\psi^{T}\frac{\partial \mathbf{R}}{\partial \vec{z}_{h}}\right)d\Omega\,. \tag{108}$$

As for the second term of the single discipline sensitivity Eq. (66), it may be evaluated by making use of the finite volume formulation implemented in FLOWer. We observe that this term is responsible for the most time-consuming computations during the solution of the adjoint equations, since it requires a complete mesh deformation for every structural degree of freedom in $\vec{z}$. In the implementation the strategy of saving 3N deformed meshes has been adopted. In this way it is possible to spare computation time, but a large amount of storage space is required. The problem is of the same kind of the previously discussed calculation of volume mesh sensitivities in the singlediscipliniary sensitivity evaluation. An accurate surface formulation, or alternatively a mesh movement adjoint formulation would be helpful in this case. The staggered serial partitioning gives rise to a convergence plot for the adjoint residual as shown in Figure 14.

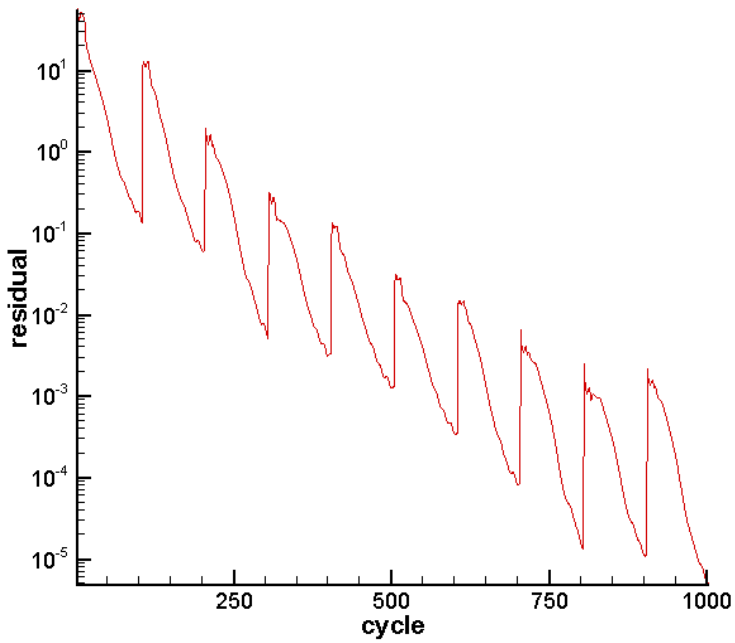

Figure 14. Adjoint flow residual during a coupled adjoint computation for the drag sensitivity, log scale.

Experience shows that a coupling every 100 flow calculation steps is enough to assure convergence in the case of the drag or lift. In the case of a coupled adjoint computation for the G stress function, however, longer calculations are necessary before performing a coupling step, or the procedure shows divergence.

5.3 Reconstruction and validation of sensitivities

After the solution of the system of discretized adjoint equations, the sensitivity may be numerically obtained from Eq. (93), via

$$\frac{dF}{da} \approx \left[\frac{\partial F}{\partial a} + \int_{\Omega} \left(\psi^T \frac{\partial \mathbf{R}}{\partial a} \right) d\Omega \right]_h + \left(\tilde{\phi}_h^T \frac{\partial \tilde{\mathbf{S}}_h}{\partial a} \right). \tag{109}$$

The subscript on the square parenthesis of the first term on r. h. s. means that it has been evaluated on the basis of the discrete solution of the flow primal and adjoint problem. The evaluation has already been discussed in the singlediscipliniary adjoint flow formulation. The third term reduces to the scalar multiplication of the discrete structural adjoint field $\tilde{\phi}_h$ by the term

$$\frac{\partial \tilde{\mathbf{S}}_h}{\partial a} = \frac{\partial K}{\partial a} \tilde{z}_h - \frac{\partial \tilde{M}_h}{\partial a}, \tag{110}$$

where K is the stiffness matrix of the primal problem and $\tilde{M}_h$ the applied generalized six-force coming from the aerodynamic side. Eq. (110) represents the variation in the residual of the structural equation after applying a geometry deformation δa, keeping the displacement $\tilde{z}_h$ and the aerodynamical pressure P constant. It has been evaluated numerically by means of a sequence of input files making use of the Nastran programming facility that evaluate K on a deformed CSM mesh and by calling the interpolation module on deformed CSM and CFD geometries, by keeping constant the pressure information evaluate by the CFD code. The contribution of this term to the sensitivity with respect to shape alterations is in general negligible for aerodynamical quantities, being about 1% with respect to the total. When Eq. (109) is used for the sensitivity of the G function (stress envelope), this is instead the dominating term.

5.3.1 Validation against finite differences

The validation of both the theory and the implementation of the adjoint formulation for the aeroelastic system is achieved as in the singlediscipliniary case by comparison with the finite difference method. This means that, after a deformation of the baseline shape of the CFD and CSM meshes, an aero elastic coupling is called and a stationary state is reached. The comparison of the values of drag, lift and stress function with the values where no design has been altered gives thus the sensitivities as shown in Chapter 4.3. The operation is repeated for every design parameter, which is in this case represented by the x or y coordinate of a free form deformation control point. The comparison of finite difference and coupled adjoint sensitivities for the G function, drag and lift are shown in the following pictures.

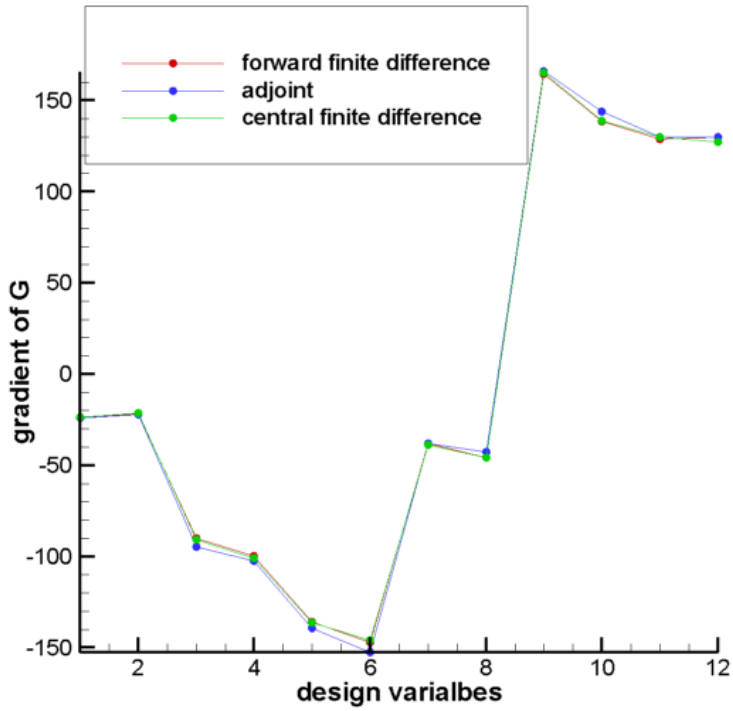

Figure 15. Sensitivities of the G stress function after aeroelastic coupling with respect to shape design variables, from adjoint calculation and finite differencing.

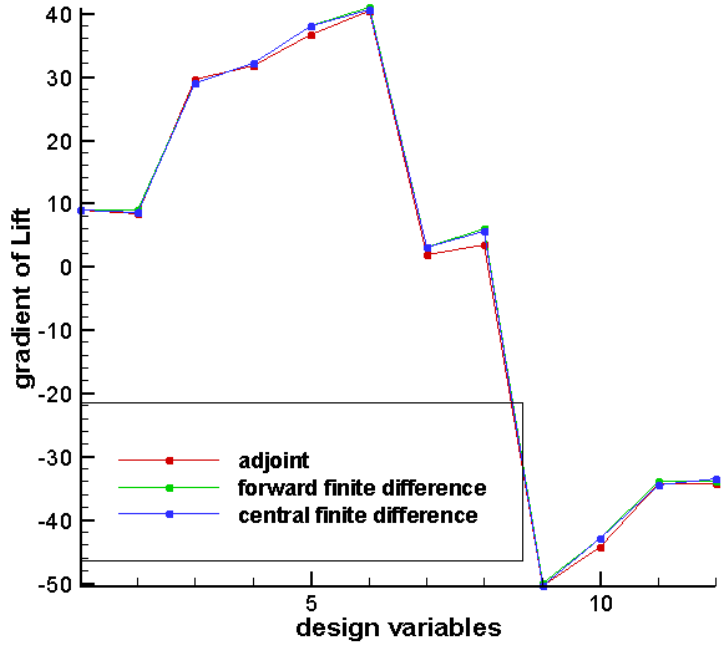

Figure 16. Sensitivities of lift after aeroelastic coupling, with respect to shape design variables, from adjoint calculation and finite differencing.

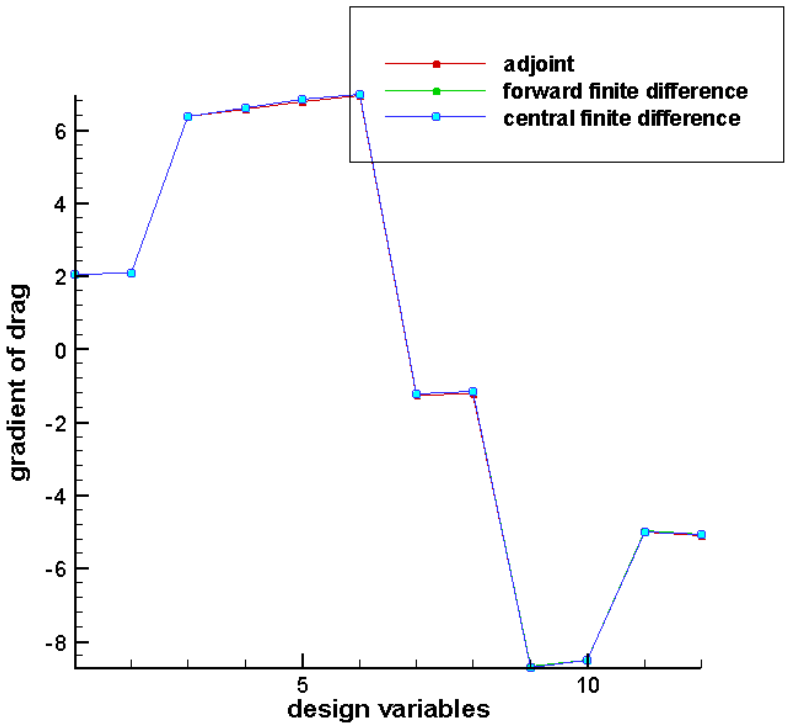

Figure 17. Sensitivities of drag after aeroelastic coupling, with respect to shape and thickness design variables, from adjoint calculation and finite differencing.

The accordance between finite-differences and adjoint for shape design variables is in all three cases good, and very good in the case of the drag, which has the smallest values of sensitivity. In all the sensitivity calculations based on continuous adjoint formulation there is a small systematic error due to the fact that the adjoint discrete equation solved represents the discretization of the continuous adjoint equation, and not the adjoint of the primal discrete equation, as outlined in [**87**]. In computing the mean deviation, care must be taken for values of the sensitivity near to zero. For such design parameters, this systematic error is amplified by the division, giving large values of absolute fractional deviation. These parameters, like design parameters 7 and 8 in the Figures, increment the mean value of absolute deviation, but have in reality no effect on the optimization, and can be removed from the computation of the mean deviation. With this caveat, the mean absolute deviation remains under 2% for all shape design variables for all the three cases shown in Figure 15, Figure 16 and Figure 17. Due to the inclusion of term (110) in the calculation of the sensitivity, also structural parameters can be used as design variables, and the associated sensitivity calculated in the very same way as for shape parameters. In fact, the last term in Eq. (109) contains the effect of the design parameter a on the applied generalized force $\tilde{M}$ and on the structural stiffness matrix K. If the alteration involves the structural model nodes coordinates, as for shape design, both these terms are different from zero. But the alteration can also involve structural element parameters, like beams thickness, the variation of which has effect only on the stiffness matrix. In this case, sensitivity is obtained with respect to this purely structural design variables, as shown in Figure 18 for the drag.

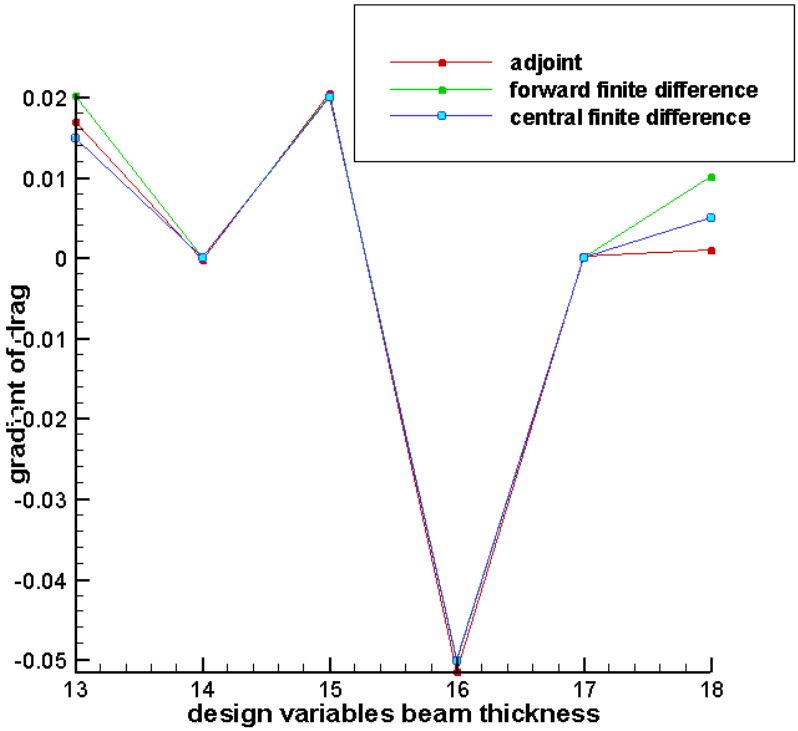

Figure 18 Sensitivity of drag with respect to beam thickness from adjoint and from finite differencing.

The agreement with the central finite-difference is good (mean absolute deviation 3%). This type of design variable has not been used in the optimization test cases.

6 Application to multidisciplinary shape optimizations

In this section, the previously described method for the efficient evaluation of sensitivities in presence of static aeroelastic interaction is applied with several kinds of shape parameterisation and optimization strategies, in order to find a combination that maximizes the effectiveness of the optimization. The test case is the AMP wing in transonic flight regime as described in the Introduction. The optimization goal is drag reduction at constant lift that is expected to lead to a shock-smeared flow with an up to 30% decreased value of the inviscid drag. Once this task has been successfully completed, the same strategy is applied to an optimization aimed at increase range in terms of the Breguet formula, assuming a stress penalty for the structural weight and again constant lift and angle of attack.

6.1 Effect of the shape parametrization and number of design parameters

In a first optimization run, Bernstein polynomials as bumping function have been chosen. The bumping functions have been calculated using the *(i,j)* indexing instead of the wing surface nodes coordinates. The use of the *(i,j)* indexing in the calculation of the bumping allows keeping the planform fixed (since the planform is defined by fixed values of *i* and *j*), and to concentrate the bumping in the median zone of the wing. This also permits avoiding the alteration of zones that are known as “critical”, like the leading and trailing edges. Later experience has shown that this restriction is not necessary, and that the sensitivity is robust enough to treat also leading and trailing edge alterations. Examples of geometry deformations that can be realized with this method are show in Figure 19.

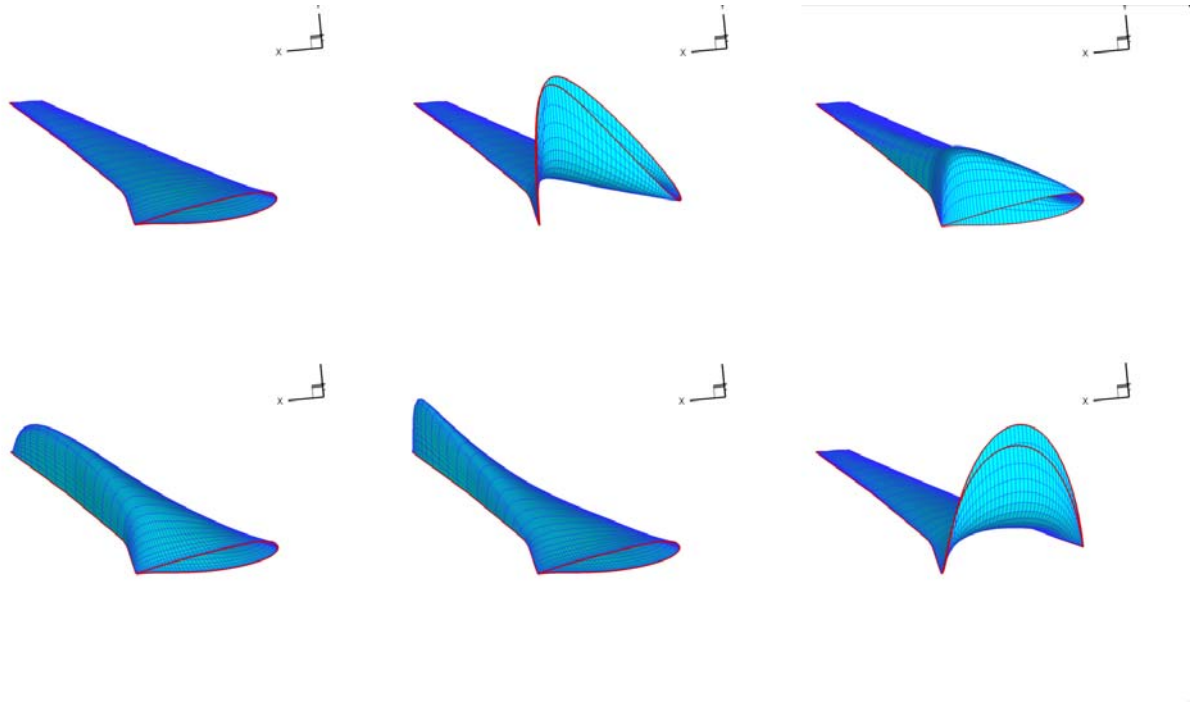

Figure 19. Geometry deformation obtained with Bernstein polynomial as bumps functions.

The number of bump functions is 60 for each surface of the wing, giving a total of 120 design variables. According to the steepest descent strategy, a line search in the direction of the sensitivity of the drag projected on the space orthogonal to the sensitivity of the lift, gave the output shown in Figure 20.

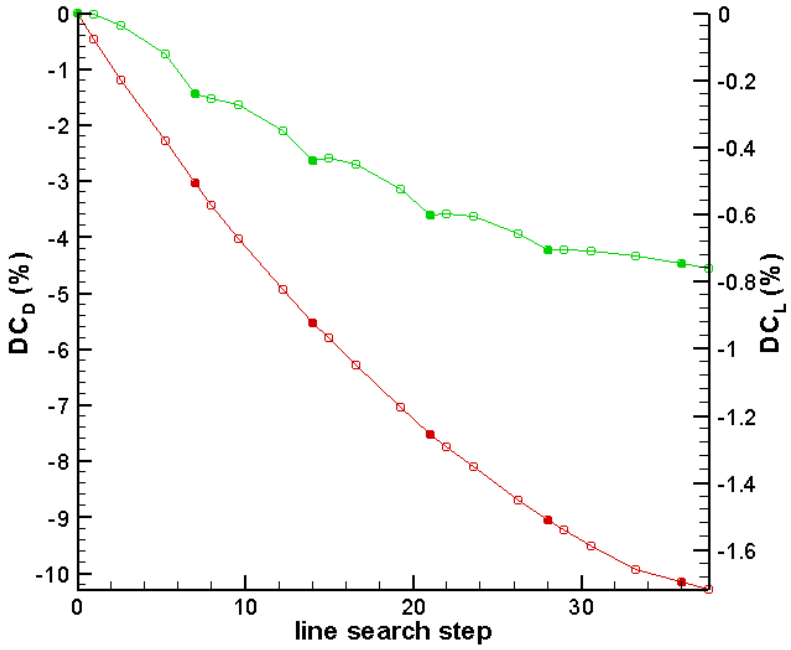

Figure 20. Drag and lift percentage variation during the line search in the direction of projected drag sensitivity. Filled spots correspond to a new sensitivity computation.

Every five steps, the direction was updated according a new gradient evaluation and projection. After 22 state evaluations and 6 sensitivities evaluations, the drag showed a decrease of about 10%, while the lift decreased of about 0.8 %. This is a nice result from theoretical point of view, confirming that the gradients are accurate and the projection strategy is effective. The variation of the lift can be understood from the fact that the projected gradient assures a constancy of the constraint only locally in the neighbourhood of the design point where it has been evaluated. However, as the design point moves away from the point where the gradients have been evaluated, also the lift start to decrease. This behaviour can be depicted in the following 2D idealization.

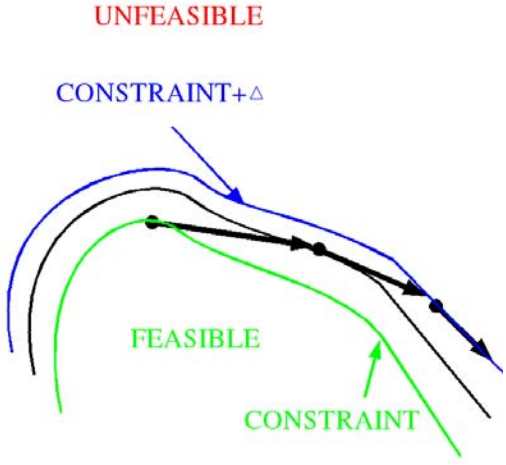

Figure 21. 2D idealization of the path in the design space spanned by *A* according steepest descent strategy with projected gradient.

In mathematical terms, if $l(\mathbf{A})$ is the constraint and $g(\mathbf{A})$ the cost function to be decreased, a (small) step $d\mathbf{A}$ in the direction of $\nabla g(\mathbf{A}) - \frac{(\nabla g(\mathbf{A}))^T \nabla l(\mathbf{A})}{\|\nabla l(\mathbf{A})\|^2} \nabla l(\mathbf{A})$, which is the projection of $\nabla g(\mathbf{A})$ onto the orthogonal to $\nabla l(\mathbf{A})$, assures a constancy of $l(\mathbf{A})$ to the first order in $d\mathbf{A}$. Since the real step $\Delta\mathbf{A}$ taken by the optimizer is finite, this realizes a variation in the constraint given by $\Delta l(\mathbf{A}) = l(\mathbf{A}) - l(\mathbf{A}+\Delta\mathbf{A})$, which is a small but finite quantity. Once the constraint is violated, the method has no way of recovering the violation. The new line step taken according the gradients evaluated the design point $\mathbf{A}+\Delta\mathbf{A}$ will assure a small variation of the lift with respect to the value $l(\mathbf{A}+\Delta\mathbf{A})$, thus conserving the error introduced in the first step. A sequence of such steps is likely to accumulate errors of the same sign, giving at the end a substantial, although not big, variation of the lift. Thus, this strategy is well suited for a slowly varying constraint. From Figure 20 it can be noted instead the wavy behaviour of the lift, which requires many sensitivity evaluations to be captured. This is very different from the behaviour of the lift in a transonic 2D case, where the lift varies slowly. Since from a designer point of view, the 0.8 % variation of the lift is not acceptable, the strategy must be modified to take control of the constraint value. For this reason, an optimizer has been chosen, that relies on the method of modified feasible directions [**27**]. According to this method, the optimizer seeks a direction in the design space to realize the maximal cost function decrease by keeping constant the constraint(s), and performs a series of steps in this direction. After realizing a decrease in the cost function, the optimizer checks if the constraint (in this case the lift) has been violated. If this is the case, the next direction-finding problem is augmented with a penalty factor that is proportional to the amount of constraint violation. As consequence, the next step will bring back the design to an acceptable value (within some allowed tolerance which is usually 0.3 %). This behaviour is schematised in Figure 22:

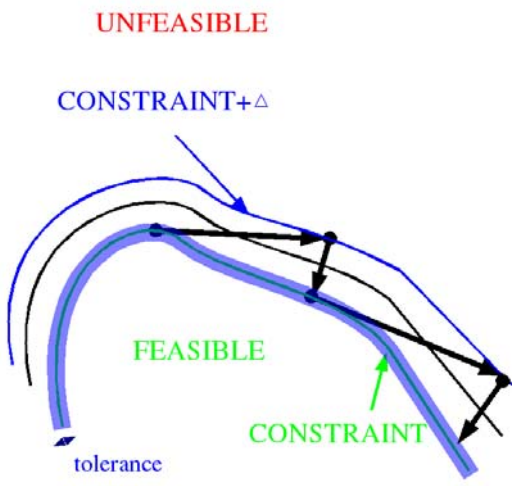

Figure 22. 2D idealization of the path in design space according feasible direction strategy.

The resulting optimization history is shown in Figure 23.

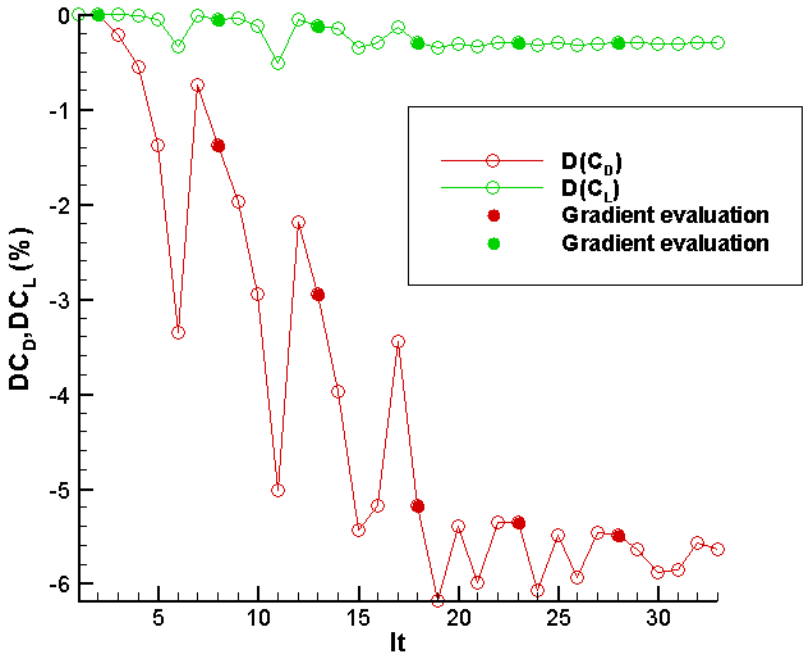

Figure 23. Optimization history for drag reduction with constant lift, method of feasible directions and surface bumping. Percentage variation of drag ad lift is shown. Filled spots represent state and gradients evaluations.

After 33 state evaluations and 6 sensitivity evaluations the wing showed a decrease of about 6.5 % in drag, with a decrease of 0.3 % in lift, which corresponds to the amount of constraint violation allowed by the optimization algorithm. Despite the high number of design variables used, the amount of drag decrease was unsatisfactory, indicating that the choice of limiting the bumping to the median zone of the wing, where the shock occurs, is invalid, and that the geometry must be altered in a more extensive way to obtain a successful optimization. One solution could have been to extend the polynomials to a bigger part of the wing, and to add twist deformation to the set of design variables. Instead, a completely new geometry deformation module has been written, based on the free form deformation algorithm. This method is based on a rectangular 3D grid of control points surrounding the shape. The displacement of such points generates a volumetric deformation in the entire domain. In this case the grid was of 6x2x5 points along respectively x, y and z (spanwise) directions. The control points were allowed to move on the (x, y) plane, giving again a total of 120 design variables, as depicted in Figure 24.

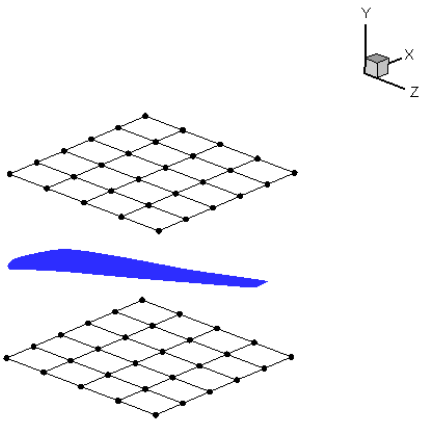

Figure 24. Free form deformation control points box used in the optimization.

The optimization history is shown, with adjusted scaling, in Figure 25.

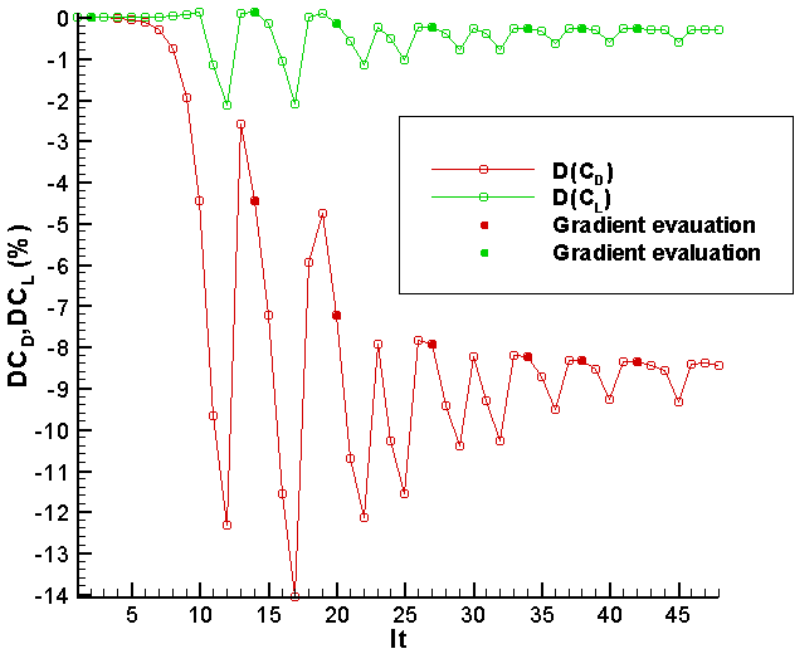

Figure 25. Optimization history for drag reduction at constant lift, method of feasible directions and free form deformation with 120 control points. Percentage variation of drag and lift is shown. Filled spots represent state and gradients evaluations.

After 48 state evaluations and 7 sensitivity evaluations the drag has been decreased by about 8.5%, while the lift remained constant within a bound of 0.3%. With the same number of design variables, the FFD approach has been thus more efficient in reducing the drag of the transonic wing profile. Nevertheless, an inspection of the pressure distribution across the wing surface shows the persistence of the shock, as can be seen in Figure 26.

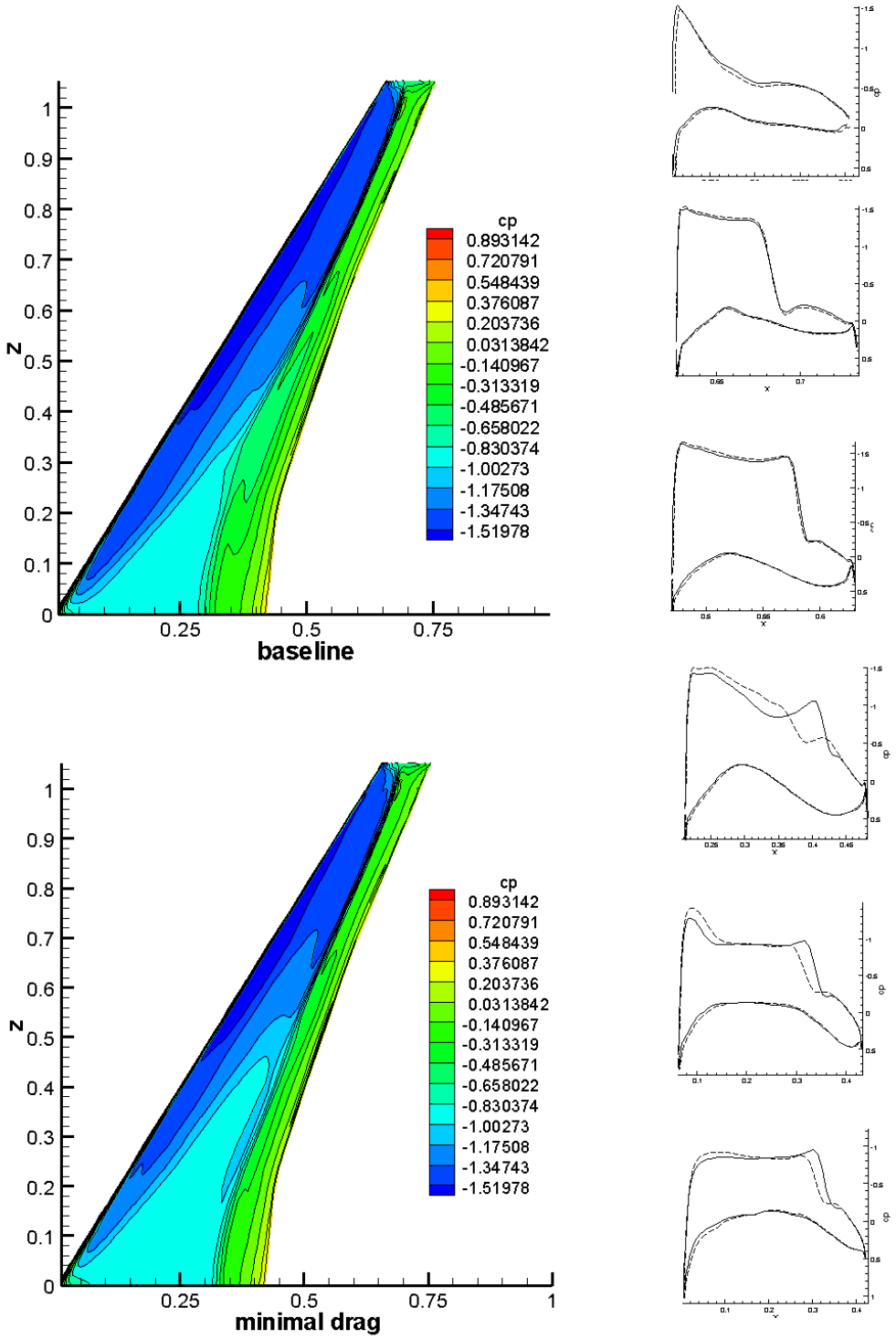

Figure 26. Pressure distribution on baseline (continuous) and optimized wing (dashed) at six stations uniformly spaced from the wing´s root (bottom) to wing´s tip (top). Also the baseline and optimized pressure distribution as contour plots are shown. The optimization was based on free from deformation with 120 control points allowed to move in the x and y directions, and lead to a 8.5 % decrease in drag.

The addition of the angle of attack to the set of design variables has not been of appreciable effect, evidently due to the fact that this variable is not linearly independent of a collective motion of the control points. Thus, a further optimization was performed, based on FFD as before, but with double the number of control points in th x direction, for a total of 240 instead of 120. The outcome of the optimization is shown in Figure 27.

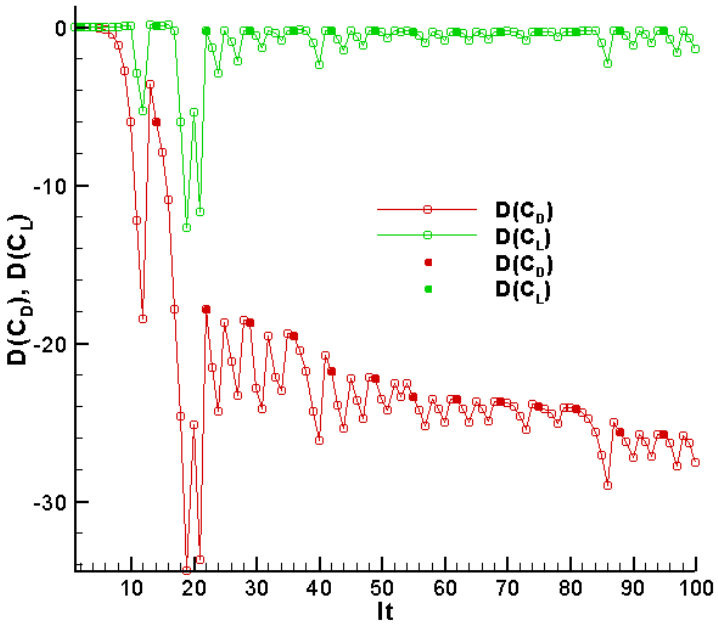

Figure 27. Optimization history for drag reduction with constant lift, method of feasible directions and free form deformation with 240 control points. Percentage variation of drag and lift is shown. Filled spots represent state and gradients evaluations.

Doubling the number of design variables is associated with an increase of the effectiveness of the optimization by a factor 3, giving in this case a decrease of the drag of about 26%. The lift has been kept constant within 0.1 %, thus not only the efficiency but also the fulfilment of the constraint is increased by the doubling of design parameters. The number of steps necessary to reach convergence scales linearly with the number of design parameters, going roughly from 50 to 100. The cost of a single gradient evaluation, according to the adjoint method, is instead only weakly dependent on the number of design variables. An inspection of the pressure distribution on the wing surface shows an evident reduction of the shock on the upper side and a general smoothing of the distribution, shown in Figure 28.

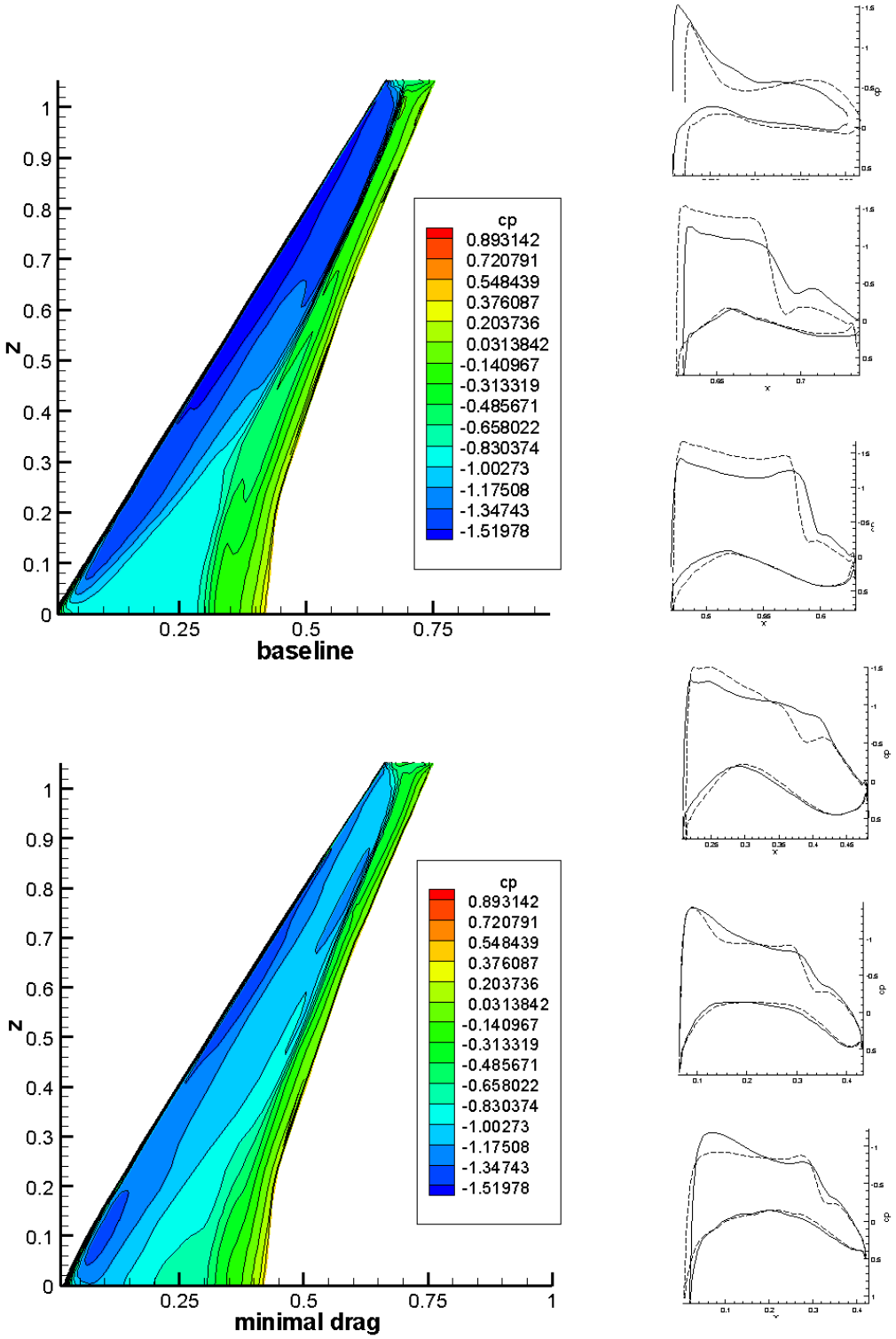

Figure 28. Pressure distribution on baseline (dashed) and optimized wing (cont. line) at six stations uniformly spaced from the wing´s root (bottom) to wing´s tip (top). Also the baseline and optimized pressure distribution as contour plots are shown. The optimization was based on free from deformation with 240 control points allowed to move in the x and y directions, and lead to a 26 % decrease in drag.

The sensitivity of the cost function (drag), projected onto the hyperplane orthogonal to the sensitivity of the constraint (lift) showed a reduction of about 75 % in the Euclidean norm, suggesting the effective approach to the nearest constrained minimum design point, where this vector is formally zero. Such a sensitivity evaluated at the beginning and at the end of optmization, is shown in Figure 29.

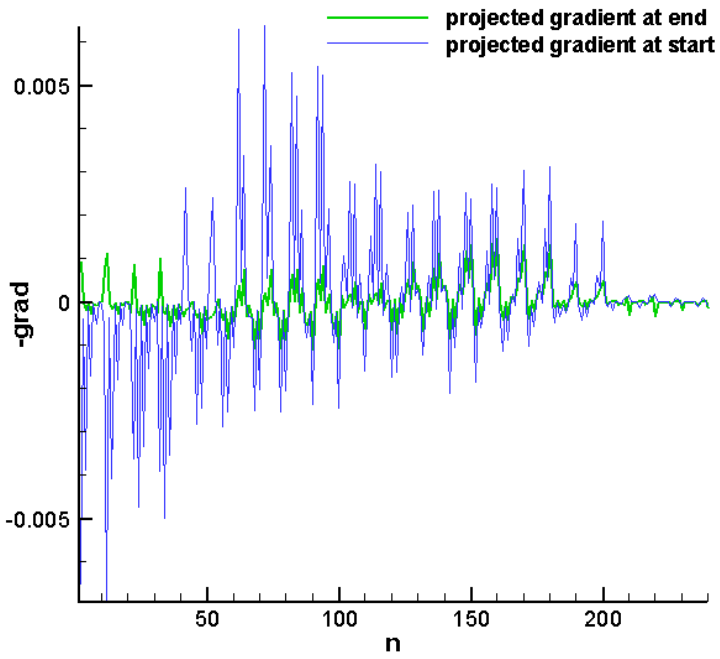

Figure 29. Projected sensitivities of drag at start (blue) and at end (green) of the optimization. In the constrained minimum design point, the projected sensitivity is expected to be zero.

Figure 30 shows the lift distribution of the baseline and optimized wing. A comparison with the outcome of the optimization with constant deflection previously performed in Chapter 4.3 shows that the lift distribution of the optimized wing is almost coincident for both optimizations.

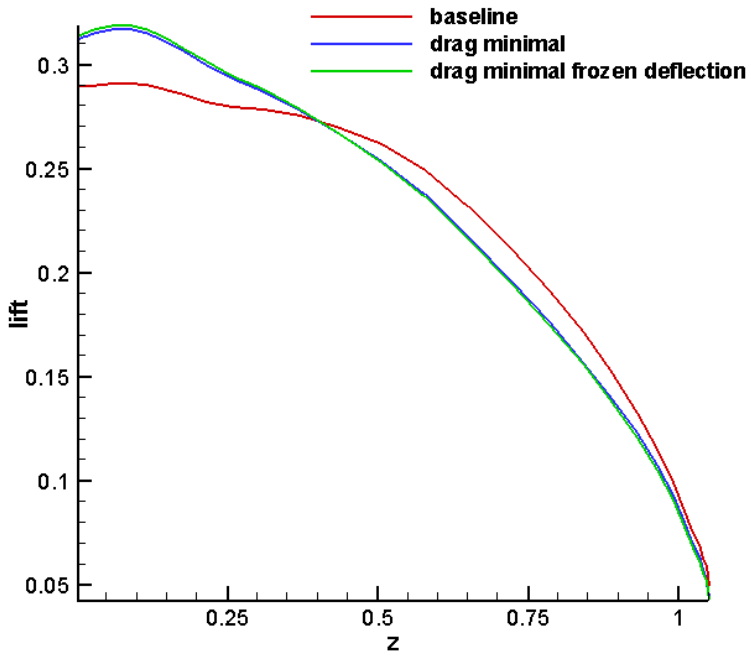

Figure 30. Lift distribution for the baseline, optimized and rigidly optimized wing.

Also the CFD surface meshes obtained in the two optimizations are almost coincident, as shown in Figure 31.

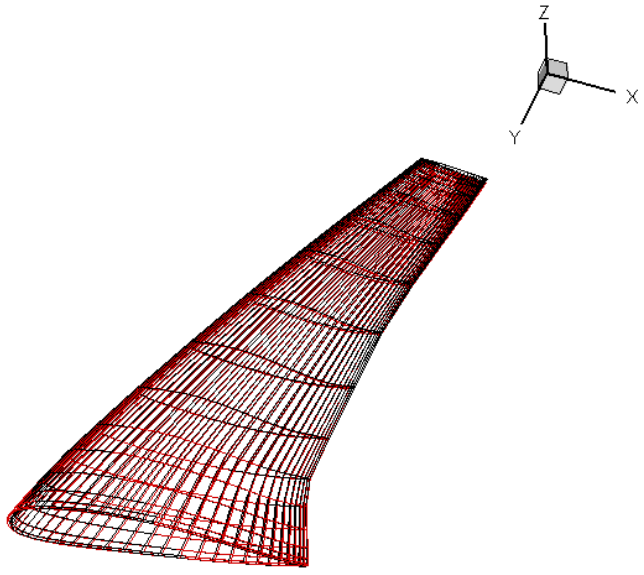

Figure 31. Optimal wing shape for minimal drag obtained by singlediscipliinary adjoint (black mesh) and coupled adjoint (red mesh) optimizations.

This indicates that the same, or a nearly equivalent, geometrical optimum has been reached by both processes, and that no essential loss in accuracy has been introduced by the coupling and adjoint coupling formalism with respect to a singlediscipliniary optimization. It must be noted that the optimized shape is sum of two effect, deflection (from elasticity) and deformation (from design update), which are not the same for the two cases. For the singlediscipliniary optimized wing the deflection was assumed constant from beginning, and the optimization was essentially singlediscipliniary while for the actual aero-elastic optimization the deflection is updated with the design. Only the *sum* of deformation and deflection is the same in both cases, giving almost identical final wing shapes. As previously shown, the optimum obtained with the singlediscipliniary procedure is not an aeroelastic stationary state, because the deflection has not been taken into account during the optimization, as has been done during the coupled aeroelastic optimization. The almost coincidence of drag optimal shapes can be viewed as a realization of the *jig design* method, that presupposes to know an optimal wing shape and is aimed to find a shape that after elastic deflection coincides with that optimal shape. A similar result has been obtained for an elastic cylinder in incompressible viscous fluid, as reported in [**88**]. It must be noted that it is possible to achieve this optimal design also without using a multidisciplinary feasible approach, but with a serial optimization procedure that alternates singlediscipliniary drag optimizations at constant deflection and structural optimizations with constrained deflection.

6.1.1 Efficiency gain with respect finite differencing

The optimization shown above required 14 sensitivity evaluations and 100 state evaluations, taking about 18 days to complete on a Pentium IV 2,08 GHz desktop machine. Obtaining the same result with the finite difference method, where the computational cost of a sensitivity evaluation is linearly dependent on the number of design variables, would have required about 288 days of computation.

6.2 Range optimization at constant lift

Having at disposal an efficient method for the evaluation of coupled sensitivities of both aerodynamical and structural cost functions with respect to both shape and structural design variables, it is in principle possible to assemble and solve in an efficient way MDOs with cost functions or constraints obtained from combinations of terms belonging to the two disciplines, provided that the terms are defined by means of differentiable functions. Unlike in the case of pure aerodynamical cost function, the optimal design for such kind of cost function cannot be achieved by a series of alternating singlediscipliniary optimizations. Our goal in this Chapter is to show that a coupled-sensitivities approach allows the solution of this kind of multidisciplinary optimization problem in natural way, and that the result is a multidisciplinary optimum, different from the aerodynamical optimum for minimal drag obtained in the previous Chapter. The choice of Ref. [**58**] for the range optimization of a supersonic business jet was maximizing the range as function of drag, lift and weight, with constraints on the stress of the structure and on the lift and keeping free the angle of attack. However, one must observe that the lumping the constraint on the stresses with a single Kreisselmeier-Steinhauser enveloping function G of the form already discussed in Eq. (71),

$$G(\sigma_n) = \frac{1}{\rho} \ln \sum_n \exp(\rho \frac{\sigma_n - \sigma_0}{\sigma_0}) \tag{111}$$

does not allow a complete optimization of the structure, leaving elements under-stressed. We will instead incorporate the stresses inside an analytical model for the weight, and constrain the lift and the angle of attack to be constant by using the modified feasible direction strategy, as done in previous optimizations. Although the structure is not directly optimized, it is possible in this way to avoid an over-stressing of the elements, which is paid for with an increase of the weight. To model this penalty, we can assume the total gross weight *W* to be a linear function of the type

$$W_T = W_0(1+\alpha G), \tag{112}$$

where α is some parameter to be set and *G* is evaluated on aero-elastic stationary state. The Kreisselmeier-Steinhauser functional is usually used as lumped constraint in structural optimization problems. We will instead use it as penalty function for the weight. This choice has the purely demonstrative value of showing that the method is able to handle this kind of problem, and has not to be intended as corresponding to some realistic design problem. With this assumption, the Breguet range function defined in (14) becomes

$$R \propto \frac{L}{D}\ln\left(\frac{W_T}{W_T - M_F}\right) = \frac{L}{D}\ln\left(\frac{W_0(1+\alpha G)}{W_0(1+\alpha G - FF)}\right) = \frac{L}{D}\ln\left(\frac{(1+\alpha G)}{(1+\alpha G - FF)}\right) = R'(a,u,\omega), \tag{113}$$

where we introduced the fuel fraction *FF* as the ratio of fuel mass *F* to the total gross weight W_T. Having available the sensitivities of lift, drag and of *G* from the coupled adjoint formulation, the sensitivity of the range is easily found by differentiating Eq. (113) as

$$\frac{dR'}{da} = \left(\frac{dL}{da}\frac{1}{D} - \frac{dD}{da}\frac{L}{D^2}\right)\ln\left(\frac{(1+\alpha G)}{(1+\alpha G - FF)}\right) + \frac{dG}{da}\frac{L}{D}\frac{(-\alpha FF)}{(1+\alpha G)(1+\alpha G - FF)} \tag{114}$$

As numerical parameters, the value of *FF=0.476* and $\alpha = 20$ have been taken. The first is the value of the fuel fraction for an Airbus A310 or a Boeing 747, the second is an arbitrary weighting of the stress penalty. As parameters for the G function, $\sigma_0 = -20000$ and $\rho = 20$ have been taken. An optimization has been run, taking the range as cost function to be maximized and the lift as a constraint and using the same modified feasible direction strategy in conjunction with 240 free form deformation control points used in the previous Chapter. The optimization history is shown in Figure 32.

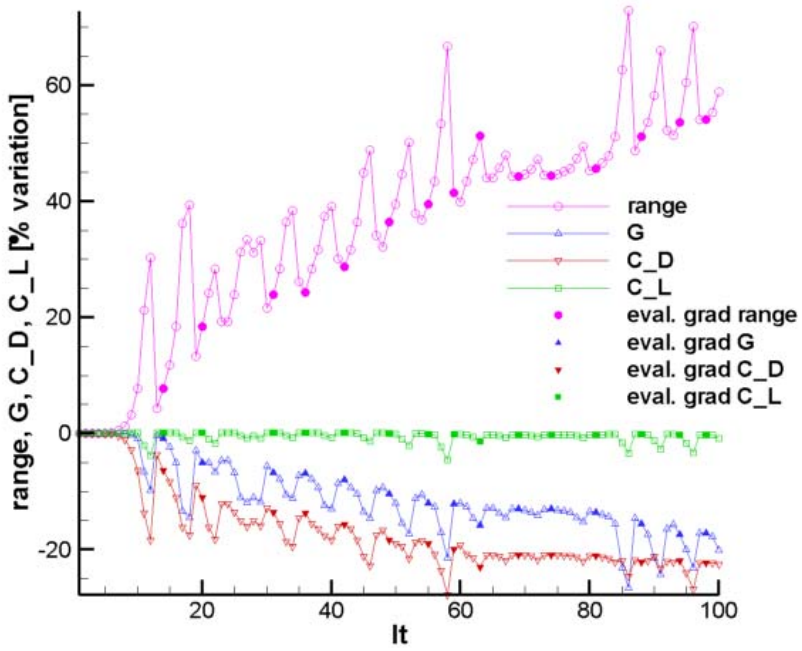

Figure 32. Optimization history for range optimization with constant lift, method of feasible directions and free form deformation with 240 control points. Percentage variation of drag, range, G stress function and lift is shown. Filled spots represent state and gradients evaluations.

After 98 state evaluations and 16 sensitivity evaluation the Range showed an increase of about 50%, due to a decrease of the Drag of about 22% and of the G function of about 17%. As usual the Lift has been kept constant within the 0.3 %. More meaningful than the range gain with respect to the initial configuration, is the comparison of the range optimal value with the value calculated by means of Eq. (113) on a minimal drag configuration, like that obtained in the previous Chapter. Such a calculation shows that range increased of about 7%. This is due to the trade-off between the instances of low drag and low stress that the penalty factor in the cost function introduced into the optimization. For this aspect, the comparison between the drag and stress value histories of the drag minimal optimization and the present one is meaningful. The comparison is shown in Figure 33.

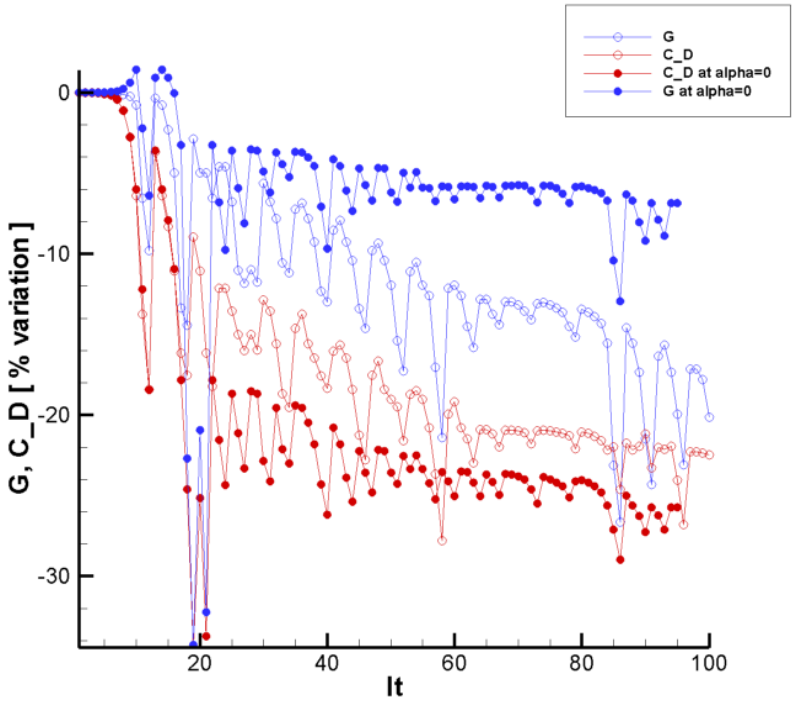

Figure 33. Drag (red spots) and stress (blue spots) values during a drag minimization (filled spots) and a range optimization (empty spots).

The presence of a stress term in the cost function and in its sensitivity, leads to a different (although simiar in form) optimization history. At the end of the range optimization, the result is that the drag has been increased of about 4% with respect the optimal drag design, while the stress, expressed by means of the G function, has been decreased of about 6%. In order to obtain a stress-reduced configuration, the optimizer found a shape, characterized by a different lift distribution with respect to the minimal-drag lift distribution. A comparison of the drag minimal and range optimal lift distributions is shown in Figure 34.

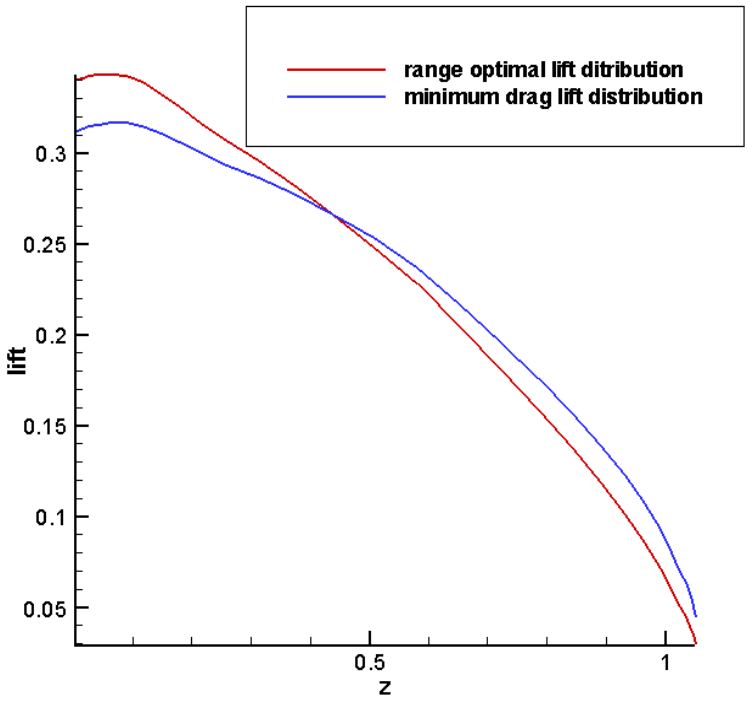

Figure 34. Optimal range and minimal drag lift distributions.

The range optimal lift distribution shows a span load shifted towards the root of the wing, in qualitative accordance with analytical [**41**] and computational [**42**], [**18**]**,** [**58-60**] results from the literature. The value of the shifting depends on the value adopted for the penalty parameter α, as well as on the parameters in the G function. The decrease of the stress can be appreciated also by looking directly at the bending stress distributions, as shown in Figure 35.

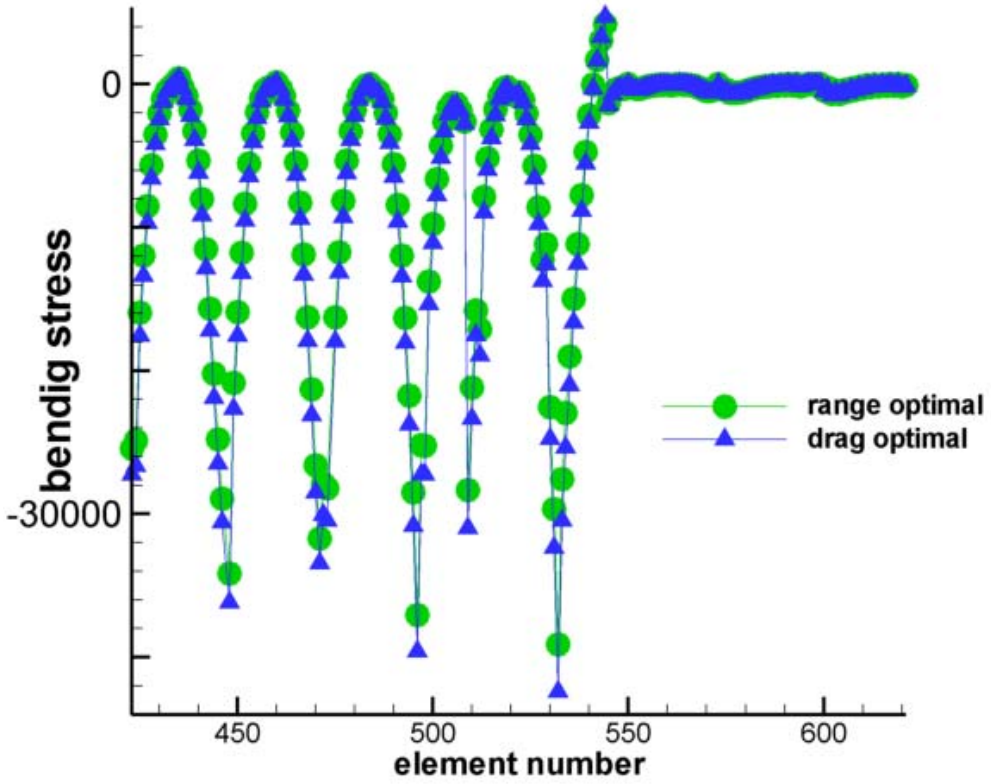

Figure 35. Beam bending stress distribution for the minimal drag and optimal range designs.

The distribution shows a decrease of 7% of the stress of the most stressed element (element 532), with respect to the minimal-drag design. The decrease of the stress has been realized at cost of some drag increase, caused by a different pressure distribution, showing some resurgence of the shock in the root-near section of the wing. The minimal drag and optimal range pressure distributions are shown in Figure 36.

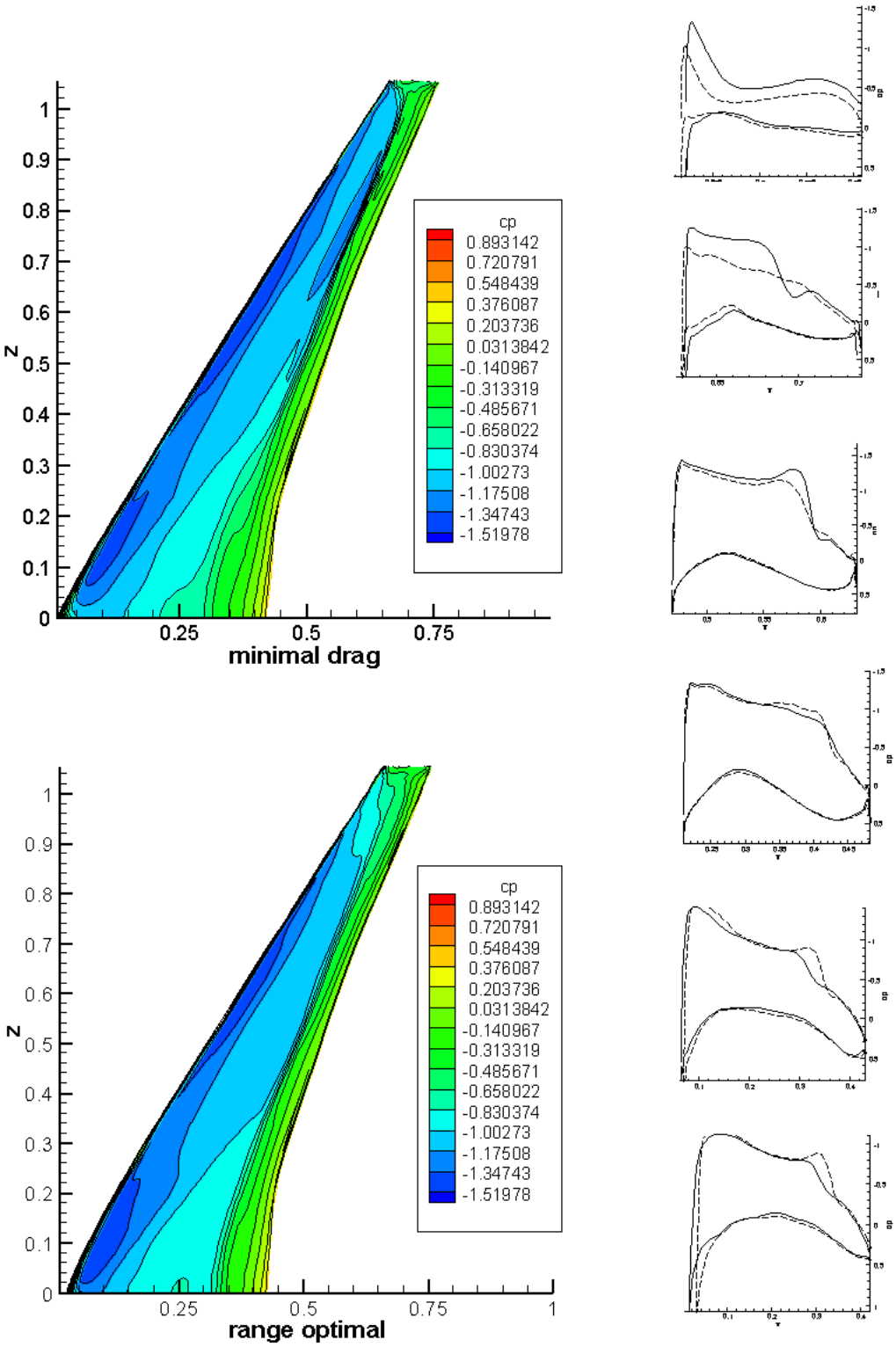

Figure 36. Pressure distribution on the minimal drag (cont. line) and optimal range (dashed) wing at six stations uniformly spaced from the wing root (bottom) to wing´s tip (top). Also the pressure distributions as contour plots are shown. Both optimizations were based on free from deformation with 240 control points allowed to move in the x and y directions.

7 Conclusions

A consistent method of evaluating sensitivities of cost functions and constraints in the presence of aero-elastic stationary coupling by means of the solution of coupled flow and structure adjoint equations has been presented. The method is based on a completely continuous adjoint formulation for the fluid-structure coupling, while existing approaches are either completely discrete, or only partially continuous. This formulation allows some saving of computational time and disk storage with respect to the other formulations. As for other coupled adjoint formulations, the multi discipline feasible sensitivities (including the effect of elasticity) are evaluated with a greater efficiency with respect to the method of finite-differences. The coupled adjoint method is able to handle cost functions and constraints of pure aerodynamical type like lift and drag, of purely structural type, such as lumped functions of the stress distribution, or combinations of the both. The design variables may be of both types, topological (shape) or structural (e.g. beam thickness), although the test case presented involved only shape design. The necessity of calculating high fidelity (multi discipline feasible) sensitivities that contain information about the elasticity for maximizing the effectiveness of the optimization has been demonstrated. The effectiveness of the free form deformation method in conjunction with a high number of design variables has also been shown, justifying the effort of building a coupled adjoint framework aimed at the efficient evaluation of sensitivities. Test cases have involved the Euler inviscid transonic flow on a 3D transonic geometry and a structural model assembled with linear elastic elements, associated with a 10% wing span-tip deflection ratio. Optimization results generated a shock-free flow in the case of drag minimization and a stress-reduced lift distribution in the case of range optimization.

Extension of the method to the Navier-Stokes equations can be performed if a Navier-Stokes adjoint option of the FLOWer-code is available. An unstructured CFD code with adjoint option (e. g. the DLR code TAU) can be adapted to the method with some work on the definition of the boundary conditions that embody the adjoint coupling. The use of a higher definition CSM model with a high N, number of nodes, is possible but it implies a large number of mesh deformation operations during the coupled adjoint computation, since on every adjoint coupling step either the flow mesh has to be deformed 3N times, or 3N deformed meshes have to be stored. This can be avoided either using a very accurate surface formulation or an adjoint formulation for the evaluation of mesh-sensitivity terms. Extension to non-linear elasticity, which requires the evaluation of the derivative of the stiffness matrix and the modification of the problem solved by the CSM solver, requires an extensive modification of the input files implemented within Nastran for the solution of the primal and adjoint coupling loops. Extension to the treatment of a combined wing-body CFD/CSM geometry is possible, since all codes involved are multi-block capable.

Bibliography

[**1**] S. Kodiyalam, J. Sobieszczanski-Sobiesky. *Multidisciplinary Design Optimization – Some Formal Methods, Framework Requirements, and Application to Vehicle Design* int. j. Vehicle Design (Special Issue), pp.3-22, 2001.

[**2**] S. Kodiyalam. *Evaluation of Methods for Multidisciplinary Design Optimization (MDO), Phase I,* NASA contractor report, NASA/CR-1998-208716, 1998.

[**3**] S. Kodiyalam, C. Yuan. *Evaluation of Methods for Multidisciplinary Design Optimization (MDO), Part II,* NASA contractor report, NASA/CR-2000-210313, 2000.

[**4**] J. S. Sobiesky, R. T. Haftka. *Multidisciplinary aerospace design optimization: survey of recent developments*, AIAA paper 96-0711, 1996.

[**5**] R. M. Hicks , P. A. Henne. *Wing design by numerical optimization*, Journal of Aircraft 15:407-412, 1978.

[**6**] F. T. Johnson, E. N. Tinoco ,N. J. Yu. *Thirty years of development and application of CFD at Boeing commercial airplanes, Seattle,* AIAA paper 2003-3439, 2003.

[**7**] C. M. Österheld, W. Heinze, P. Horst. *Preliminary design of a Blended Wing Body Configuration using the design tool PrADO* , Proceedings of the CEAS conference On Multidisciplinary Aircraft Design and Optimization, Köln, 25/26 June 2001.

[**8**] A. Jameson, D. A. Caughey. *A Finite Volume Method for Transonic Potential Flow Calculations*, Proceedings of AIAA 3rd Computational Fluid Dynamic Conference, pp. 35-54, 1977.

[**9**] W. H. Manson. *On the Use of the Potential Flow Model for Aerodynamic Design at Transonic Speeds*, AIAA paper 95-0741, 1995.

[**10**] A. Jameson, W. Schmidt, E. Turkel. *Numerical Solution of the Euler equation by finite volume methods using Runge-Kutta time stepping schemes* AIAA paper 81-1259, 1981.

[**11**] J. Reuther, A. Jameson, J. Farmer, L. Martinelli and D. Saunders. *Aerodynamic shape optimization of complex aircraft configurations via an Adjoint Formulation* AIAA paper 96-0094, 1996.

[**12**] S. Kim, J. J. Alonso, A. Jameson. *A Gradient Accuracy Study for the Adjoint-Based Navier-Stokes Design Method*, AIAA paper 99-0299, 1999.

[**13**] A. Jameson, L. Martinelli, N. A. Pierce. *Optimum aerodynamic design using the Navier-Stokes equations*, AIAA paper 97-0101, 1997.

[**14**] G. W. Burgreen, O. Baysal. *Three-Dimensional Aerodynamic Shape Optimization of Wings Using Discrete Sensitivity Analysis*, AIAA journal, Vol. 34, No. 9, pp. 1761-1770, 1996.

[**15**] W. K. Anderson, V. Venkatakrishnan. *Aerodynamic Design Optimization on Unstructured Grids with Continuous Adjoint Formulation*, AIAA paper 97-0643, 1997.

[**16**] A. Jameson, L. Martinelli. *A continuous adjoint method for unstructured grids*, AIAA paper 2003-3995, 2003.

[**17**] S. K. Nadarajah, A. Jameson. *Studies on the continuous and discrete adjoint approaches to viscous automatic aerodynamic shape optimization*, AIAA paper 2001-2530, 2001.

[**18**] J. R. Martins, J. J. Alonso, J. J. Reuther. *High-Fidelity aero-structural design optimization of a supersonic business jet*, AIAA 2002-1483, 2002.

[**19**] K. Maute, M. Nikbay, C. Farhat. *Sensitivity analysis and design optimization of three-dimensional non-linear aeroelastic systems by the adjoint method*, Int. J. Numer. Meth. Engng 2003;**56**:911-933, 2003.

[**20**] J. Wild. *Multi objective constrained optimization and high lift device applications*, Von Karman Institute for Fluid Dynamics, Lecture Series 2004-07, Optimization methods & tools for multicriteria/multidisciplinary design - applications to aeronautics and turbomachinery, November 15-19, 2004.

[**21**] A. Vicini, D. Quagliarella. *Airfoil and wing design using hybrid optimization strategies* AIAA paper 98-2729, 1998.

[**22**] G. Carrier. *Multi-Disciplinary Optimisation of a supersonic transport aircraft wing planform* ECCOMAS 2004, Jyväskylä 24-28 July 2004.

[**23**] J. A. Nelder, R. Mead. *A simplex method for function minimization*, Computer Journal, 7.308-313, 1965.

[**24**] J. A. Desideri, A. Janka. *Multilevel Shape Parametrization for Aerodynamic Optimization – application to drag and noise reduction of transonic/supersonic business jet.* ECCOMAS 2004, Jyväskylä 24-28 July 2004.

[**25**] G. N. Vanderplaats. *Numerical Optimization Techniques for Engineering Design* Mc.Graw-Hill, New York, USA, 1984.

[**26**] J. Nocedal, S. J. Wright. *Numerical Optimization*, Springer series in operations research, Springer Verlag New York inc., 1999.

[**27**] *DOT – design optimization tools*, Vanderplaats Research & Development, Inc. 1767 S. 8th Street, Suite 210 Colorado Springs, CO 80906.

[**28**] A. Jameson. *Efficient Aerodynamic Shape Optimization*, AIAA paper 2004-4369, 2004.

[**29**] J. A. Samareh. *Multidisciplinary Aerodynamic-Structural Optimization Using Deformation (MASSOUD)* AIAA paper 2000-4911, 2000.

[**30**] J. J. Alonso, J. R. R. A. Martins, J. J. Reuther, R. Haimes, C. A. Crawford. *High-Fidelity Aero-Structural Design Using a Parametric CAD-Based Model*, AIAA paper 2003-3429, 2003.

[**31**] J. Brezillon, N. R. Gauger. *2D and 3D aerodynamic shape optimization using the adjoint approach,* Aerospace Science and Technology Vol. 8, No. 8, 2004.

[**32**] T. W. Sedemberg, S. R. Parry. *Free-Form Deformation of Solid Geometric Models*, Computer Graphics Vol. 20, No. 4, pp. 151-160, 1986.

[**33**] A. Ronzheimer. *Post-parametrization of CAD geometries using freeform deformation and grid generation techniques*, Notes on Numerical Fluid Mechanics and Multidisciplinary Design, Vol. 87, Contributions to the 13th STAB/DGLR Symposium Munich, pp. 382-389, 2002.

[**34**] J. A. Samareh. *Aerodynamic shape optimization based on free-form deformation*, AIAA paper 2004-4630, 2004.

[**35**] R. M. Hicks, P. A. Henne. *Wing design by numerical optimization*, AIAA 77-1247, 1977.

[**36**] G. N. Vanderplaats. *Approximation concepts for numerical airfoil optimization* NASA TP-1370, 1979.

[**37**] J. R. R. A. Martins, I. M. Kroo, J. J. Alonso. *An Automated Method for Sensitivity Analysis using Complex Variables*, Proceedings of the 38th Aerospace Science Meeting, Reno, NV, January 2000. AIAA 2000-0689, 2000.

[**38**] J. D. Müller, P. Cusdin. *On the performance of discrete adjoint CFD codes using automatic differentiation*, Int. J. Numer. Meth. Fluids 2000; **00**:1-6, 2000.

[**39**] A. Griewank. *Evaluating derivatives, Principles and techniques of algorithmic differentiation*, SIAM Publisher, Philadelphia, 2000.

[**40**] T. A. Zang, L. L. Green. *Multidisciplinary design Optimization Techniques : Implications and Opportunities for Fluid Dynamics Research*, 30th AIAA Fluid Dynamics Conference Hune 28-July 1 , 1999 Norfolk, VA. AIAA 99-3798, 1999.

[**41**] L. Prandtl. *Über Tragflügel des kleinsten induzierten Widerstandes*, Zeitschrift für Flugtechnik und Motorluftschifffahrt 24 Jg, 1933. Reprinted in Gesammelte Abhandlungen zur angewandten Mechanik, Hydro- und Aerodynamik, Tollmien, W, Schlichting, H., and Görtler, H., eds, Springer-Verlag, Berlin, pp. 556-561, 1961.

[**42**] S. Iglesias, W. H. Mason. *Optimum Spanloads Incorporating Wing Structural Weight,* AIAA paper 2001-5234, 2001.

[**43**] T. McGeer. *Wing design for minimum drag with practical constraints,* Journal of Aircraft, Vol. 12, pp. 879-886, Nov. 1984.

[**44**] A. Craig, J. McLean. *Spanload optimization for strength designed lifting surfaces,* AIAA paper 88-2512, 1988.

[**45**] K. Eoviriyakit, A. Jameson. *Case Studies in Aero-Structural Wing Planform and Section Optimization* AIAA paper 2004-5372, 2004.

[**46**] J. L. Walsh, R. P. Weston, J. A. Samareh, B. H. Mason, L. L. Green, and R. T. Biedron. *Multidisciplinary High-Fidelity Analysis and Optimization of Aerospace Vehicles, Part 2: Preliminary Results,* AIAA paper 2000-0419, 2000.

[**47**] A. E. Arslan, D. A. Carlson. *Integrated determination of sensitivity derivatives for an aeroelastic transonic wing.* AIAA paper 94-4400, 1994.

[**48**] J. C. Newman III, P. A. Newman, A. C. Taylor. *Nonlinear aerodynamic design optimization of a flexible wing.* AIAA paper 96-4108, 1996.

[**49**] R. P. Weston, J. C. Townsend, T. M. Eidson and R. L. Gates. *A distributed computing environment for multidisciplinary design,* 5th AIAA/NASA/ISSMO Symposium on multidisciplinary analysis and optimization, Panama city beach, FL, AIAA paper 94-4374-CP, pp. 1091-1097, Sept. 1994.

[**50**] D. L. Knill, A. A. Giunta, C. A. Baker, B. Grossman, W. H. Manson, R. T. Haftka and L. T. Watson. *HSCT configuration design using response surface approximations of supersonic Euler aerodynamics,* AIAA paper 98-0995, 1998.

[**51**] N. M. Alexandrov, R. M. Lewis. *Analytical and computational properties of distributed approaches to MDO,* AIAA paper 2000-4718, 2000.

[**52**] I. P. Sobieski , I. Kroo. *Collaborative optimization using response surface estimation,* AIAA Journal, 38:1931-1938, 2000.

[**53**] P. A. LeGresley, J. J. Alonso. *Improving the performance of design decomposition methods with POD,* AIAA paper 2004-4465, 2004.

[**54**] C. R. Gumbert, G. J. W. Hou, P. A. Newman. *Simultaneous Aerodynamic and Structural Design Optimization (SASDO) for a 3-D Wing,* AIAA paper 2001-2527, 2001.

[**55**] J. Sobieszczanski-Sobiesky. *Sensitivity of complex, internally coupled systems,* AIAA journal Vol. 28, No. 1, pp. 153-160, January 1990.

[**56**] J. C. Newman III, A. C. Taylor III, R. W. Barnwell. *Aerodynamic shape sensitivity analysis and design optimization of complex configurations using unstructured grids*, Proc. 12th AIAA computation fluid dynamics conference, AIAA paper 95-1646, 1995.

[**57**] A. A. Giunta, J. Sobieszczanski-Sobiesky. *Progress towards using sensitivity derivatives in a high-fidelity aeroelastic analysis of a supersonic transport*, AIAA paper 90-4763, 1998.

[**58**] J. R. R. A. Martins, J. J. Alonso. *Aero-structural wing design optimization using high fidelity sensitivity analysis*, CEAS conference on multidisciplinary analysis and optimization, Cologne, Germany, June 2001.

[**59**] J. J. Reuther, J. J. Alonso, J. R. R. A. Martin, S. C. Smith. *A Coupled Aero-Structural Optimization Method For Complete Aircraft Configurations*, AIAA Paper 99-0187,1999.

[**60**] J. R. R. A. Martins, Juan J. Alonso, James J. Reuther. *Complete Configuration Aero-Structural Optimization Using a Coupled Sensitivity Analysis Method*, AIAA paper 2002–5402, 2002.

[**61**] N. Kroll, C. C. Rossow, D. Schwamborn, K. Becker, G. Heller. *MEGAFLOW – A numerical flow simulation tool for transport aircraft design*, ICAS Congress 2002, Paper No. 1.10.5, 2002.

[**62**] MSC. Software Corporation, 2 MacArthur Place Santa Ana, CA 92707, USA.

[**63**] A. Fazzolari, N. R. Gauger and J. Brezillon. *Sensitivity evaluation for efficient aerodynamic shape optimization with aeroelastic constraints*, European Congress on Computational Methods in Applied Sciences and Engineering ECCOMAS 2004, P. Neittaanmäki, T. Rossi, S. Korotov, E. Oñate, J. Périaux, and D. Knörzer (eds.), Jyväskylä, 24—28 July, 2004.

[**64**] A. Fazzolari, N. R. Gauger and J. Brezillon. *Efficient aerodynamic shape optimization in MDO context*, Journal of Computational and Applied Mathematics, accepted for publication in 2006.

[**65**] A. Fazzolari, N. R. Gauger and J. Brezillon. *Efficient aerodynamic shape optimization in MDO context*, Proc. Appl. Math. Mech., Vol. 5, pp. 739-740, 2005.

[**66**] A. Fazzolari, N. R. Gauger and J. Brezillon. *An Aero-Structure Adjoint Formulation for Efficient Multidiscipinary Optimization*, to appear in Evolutionary and Deterministic Methods for Design, Optimization and Control with Applications to Industrial and Societal Problems EUROGEN 2005, R. Schilling, W.Haase, J. Periaux, H. Baier, G. Bugeda (Eds) © FLM, Munich, 2005.

[**67**] R. Heinrich, R. Ahrem, G. Guenther, H.P, Kersken, W. Krueger, J. Nemann. *Aeroelastic Computation Using the AMANDA Simulation Environment*, CEAS Conference of Multidisciplinary Aircraft Design and Optimization, Maternushaus, Köln, Germany, 25-26 June 2001.

[**68**] O. Brodersen, M. Hepperle, A. Ronzheimer, C. C. Rossow and B. Schoening *The parametric grid generation system Megacads.* Proc of the 5th International Conference on numerical grid generation in comp field simulations (Ed. B.K. Soni, J. F. Thompson, J. Haeuser, P. Eiseman), NSF Eng. Center, Mississipi, pages 353-362, 1996.

[**69**] M. Abdo, R. L'Heureux, F. Pepin, F. Kafyeke. *Equivalent Finite Element Wing Structural Models used for Aerodynamics-Structure Interaction*, Canadian Aeronautics and Space Institute 50th AGM and Conference 16th Aerospace Structures and Materials Symposium, Montréal, 28-30 April 2003.

[**70**] A. Jameson. *Optimum transonic wing design using control theory*, Symposium transonicum iv, International Union of Theoretical and Applied Mathematics, Göttingen, Germany, September 2002.

[**71**] E. Previato et. al. *Dictionary of Applied Math for Engineers and Scientists*, CRC press, 2003.

[**72**] I. M. Gelfand, S. V. Fomin. *Calculus of Variations, Prentice-Hall, Inc, 1963.*

[**73**] A. Jameson, W. Schmidt, E. Turkel. *Numerical solution of the Euler equations by finite volume methods using Runge-Kutta time stepping schemes*, AIAA paper 81-1259, 1981.

[**74**] N. R. Gauger. *Das Adjungiertenverfahren in der aerodynamischen Formoptimierung*, DLR-Report No. DLR-FB--2003-05 (ISSN 1434-8454), 2003.

[**75**] O. Enoksson, P. Weinerfelt. *Numerical Methods for Aerodynamic Optimisation*, 8th International Symposium on Comp. Fluid Dynamics, Sep. 5-10 1999, Bremen, 1999.

[**76**] A. Jameson, S. Kim. *Reduction of the adjoint gradient formula in the continuous limit*, AIAA paper 2003-0040, 2003.

[**77**] E. J. Nielsen, M. A. Park. *Using an adjoint approach to eliminate mesh sensitivities in computational design*, AIAA paper 2005-0491, 2005.

[**78**] *Introduction to Finite Element Methods* (ASEN 5007) teaching course of the Department of Aerospace Engineering Sciences University of Colorado at Boulder. Lecture notes by Carlos Felippa: carlos.felippa@colorado.edu, 2005.

[**79**] M. A. Akgün, R.T. Haftka, K.C. Wu and J.L. Walsh. *Sensitivity of lumped constraints using adjoint method* AIAA paper 99-1314, 1999.

[**80**] A. Uzum, H. U. Akay and C. E. Bronnenberg. *Parallel computations of unsteady Euler equations on dynamically deforming unstructured grids*, Proceedings of the Parallel CFD´99´ Conference, May 23-26, Williamsburg, VA USA, 1999.

[**81**] H. G. Matthies , J. Steindorf. *Strong Coupling Methods* in W.L Wendland, M. Efendiev (Eds.) Analysis and Simulation of Multifield Problems, Springer-Verlag, Berlin, 2003.

[**82**] A. Beckert. *Coupling fluid (CFD) and structural (FE) models using finite interpolation elements* Aerosp. Sci. Technol. 4 (2000), 13-22, 2000.

[**83**] H. Doi, J. J. Alonso. *Fluid/structure coupled aeroelastic computations for transonic flow in turbomachinery*, proceedings of ASME Turbo Expo 2002, June 3-6 2002, Amsterdam, The Netherlands, 2002.

[**84**] G. J. W. Hou, A. Satyanarayana. *Analytical sensitivity analysis of a static aeroelastic wing*, AIAA paper 2000-4824, 2000.

[**85**] A. Beckert, H. Wendland. *Multivariate interpolation for fluid-structure-interaction problems using radial basis functions,* Aerosp. Sci. Technol. 00 (2001) 1-11, 2001.

[**86**] J. J. Alonso, P. LeGresley, E. van der Weide. *pyMDO: A Framework for high-Fidelity Multi-Disciplinary Optimization* AIAA paper 2004-4480, 2004.

[**87**] M. B. Giles , N.A. Pierce. *An introduction to adjoint approach to design*, Flow, Turbulence and Combustion, 65(3-4), pp. 393-415, 2000.

[**88**] E. Lund, H. Møller, L. A. Jakobsen. *Shape design optimization of steady fluid-structure interaction problems with large displacements,* AIAA paper 2001-1624, 2001.

Curriculum Vitae

Antonio Fazzolari

Juli 2005

Geburtsdatum: 19. Februar 1975
Geburtsort: Empoli (FI), Italien
Familienstand: ledig
Adresse: Via Valicarda 50
50056 Capraia e Limite (FI), Italia

Lebenslauf

1980-1993	Besuch der Grundschule, Mittelschule und des Gymnasiums in Empoli
1993	Maturitá (Abitur)
1993-1999	Studium an der Universität Pisa, Fachrichtung Physik
1999-2001	Studium an der Universität Florenz, Fachrichtung Physik
2001	Laurea (Diplom)
2002-2005	Promotionstipendiat / Doktorand im Rahmen des Graduiertenkollegs „Wechselwirkung von Struktur und Fluid“ an der Technischen Universität Braunschweig